Applications of Absorption Heat Transformers in Desalination, Cogeneration and the Use of Alternative Working Pairs

Kiyan Parham

Submitted to the
Institute of Graduate Studies and Research
in partial fulfillment of the requirements for the Degree of

Doctor of Philosophy
in
Mechanical Engineering

Eastern Mediterranean University
January 2014
Gazimağusa, North Cyprus

Approval of the Institute of Graduate Studies and Research

Prof. Dr. Elvan Yılmaz
Director

I certify that this thesis satisfies the requirements as a thesis for the degree of Doctor of Philosophy in Mechanical Engineering.

Prof. Dr. Uğur Atikol
Chair, Mechanical Engineering Department

We certify that we have read this thesis and that in our opinion it is fully adequate in scope and quality as a thesis for the degree of Doctor of Philosophy in Mechanical Engineering.

Prof.Dr.Mortaza Yari
Co-Supervisor

Prof. Dr. Uğur Atikol
Supervisor

Examining Committee

1. Prof. Dr. Uğur Atikol

2. Prof. Dr. Fuat Egelioğlu

3. Prof. Dr. Arif Hepbaşlı

4. Prof. Dr. Adnan Midilli

5. Prof. Dr. Mortaza Yari

ABSTRACT

In recent years considerable attention has been given to reduce the use of fossil fuels for heating and cooling applications. Large amounts of thermal energy at low temperatures from the process industries are released into the atmosphere, which causes thermal pollution. The Absorption Heat Transformer (AHT), being principally heat operated, is a useful tool to upgrade this low temperature rejected heat to the required heat energy at higher temperatures for useful applications. The desalination of seawater is one of such applications, which requires heat input at higher temperatures. Therefore, integrating the AHT and the desalination system for the aim of seawater desalination can significantly contribute to improve energy utilization and also the energy conservation. This thesis presents theoretical investigations on AHT based desalination systems.

Alternative configurations of AHT systems using $LiBr/H_2O$ as the working fluid and integrated with a water purification system are analyzed and optimized thermodynamically. First, the waste heat from a textile factory is utilized to run the AHT systems and the generated high temperature heat is employed for the purpose of desalination. A computer program is developed in the EES (Engineering Equation Solver) to investigate the effects of different parameters on four different configurations of AHT and the desalination system. It is shown that applying different modifications can increase the coefficient of performance (*COP*) of the AHT and consequently the productivity of the desalination system. The maximum flow rate of the distilled pure water reaches 0.2435 kg/s when waste heat from the

condenser is utilized by the evaporator. The risk of crystallization of LiBr is lowered in the modified configurations.

In the subsequent section of the study the waste heat from a novel cogeneration cycle based on the recompression supercritical carbon dioxide (S-CO_2) Brayton cycle is utilized to produce power through a transcritical CO_2 power cycle and pure water by means of distillation process. Alternative configurations of AHT systems are employed to upgrade the lower temperature waste heat in order to run desalination system. It was found that in the best configuration, both the energy and exergy efficiencies are about 5.5–26% and 9.97-10.2% higher.

The thermodynamic performance of the absorption chiller using (H_2O+LiCl) as the working pair was simulated and compared with the absorption chiller using (H_2O+LiBr). The effects of evaporation temperature on the performance coefficient, COP, generation temperature, concentration of strong solution and flow rate ratio were also analyzed. The results showed that the coefficient of performance of the absorption chiller, using (H_2O+LiBr) at the optimum conditions, was around 1.5–2% higher than that of (H_2O + LiCl).

Keywords: Absorption Heat transformer, absorption chiller, Alternative configurations, Desalination, LiBr+H20, crystallization

ÖZ

Son yıllarda, ısıtma ve soğutma uygulamalarında fosil yakıt kullanımının azaltılmasına özen gösteriliyor. Proses sanayilerinde açığa çıkan çok miktarda düşük sıcaklıktaki ısıl enerji atmosfere bırakılarak termal kirlilik yaratılıyor. Esasen ısı ile çalıştırılan Absorbsiyonlu Isı Dönüştürücüsü (AID), bu düşük sıcaklıkta atılan ısıyı bazı uygulamalarda ihtiyaç duyulan daha yüksek sıcaklıktaki ısı enerjisine yükseltmek için kullanılabilecek yararlı bir gereçtir. Deniz suyunun tuzdan arındırılması, yüksek sıcaklıkta ısı girdisine ihtiyaç duyulan bahse konu uygulamalardan biridir. Bu yüzden, deniz suyunu tuzdan arındırmak için, AID'ı arıtma sistemi ile entegre ederek enerjiyi daha etkili kullanma ve enerji tasarrufu konularına katkıda bulunmak mümkündür. Bu tez raporu, AID ile birleşik su arıtma sistemlerinin kuramsal araştırmalarını içermektedir.

Bir su arıtma sistemi ile entegre edilen ve $LiBr/H_2O$ çalışma akışkanını kullanan farklı AID yapılandırmaları analiz edilerek termodinamik optimizyasyonlar yapıldı. Önce, bir tekstil fabrikasında açığa çıkan atık ısıdan yararlanılarak AID sistemleri çalıştırılmış ve bunlardan elde edilen yüksek sıcaklıktaki ısı, su arıtma maksatlı kullanılmıştır. Dört alternatif düzende kurulmuş AID üniteleri ile entegre edilmiş su arıtma sistemlerinin değişik parametrelerini incelemek için EES (Engineering Equation Solver) yazılımı kullanarak bir bilgisayar programı geliştirilmiştir. AID'lerde uygulanan değişikliklerin soğutma tesir katsayılarını (*STK*) ve buna bağlı olarak arıtma sisteminin üretkenliğini artırdığı gözlemlenmiştir. Yoğuşturucudan çıkan atık ısı, buharlaştırıcı tarafından kullanıldığı zaman arıtılmış suyun azami akış

hızı 0.2435 kg/s'ye ulaşıyor. Sözkonusu alternatif AID sistemlerde, LiBr akışkanının kristalleşme riski de azalıyor.

Araştırmanın daha sonraki kısmında, yeniden sıkıştırma kritik üstü karbondiyoksit (S-CO_2) Brayton çevrimine dayalı yeni bir kojenerasyon çevriminden açığa çıkan atık ısı kullanılarak, transkritik CO_2 çevrimde güç üretimi elde edilmiş ve damıtma işlemi yapılarak saf su elde edilmiştir. Değişik düzeneklerde tasarlanan AID kullanılarak düşük sıcaklıkta elde edilen atık ısıyı daha yüksek sıcaklıklara çıkarmak suretiyle tuzdan arındırma sistemi beslenerek çalıştırılmıştır. En iyi düzenekte, enerji ve exerji verimliliklerinin yaklaşık yüzde 5.5-26 ve 9.97-10.2 daha yüksek olduğu gözlemlenmiştir.

Akışkan çifti olarak (H_2O+LiCl) kullanan absorbsiyonlu soğutma gurubunun termodinamik performansı simule edilmiş ve (H_2O+LiBr) kullanan soğutma gurubuyla kıyaslanmıştır. Ayni zamanda, buharlaşma sıcaklığının *STK*'na, üretim sıcaklığına, güçlü solusyonun konsantrasyonuna ve akış hızı oranına etkileri değerlendirilmiştir. Sonuçlar, (H_2O+LiBr) çiftini optimum şartlarda kullanan absorbsiyonlu soğutma gurubunun, (H_2O + LiCl) kullanana göre, *STK*'nın yüzde 1.5 – 2 civarında daha yüksek olduğunu göstermiştir.

Anahtar Kelimeler: Absorbsiyonlu ısı dönüştürücüsü, absorbsiyonlu soğutma gurubu, alternatif düzenekler, tuzdan arındırma, LiBr+H_20, kristalleşm

To My Family

ACKNOWLEDGMENT

First and foremost, I would like to express my sincere gratitude to my supervisor **Prof. Dr. Ugur. Atikol** for the continuous support during my Ph.D studies and research, his patience, motivation, and immense knowledge. His guidance helped me in all the times of research and writing of this thesis. The good advice, support and friendship of **Prof. Atikol**, has been invaluable on both an academic and personal life, for which I am extremely grateful. In fact it is an honor for me to have been working with him.

I would like to express my special appreciation and thanks to my co-supervisor **Prof. Dr. Mortaza. Yari** whom has been a tremendous mentor for me. It would not have been possible to write this doctoral thesis without the help and support of this kind man.

A special thanks to my family. Words cannot express how grateful I am to my mother and father for all of the sacrifices that they have made on my behalf. Their prayer for me was what sustained me thus far.

At the end I would like to express appreciation to my lovely friends who supported me in doing and writing my thesis, and heartened me to strive towards my goal.

TABLE OF CONTENTS

LIST OF TABLES

LIST OF FIGURES

LIST OF ABRIVATIONS

abs	Absorber
AB/EV	Absorber/evaporator
con	Condenser
COP	Coefficient of Performance
DAHT	Double Absorption Heat Transformer
ECOP	Exergetic Coefficient of Performance
eva	Evaporator
gen	Generator
GTL	Gross Temperature Lift
HEX	Heat Exchanger
SAHT	Single absorption heat transformer
TAHT	Triple absorption heat transformer

LIST OF SYMBOLS

ε	Economizer efficiency(dimensionless)
X	Concentration (wt)
f	Flow ratio
T	Temperature (^{o}C)
P	Pressure (kPa)
$\dot{Q}$	Heat Capacity (KW)
$\dot{m}$	Mass flow rate (kg/s)
h	Enthalpy (kJ/kg)

LIST OF SUBSCRIPTS

O	Ambient
S	Strong
w	Weak
u	Utilized

Chapter 1

INTRODUCTION

1.1 Background

With fast economic growth and constantly increasing energy consumption, the utilization of low-grade energy is becoming more and more important for the world. Large amounts of low-temperature waste heat are released daily from many industrial plants to the atmosphere at temperatures between 60 and 100 ^{o}C.

A heat transformer is a device, which can deliver heat at a higher temperature than the temperature of the fluid, by which it is fed. Absorption heat transformer systems are attractive for upgrading the waste heat from industrial processes and the heat generated from solar and geothermal sources. In addition, they can be used to upgrade the low temperature waste heat from a process to be used in a secondary process. The integration of AHTs with different kinds of cycles plays an important role in energy saving or even energy efficiency increment.

Figure 1.1 shows the general schematic of the absorption heat transformer in a single stage mode. The single stage absorption heat transformer (SAHT) basically consists of an evaporator, a condenser, a generator, an absorber and a solution heat exchanger (SHE). The generator and evaporator are supplied with waste heat at the same temperature leading to increased heat that can be collected at the absorber. The AHT performs in a cycle, which is the reverse of absorption heat pump [1].

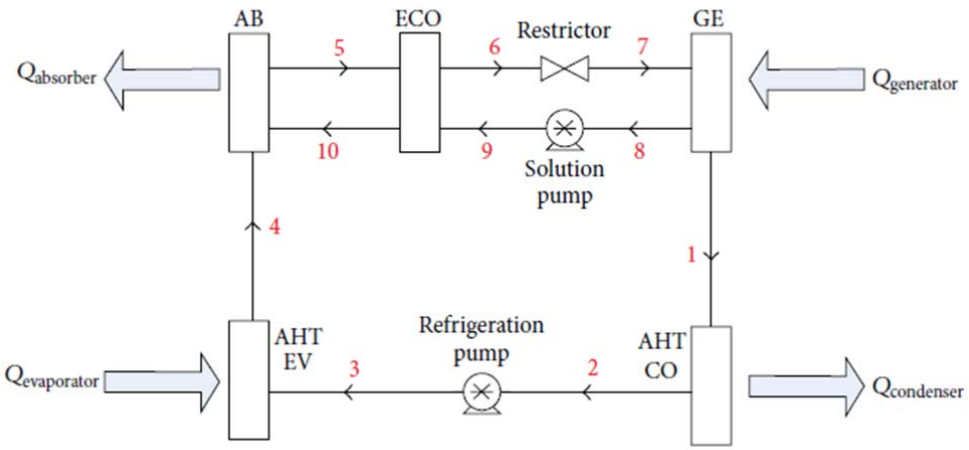

Figure 1. 1 Single stage absorption heat transformer [2]

1.2 Absorption Heat Transformers

The operating system of the basic absorption cycles is briefly explained as follows: Refrigerant vapor is produced at state 4 in the evaporator, by low or medium-grade heat source. The refrigerant vapor dissolves and reacts with the strong refrigerant-absorbent solution of $LiBr+H_2O$ that enters the absorber from state 10, and weak solution returns back to generator at state 5.

The heat released from the absorber will be higher than the heat input in the generator and evaporator due to the exothermic reaction of the absorber and refrigerant in it. In the generator some refrigerant vapor is removed from the weak solution to be sent to the condenser and consequently the strong solution from the generator is returned to the absorber. After condensing the vaporized refrigerant in the condenser, it is pumped to a higher pressure level as it enters the evaporator. The waste heat delivered to the evaporator causes its vaporization. Again the absorber absorbs the refrigerant vapor at a higher temperature. Therefore, the absorption

cycles have the capability of raising the temperature of the solution above the temperature of the waste heat [3].

1.3 State of the Knowledge

Modifications of absorption heat transformers have always been a big challenge in the area of the study. One of the major problems in AHT systems is crystallization risk, which causes the heat transfer area in the absorber to decrease and totally harms the device. Recently Horuz et al. [1] introduced alternative configurations of AHTs and after assessing their COPs they concluded that there were possibilities for improving the performance. However, in order to make a more conclusive evaluation on the performance of such modifications on the cycle, other performance parameters such as, the crystallization risk of the absorbent, gross temperature lift and the flow-ratio of the absorbent and the refrigerant need to be evaluated under different working criteria. Besides these points, optimization of the alternative cycles has not been adequately investigated before.

1.4 Scope and Objective of the Study

The present work aims at continuing Horuz and Kurt's work [1] in a more detailed study via a methodical comparative investigation. The main objective of the present work is to examine in detail the performances of alternative AHT configurations coupled with desalination and power generation systems, while at the same time exploring alternative working fluids.

A thorough and comprehensive thermodynamics analysis and efficiency assessment of the proposed configurations will be carried out. In order to identify the effects of some parameters, such as AHT heat source temperature, absorber, generator and evaporator temperatures, flow-ratio, concentration of weak and strong solutions on

the cycle performance and the quantity of distilled water, a parametric study will be conducted and validated with the experimental data. Furthermore, all the cycles will be optimized thermodynamically using the Engineering Equation Solver software.

1.5 Organization of the Thesis

The upcoming chapters in this thesis are as follows:

Chapter 2 deals with an inclusive and comprehensive literature review, which investigates the major arrangements and configurations of single stage absorption heat transformers. In chapter 3 a fascinating case study, in which four different novel configurations of SAHTs, have been coupled to desalination system has been analyzed and a multi objective optimization has been done. In chapter 4, the same configurations of AHTs have been integrated into a cogeneration cycle to analyze the benefits of such combinations. An overview of the employed working fluids in AHTs has been made in chapter 5 and as a case study an absorption chiller utilizing ($LiCl+H_2O$) has been presented. And finally the last chapter covers some concluding remarks of the thesis.

Chapter 2

LITERATURE REVIEW

Kurem and Horuz [2] analyzed the Absorption Heat Transformers using ammonia-water and water-lithium bromide (H_2O/LiBr) solutions. Their results showed that the AHT system using H_2O/LiBr solution performed better than the system using ammonia water (NH_3/H_2O) solution. Although water-lithium bromide solution was well suited for use in the AHTs, it still had some disadvantages, namely, corrosion, high viscosity, limited solubility, and a practical upper temperature limit. Horuz and Kurt [1] investigated an industrial application of the AHT system to obtain hot process water. For this purpose, a textile factory, which generated waste heat at $90\pm2^{o}C$ (15 ton/h is extracted from four different processes) and required hot water for process at $120^{o}C$ was chosen. In the first case, in a basic single AHT, the waste heat was supplied to the generator and absorber at the same time (Fig. 2.1). In the second setup the waste hot water was directed first to the evaporator and then to the generator (Fig. 2.2). In the third system, in addition to the waste hot water configuration of the second system, an absorber heat exchanger was included instead of the solution heat exchanger (Fig. 2.3).

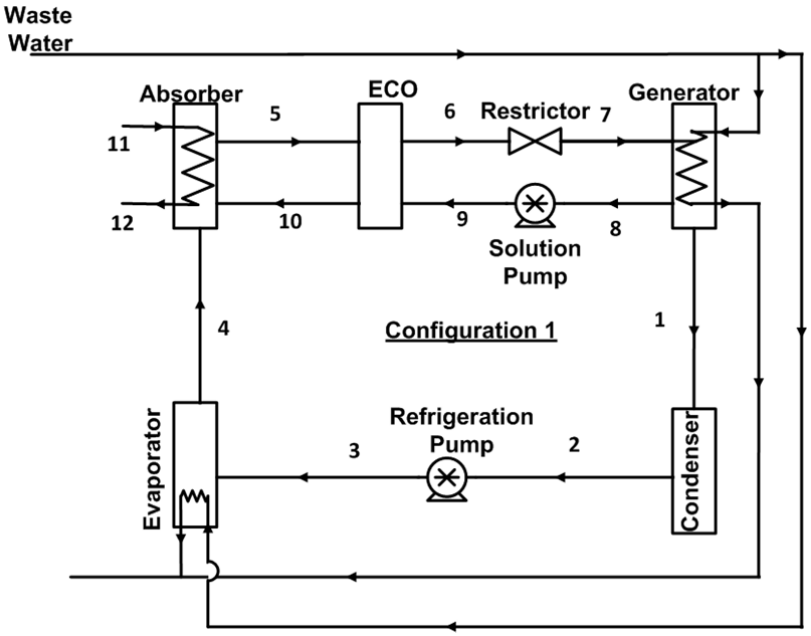

Figure 2. 1. Schematic diagram of SAHT(S-Type I) [1]

Finally, the last configuration incorporated the second and third systems with the addition of a refrigerant heat exchanger at the evaporator inlet (Fig.2.4).

It was shown that with the increase in the condenser temperature, the COPs and the absorber heat capacity decreased. On the other hand, as the evaporator and the generator temperatures increased, the COP and the absorber heat capacities were also increased. Additionally, it was proved that, when the evaporator temperature was higher than the generator temperature, the COP and the absorber heat capacity was relatively higher (Figs 2.2-2.4).

In fact the latter is the most important result of reference [1] and this leads to the motivation of proposing different configurations.

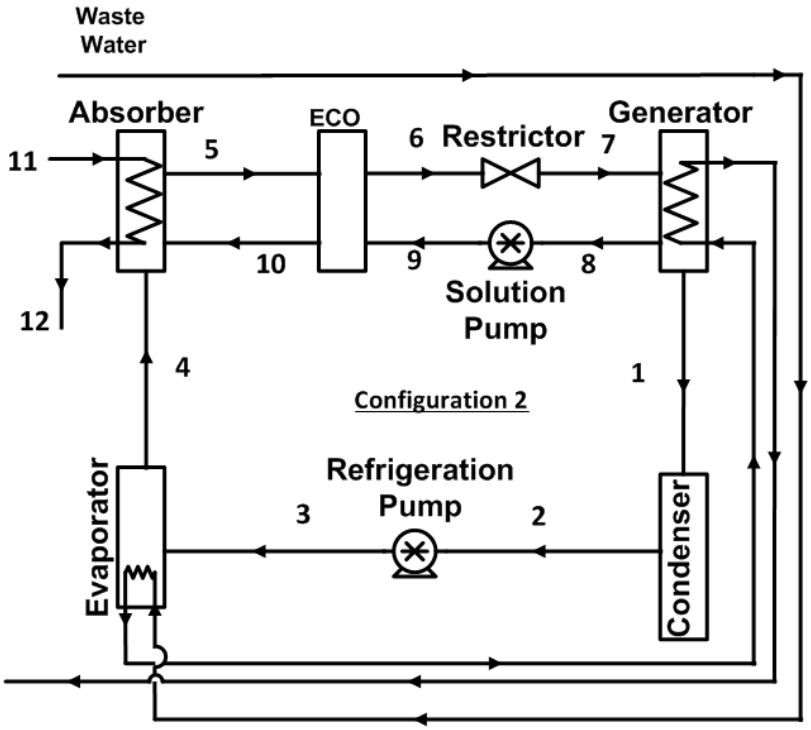

Figure 2. 2.Schematic diagram of SAHT(S-Type II) [1]

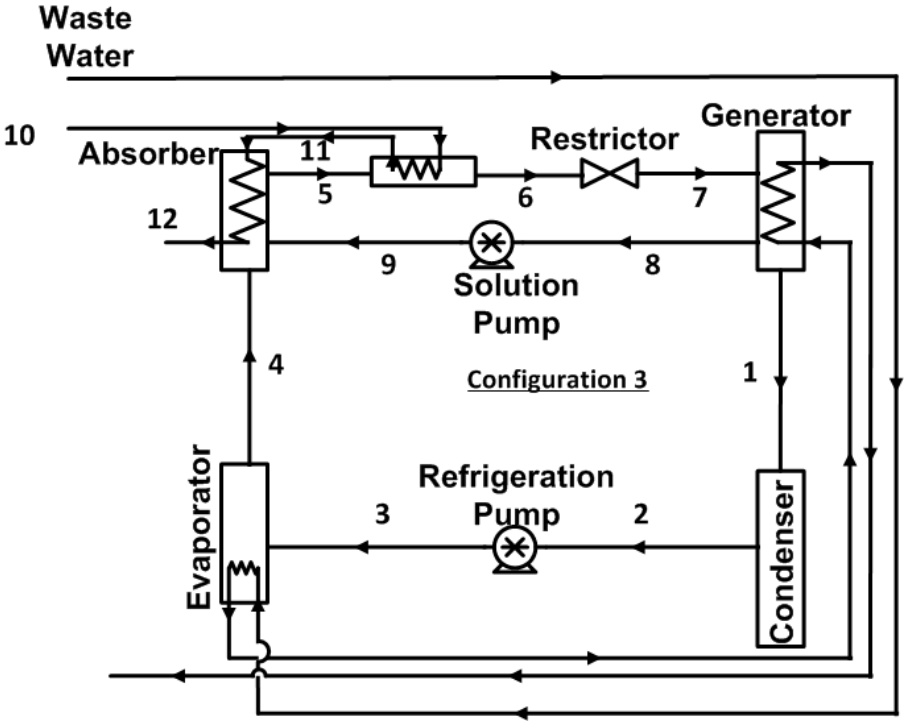

Figure 2. 3. Schematic diagram of SAHT(S-Type III) [1]

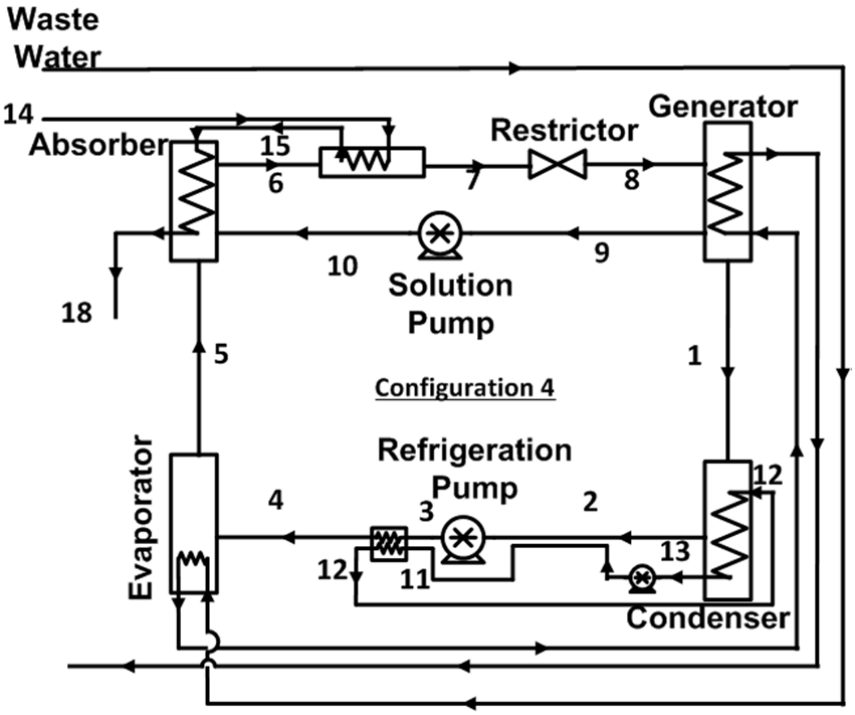

Figure 2. 4. Schematic diagram of SAHT(S-Type IV) [1]

Ma et al. [4] reported the first industrial scale heat transformer by recovering waste heat from a synthetic rubber plant, which was used to heat water from 95 to 110^{o}C with heat flow rate of 5000 kW, obtaining a mean coefficient of performance (COP) of 0.470, and a gross temperature lift of 25 ^{o}C. Furthermore in this work, economic analysis was performed and a simple payback period of 2 years was reported.

Sotelo and Romero [5] compared the performance and Gross Temperature Lift (GTL) of an absorption heat transformer with plate heat exchangers using and comparing water/Carrol to one using H_2O/LiBr. It was proved that water/Carrol mixture had a better performance and higher temperature lifts. Zhang and Hu [6] investigated the performance of a new working pair H_2O + 1-ethyl-3-methylimidazolium dimethylphosphate ([EMIM][DMP]) in an AHT and compared

the simulation results to those of H_2O/LiBr, and Tetraethylene glycol dimethyl ether (TFE/E181). It was concluded that H_2O + [EMIM] [DMP] had excellent cycle performances together with negligible vapor pressure and no possibility of crystallization. It also had a weaker corrosion tendency on iron-steel materials compared to aqueous solution of lithium bromide and could thus be used for Industrial applications.

Zebbar et al. [7] elaborated a mathematical model for a H_2O/LiBr AHT to optimize those parameters having a significant effect on the endo-irreversible cycle for an existing heat transformer with already dimensioned total area of heat exchangers. This optimization was achieved through the structural bond analysis of the heat transformer, using the coefficient of structural bond (CSB) and varied parameters such pressure P of the AHT and solution concentration X. Results showed that the irreversibility of the absorber and the generator played an important role on the total entropy of the system generated with varying concentration. On the other hand, when the pressure was varied, the generator and condenser were the critical parameters. Furthermore at an optimal pressure ratio of 0.72 a COP of 0.486 was achieved instead 0.479.

Rivera et al. [8] studied both theoretically and experimentally the performance of a single-stage heat transformer (SSHT) operating with the H_2O/LiBr and the H_2O /Carrol$_{TM}$ mixtures. It was observed that almost the same tendencies and values of the coefficient of performance and flow ratio were obtained in general for both mixtures; however, because of the higher solubility of the water/Carrol$_{TM}$ mixture the SSHT operated over a large range of generator and evaporator temperatures and with

higher GTLs. It was concluded that this alternative solution could be better, serving as working fluids in AHTs.

In another work Rivera, and Cerezo [9] introduced additives of 1-octanol and 2-ethyl-1-hexanol, in a 2 kW single-stage heat transformer utilizing H_2O/LiBr, operating at absorber temperatures in a range of 70 and 110^oC. The results showed that at the same conditions, absorber temperatures increased about 5^oC with the addition of 400 ppm of 2-ethyl-1-hexanol to the lithium bromide mixture. Also it was shown that the COP increased by up to 40% with the same additive.

Second law analysis of the latter mentioned work was performed far ahead by the same team [10]. Their results demonstrated that for absorber temperatures between (84-88) ^oC the highest COP and Exergetic Coefficient of performance (ECOP) were obtained with the use of the 2-ethyl-1-hexanol (400 parts per million) additive, reaching values of up to 0.49, 0.40 and 0.43, respectively. The lowest COP and highest irreversibilities were obtained by using the single H_2O/LiBr mixture. It was found that 2-ethyl-1-hexanol decreased the irreversibility considerably in the absorber, thereby increasing the efficiency of this component and hence that of the entire equipment.

Thermodynamic design data for AHTs without utilizing a heat exchanger and with operation employing different working fluids were proposed by several researchers [11].

Sozen and Yucesu [12] proposed a single stage AHT that used an ejector before the absorber as illustrated in Fig. 2.5. The aim of using ejector in the mentioned cycle

was to achieve a better mixing of refrigerant and absorber in the entrance of the absorber. The results demonstrated that a reduction of 12% and 10% exergy losses were possible in the absorber and generator, respectively. Sozen [13] developed a mathematical model for simulating the performance of AHT system with NH3/water as working fluid and powered by a solar pond. The maximum upgrading of solar pond's temperature by the AHT is obtained at 51.5 ^{o}C with a GTL of 93.5 ^{o}C with COP of about 0.4. The maximum temperature of the useful heat produced by the AHT was approximately 150^{o}C. The exergy analysis demonstrated that the non-dimensional exergy loss in the absorber was about 70%, while in the generator it was above 10–20% and in the condenser it increased with the condenser temperature.

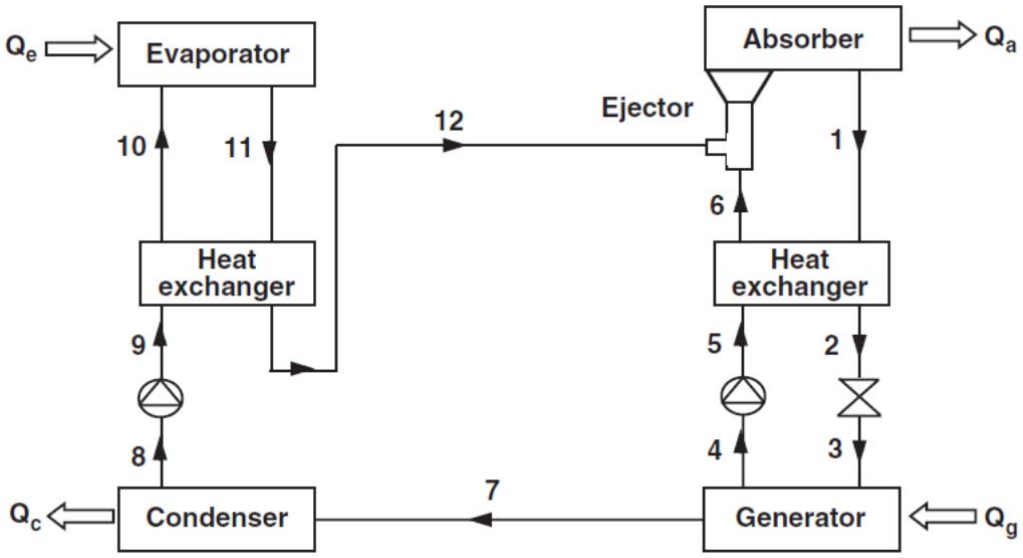

Figure 2.5. Schematic representation of Ejector-Absorption Heat Transformer (EAHT) [12]

Shi et al. [14] presented and analyzed an ejection-absorption heat transformer (EAHT) based on the performance analysis of the single stage, the two-stage and the double absorption heat transformers (Fig. 2.6).

Their results showed that EAHT had a simpler configuration than the double absorption heat transformer and two-stage heat transformer. The delivered useful temperature in the ejection-absorption heat transformer was higher than for a single stage heat transformer and simultaneously its system performance was raised.

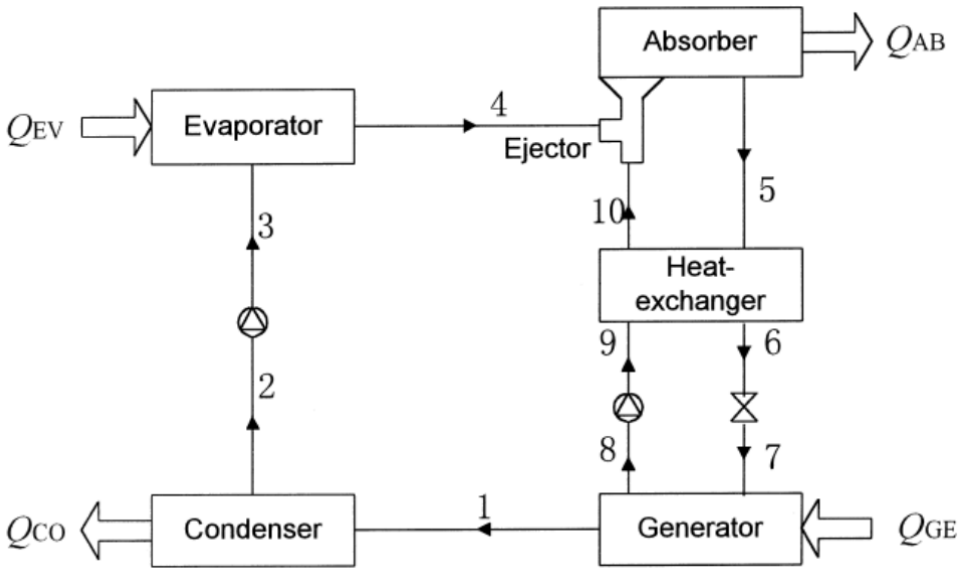

Figure 2. 6. Ejection-absorption heat transformer schematic diagram [14]

Guo et al. [15] developed a mathematical model of a vertical falling film AHT with a water/lithium bromide solution to analyze the performance of AHTs under design and off-design conditions (Fig. 2.7). The study showed that the proportion of exergy losses in auxiliary components was small in design conditions, but increased rapidly in off-design conditions. Furthermore, a novel operation strategy based on keeping the circulation ratio invariant was proposed, leading to a significantly higher COP and exergy efficiency under off design conditions.

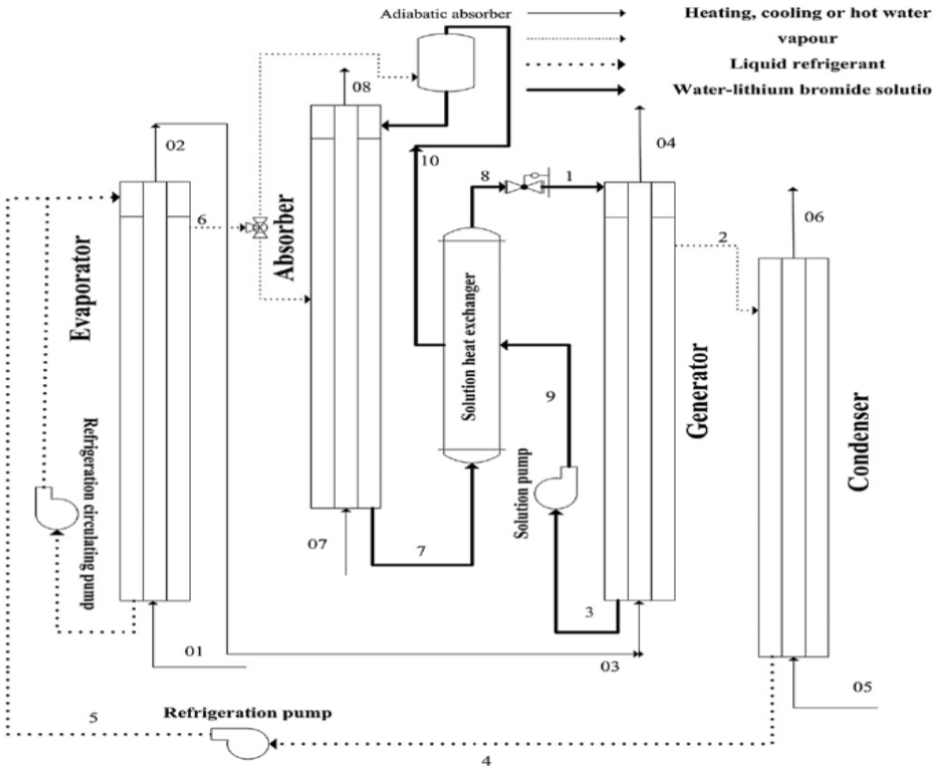

Figure 2.7. Schematic diagram of the vertical falling film AHT [15]

Olarte-Cortes et al. [16] analyzed the heat transfer of an experimentally untested geometry in absorbers (Fig. 2.8) using tar impregnated graphite disk and $LiBr/H_2O$ as working fluid. The impregnated tar was used to overcome the problem of corrosion faced by the conventionally used steel. Their results showed that as the Reynolds number increased from 110 to 144, the heat transfer coefficient increased, which led to a maximum value of 954 W/m^2K at Reynolds number of about 144, but when Reynolds number increased above 147, the heat transfer coefficient decreased.

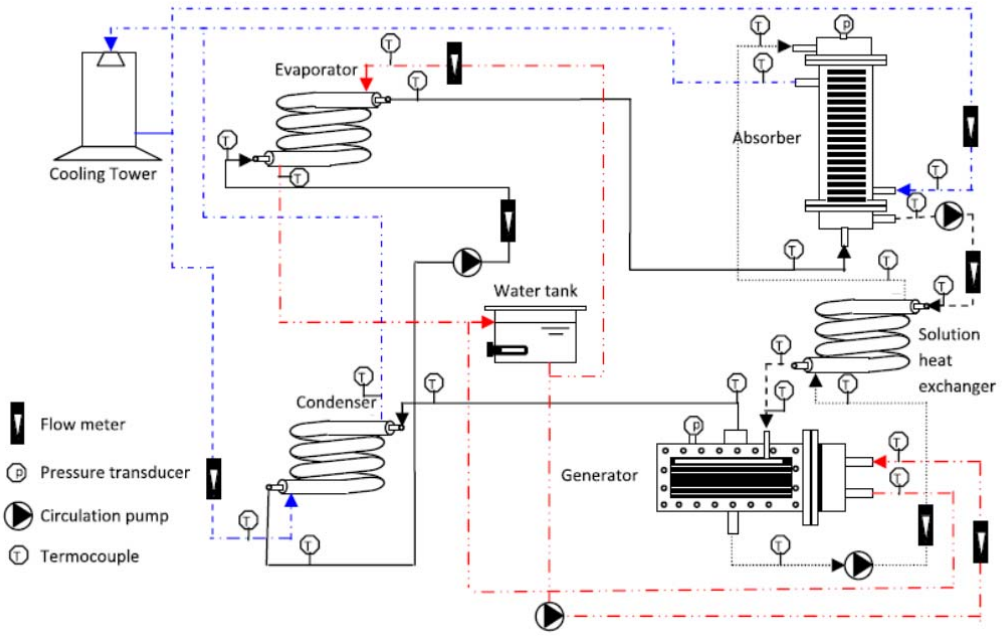

Figure 2. 8. Schematic diagram of the experimental bench using graphite disk [16]

Absorption-demixtion heat transformer (ADHT) is a kind of absorption cycle which makes use of a mixture exhibiting a miscibility gap at low temperatures. The working mixtures used in this type of AHT-process have an upper critical solution temperature (UCST) and consist of two components, with one being much more volatile than the other. At temperatures higher than the UCST the mixture is completely miscible, below this temperature it is partially miscible as shown in the phase diagram (Fig. 2.9). When utilizing this phenomenon in an AHT, absorption occurs at temperatures above the USCT and demixing (desorption) at temperatures lower than the USCT.

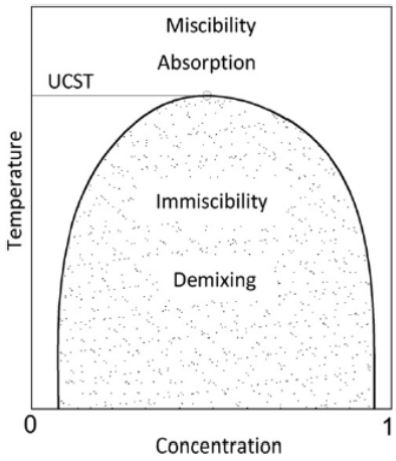

Figure 2. 9. Phase Diagram of a partially miscible solution [17]

Fig 2.10 shows a schematic of an ADHT cycle. As the working pair enters the separator, it is demixed by rejecting heat to an external heat sink. Both mixtures are pumped separately to higher pressures then heated in two internal heat exchangers. The refrigerant enters the evaporator where it absorbs heat from an external source and vaporizes, then enters through the lower part of the absorber while the absorbent enters through the upper part. In the absorber the concentration of the refrigerant decreases while its temperature increases. This results in the vapor mixture exiting at temperatures higher than the inlet temperature from the upper part of the absorber. The rest of the mixture exits from the lower part of the absorber where it is cooled in the internal heat exchanger then throttled to a lower pressure before entering the separator.

The generated vapor mixture enters the condenser, and rejects heat at high temperature level to an external heat sink while it condenses. It is later cooled down in the internal heat exchanger and throttled to the low pressure level. Finally the liquid mixture of the absorbent and refrigerant flows into the separator and mixes

there with the rest of the mixture. The COP of an ADHT-process can be defined as in reference [17], which is completely different from typical AHTs:

COP= Condenser capacity/ Evaporator capacity **(2.1)**

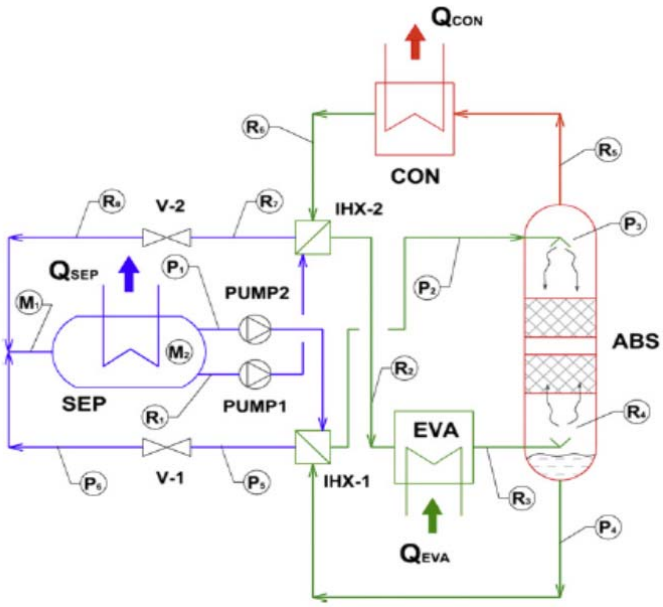

Figure 2. 10. Schematic diagram of the AHT-process using partially miscible working mixtures with upper critical solution temperature [17]

Liquid-liquid vapor equilibrium data were used by Niang et al. [18] to investigate an AHT process using a partially miscible working mixture of (H_2O/(C_3H_3OC)CHO) as an alternative to the conventional H_2O/LiBr. In their work a relatively higher COP of 0.86 was estimated. Alonso et al. [19] built the first experimental set up of an ADHT to validate its technical feasibility using n-heptane/N,N-dimethylformamide (DMF) as working mixture. In the set up used in this work, temperature lifts of maximum 8^{o}C and efficiencies of 0.3 – 0.4 were reported.

As it can be seen from the literature, the optimization of the cycles and the analysis of the crystallization risk were not paid enough attention. The present work will attempt to address these issues.

Table 2. 1.Single stage Absorption Heat Transformer

Configuration	T_{eva} (ºc)	T_{gen} (ºc)	T_{con} (ºc)	T_{abs} (ºc)	Working Pair	Flow ratio	GTL (ºc)	COP	Heat Source	Remarks	Reference
Fig. 2.2	80	80	25	130	H_2O/LiBr	9.51	50	0.48	Waste heat from a cogeneration system in a textile company	While the T_{con} increases the COPs and the Q_{abs} decrease	[1]
Fig. 2.3	80	73	25	130	H_2O/LiBr	18.63	50	0.46	Waste heat from a cogeneration system in a textile company	*Less COP than that of S-Type I *Q_{abs} and produced hot water increased by 81.1% and 2.81%	[1]
Fig. 2.4	80	73	25	130	H_2O/LiBr	18.63	50	0.53	Waste heat from a cogeneration system in a textile company	Increase in COP and f	[1]
Fig. 2.5	80	73	25	130	H_2O/LiBr	18.63	50	0.55	Waste heat from a cogeneration system in a textile company	*14.1%, , ,158.5% and 3.59% increase in COP, $Q_{abs}$and produced hot water compared to S-Type I	[1]
Fig. 2.6	58	58	20	150	H_2O - NH_3	97.5	-	0.5	Solar pond	Pressure recovery and pre-absorption in the ejector improves the efficiency of the AHT.	[14]
Same as Fig. 2.6	70	70	30	90-117	H_2O/LiBr	3-9	-	0.43-0.49	-	Higher useful delivered temperature and better performance	[12]
Same as Fig. 2.2	70-80	70-80	25-30	-	H_2O-Carrol	-	Max GTL≈ 52ºc	Max COP≈ 0.47	-	Higher GTL than that of H_2O-LiBr, less corrosivity	[20]

Chapter 3

METHODOLOGY

Typically in the thermodynamics analysis of AHTs, the most important aim is to increase the performance. Then, the whole cycle is modeled by using the energy balance for the cycle, after which weaknesses are identified. In the present work, in addition to this conventional approach, there is one major objective; namely, mitigating the crystallization risk of the absorbent. Since the proposed cycle is a combination of an AHT and a desalination system, it is important to determine, not only the COP of the considered AHT cycle, but also the GTL and the amount of distilled water.

3.1 Mathematical Model

This section describes the thermodynamic model used for the simulation of AHT integrated systems. Each component of the considered system has been treated as a control volume and the principles of mass and energy conservation are applied to them. The EES software package is used for solving the equations.

The mass balance can be expressed as:

$$\sum \dot{m}_{in} - \sum \dot{m}_{out} = 0 \qquad \textbf{(3.1)}$$

The first law of thermodynamics yields the energy balance for each component as follows:

$$\sum(\dot{m}h)_{in} - \sum(\dot{m}h)_{out} + \dot{Q}_{cv} - \dot{W}_{cv} = 0 \quad \textbf{(3.2)}$$

The following assumptions are made in this study:

I. All the processes are assumed to be steady flow processes.

II. Changes in kinetic and potential energies are neglected.

III. The pressure losses due to the frictional effects in the connecting pipes of the AHT and desalination system are neglected.

IV. Some proper values of effectiveness are considered for the heat exchangers.

V. In the AHT, the solution at the generator and the absorber outlets, as well as the refrigerant at the condenser and the evaporator outlets are all at saturated states [1].

VI. The evaporator and the generator of the AHT work at the same temperature for configuration 1, since heat is supplied to them from the same source. This assumption is made by other researchers previously [1, 21-24]. Meanwhile in configurations 2, 3 and 4 the temperature of the generator is less than that of the evaporator. (T_{gen}=T_{eva}- 7 ˚C) [1]

VII. The heat source for the AHT system is the hot water generated by a cogeneration system in a textile company. The industrial system has four different units each of them producing 15 ton/h water at 90±2˚C.

VIII. The mechanical energy consumed by pumps can be neglected.

IX. Absorber heat is transferred to impure water as latent and sensible heat.

X. The distilled water is salt free.

Table 3.1 summarizes the basic assumptions and presents the input parameters used in the simulation according to the stream numbers shown in Figures.

Table 3. 1. The input data in the simulation

Parameters	Values	References
T_{con} (°C)	25-35	[6]
T_{abs} (°C)	100–135	[25] and [26]
T_{eva} (°C)	75-90	[26]
$T_{gen} = T_{eva}$ (°C)	Configuration 1	[1], [21], [27], [22] and [23]
$T_{gen} = T_{eva} - 7$ (°C)	Configuration 2,3,4	[1]
$T_{heat\ Source}$ (°C)	90±2	[1]
$\dot{m}_{heat\ Source}$ (ton/h)	60	[1]
εECO (%)	80	[22] and [23]

3.2 Performance Evaluation

In the AHT systems the coefficient of performance (COP) is a measure of the cycle's ability to upgrade the thermal energy given to the generator and the evaporator of the system. It is defined as follows [1]:

$$COP = \frac{Q_{abs}}{Q_{gen}+Q_{eva}} \quad \text{(Configurations 1, 2)} \qquad \textbf{(3.3)}$$

$$COP = \frac{Q_{abs}+Q_{ab-ex}}{Q_{gen}+Q_{eva}} \quad \text{(Configuration 3, 4)} \qquad \textbf{(3.4)}$$

And $Q_{utilized}$ is the useful part of the utilized waste heat for desalination purposes. This quantity is the heat rate delivered to the water purification system by means of the absorber of the AHT and the pre-heater as shown in Figs. 1 and 2(a-c).

$$Q_{utilized} = \dot{m}_{13}\,(h_{14} - h_{13}) \quad \text{(Configurations 1, 2)} \qquad \textbf{(3.5)}$$

$$Q_{utilized} = \dot{m}_{12}\,(h_{14} - h_{12}) \quad \text{(Configuration 3)} \qquad \textbf{(3.6)}$$

$Q_{utilized} = \dot{m}_{16} (h_{18} - h_{16})$ (Configuration 4) **(3.7)**

The flow ratio (*f)* is an important design and optimization parameter in the AHT systems. It is defined as the ratio of the mass flow rates of the strong solution and refrigerant:

$$f = \frac{\dot{m}s}{\dot{m}r} = \frac{\dot{m}_8}{\dot{m}_4} = \frac{X_7}{X_8 - X_7} \quad \textbf{(3.8)}$$

where $\dot{m}_s$ is the strong solution mass flow rate, $\dot{m}_r$ refrigerant mass flow rate and X the LiBr concentration in the solution.

The heat capacities of the absorber and the generator as a function of flow ratio can be calculated by using the following equations [1]:

$$q_{abs} = \frac{\dot{Q}abs}{\dot{m}_4} = (f+1)h_5 - fh_{10} - h_4 \quad \textbf{(3.9)}$$

$$q_{gen} = \frac{\dot{Q}gen}{\dot{m}_4} = h_1 + fh_8 - (f+1)h_7 \quad \textbf{(3.10)}$$

$$q_{con} = \frac{\dot{Q}con}{\dot{m}_4} = (h_2 - h_1) \quad \textbf{(3.11)}$$

$$q_{eva} = \frac{\dot{Q}eva}{\dot{m}_4} = (h_4 - h_3) \quad \textbf{(3.12)}$$

In thermodynamics, the exergy of a system is the maximum useful work possible during a process that brings the system into equilibrium with a heat reservoir. Exergy is the energy that is available to be used. The second law efficiency of a process or system can be defined as the ratio of the exergy of the desired output to the exergy that is supplied to the system.

$$\eta_{II} = \frac{\text{exergy of desired output}}{\text{exergy supplied}} \quad \textbf{(3.13)}$$

3.3 Optimization Method

The results obtain from the mathematical model reveal that the optimum quantity of produced distilled water depends on the temperatures of the absorber, condenser, evaporator and generator.

Therefore, the optimum quantity of the produced distilled water of working cycle can be expressed as a function of four design parameters, as shown in the following equation:

$$\text{Maximize } \dot{m}_{distilled\text{-water}}(T_{gen}, T_{eva}, T_{con}, T_{abs}) \quad \textbf{(3.14)}$$

Subject to:

$100 \leq T_{abs} \leq 130^{\circ}C$

$20 \leq T_{con} \leq 35^{\circ}C$

$80 \leq T_{eva} \leq 90^{\circ}C$

$80 \leq T_{gen} \leq 90^{\circ}C$ (configuration 1)

$70 \leq T_{gen} \leq 80^{\circ}C$ (configuration 2, 3, 4)

Using direct search method and applying the constraints on each variable by setting the bounds, the performance of the whole cycle is optimized by using EES software from the viewpoint of quantity of produced distilled water. The direct search method is based on a successive search intended to find an extremum by directly comparing function values at a sequence of trial points without involving derivatives. This method is deemed suitable for problems involving simulation-based optimization or optimizing non-numerical functions, as well as, in practice, problems involving non-smooth or discontinuous functions [28].

3.4 Model Validation

The available data in literature were used to validate the simulation results. For the case of the AHT cycle the experimental results reported by Rivera et al. [29] were used. The conditions and assumptions used in their work are applied for the aim of validation. The assumptions were as follows:

I. Heat losses and pressure drops in the connecting pipes and the components are considered negligible.
II. The flow through the expansion valves is isenthalpic.
III. The effectiveness of the economizer is 70%.
IV. The absorber temperature is 123 °C.
V. The generator and evaporator temperatures being the same are 74.1 °C.

Fig. 3.1 shows the comparison between the COP obtained from the present work with that reported by Rivera et al. [29].

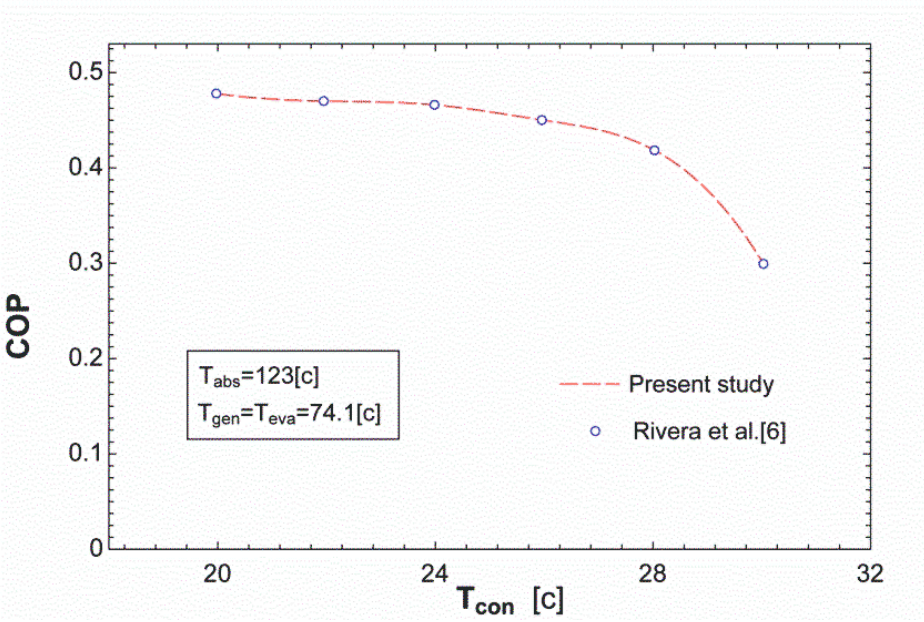

Figure 3. 1. Validation of the simulation model developed for the AHT system.

The figure shows an excellent agreement between the two outcomes and indicates a decrease in the COP as the condenser temperature of the AHT system increases. In the case of cogeneration cycle and absorption chiller some changes and modifications will be made on the earlier mentioned subjects.

Chapter 4

ALTERNATIVE ABSORPTION HEAT TRANSFORMER CONFIGURATIONS INTEGRATED WITH WATER DESALINATION SYSTEM

In this chapter, alternative configurations of AHTs, which are integrated to a desalination system, will be investigated. Water and energy are two inseparable items that govern our lives and promote civilization. In order to produce potable water from the sea or brackish water several desalination techniques are employed [30]. The most developed and widely practiced desalination method is the distillation process. The distillation of sea or brackish water can be achieved by utilizing a thermal energy source [31]. As mentioned earlier large amounts of low-temperature waste heat are released daily from many industrial plants to the atmosphere at temperatures between 60 and 100 °C [1]. Absorption heat transformers can be exploited to utilize this low-grade heat and improve energy efficiency of the plants.

The heat of absorption released in the absorber is at a temperature of about 100–140 °C. This upgraded energy now can be used in the water purification system.

The water purification system receives its required thermal energy from the absorber of the AHT system. The impure water is heated in the absorber where it is partially evaporated. The two phase flow enters into the separator vessel where it is separated into liquid and vapor. The liquid water mixes with the entering impure water before returning to the suction pump.

Recently Horuz and Kurt [1] introduced four different configurations of AHTs and developed a computer code to study the effects of condenser, evaporator and generator temperatures on the COP and absorber heat capacity of single-stage AHT systems.

In the case of the basic set-up of an AHT, the waste hot water is supplied to the generator and evaporator at the same time (shown in Fig. 2.1). The second used system has such a configuration, in which the waste hot water initially is directed to the evaporator and then generator. In the third system, in addition to the waste hot water configuration of the second system, an absorber heat exchanger is included instead of the solution heat exchanger. Finally, the last system incorporates the second and third systems with the addition of a refrigerant heat exchanger at the evaporator inlet. However, the study did not investigate the effect of parameters such as the flow ratio, weak and strong solution concentration, heat source and gross temperature quantities. Moreover, it would be interesting to conduct the simulations for more conditions.

The present work aims to address this shortage and continuing Horuz and Kurt's work [1] through in a more detailed study via a methodical comparative approach.

4.1 Performance Analysis of Alternative Configurations

Figs 4.1-4.3 display three alternative designs of AHTs integrated with seawater desalination systems, which were described in the second chapter and in more detail in [1].

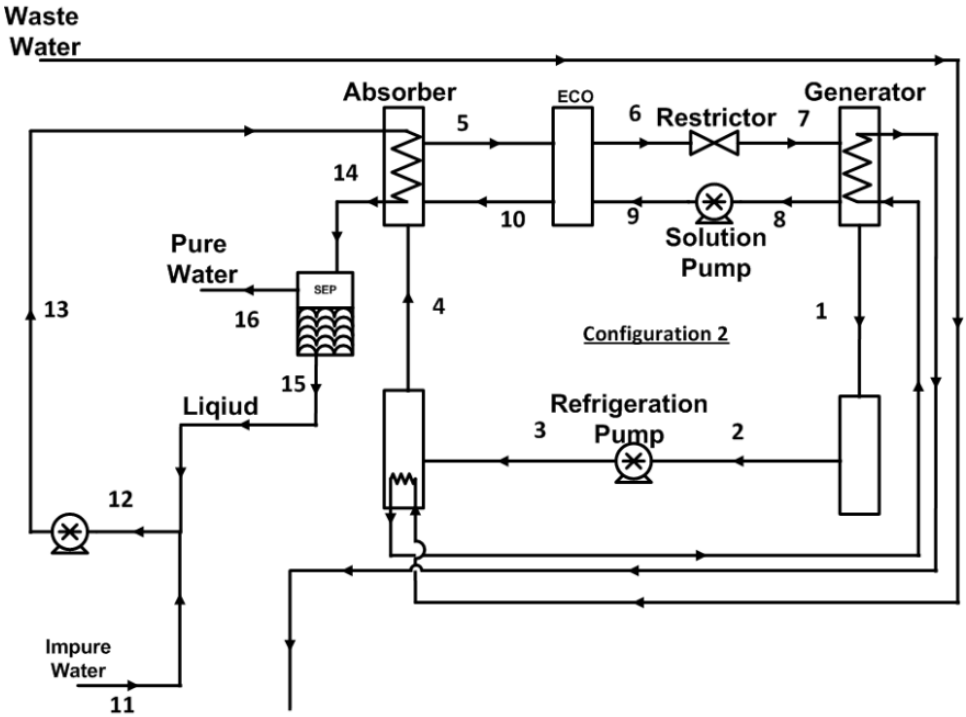

Figure 4. 1. Schematic diagram of seawater desalination system integrated to a single effect absorption heat transformer (Configuration 2)

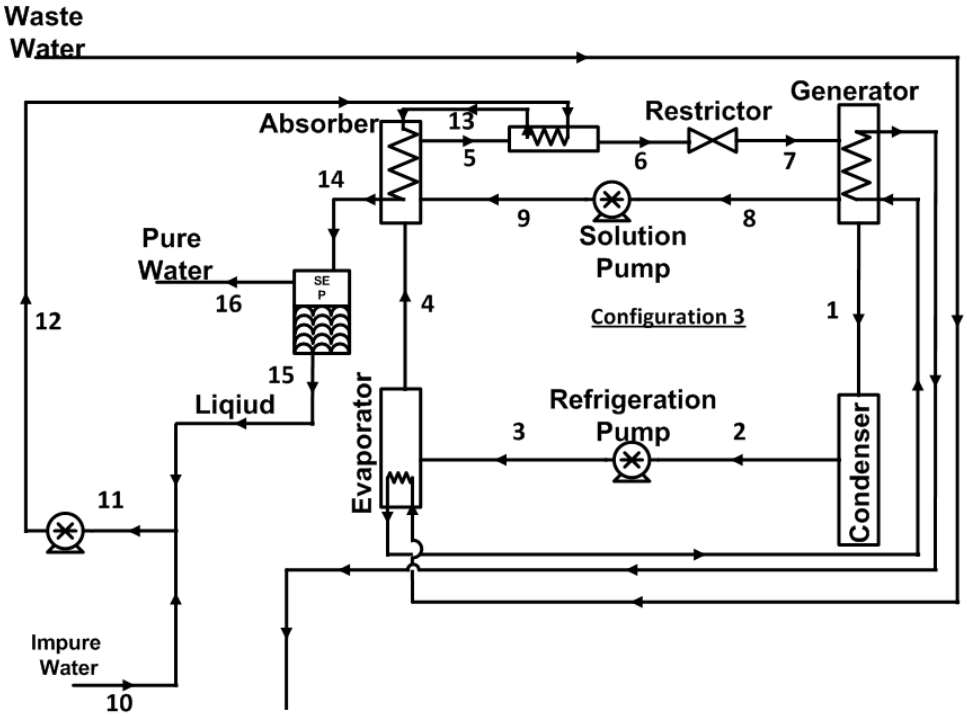

Figure 4. 2. Schematic diagram of seawater desalination system integrated to a single effect absorption heat transformer (Configuration 3)

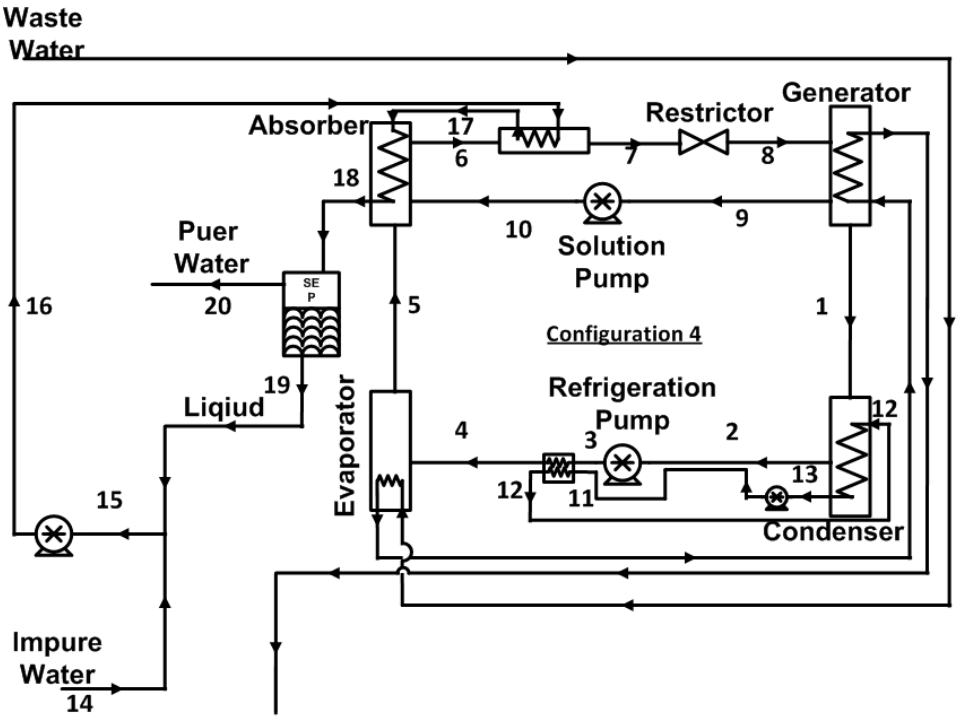

Figure 4. 3 Schematic diagram of seawater desalination system integrated to a single effect absorption heat transformer (Configuration 4)

The methodology described in chapter three was employed in the analysis. Energy equations were used in EES in order to perform the simulation.

4.2 Simulation Results and Discussion

The energy, mass flow rate, flow ratio and concentration values for four different configurations are compared for the same absorber and condenser temperatures in Table 4.1. As the table indicates, in configuration 4, the utilized heat for the aim of desalination is 2.2 times more than that of the heat utilized from a typical AHT. Meanwhile the increase in the quantity of the distilled water displays a similar trend.

Table 4. 1. Comparison of input and calculated properties of different AHT configurations

	Unit	Configuration 1	Configuration 2	Configuration 3	Configuration 4
Absorber Temperature	˚C	130	130	130	130
Condenser Temperature	˚C	25	25	25	25
Generator Temperature	˚C	80	73	73	73
Evaporator Temperature	˚C	80	80	80	80
Solution heat exchanger outlet temperature	˚C	120	118.6	-	-
Absorber heat exchanger outlet temperature	˚C	98.02	89.37	80	80
Evaporator heat exchanger outlet temperature	˚C	-	-	-	68
f (flow ratio)		9.28	18.72	18.72	18.72
COP_{AHT}		0.4876	0.4584	0.4976	0.516
$\dot{m}_r$ (Refrigerant flow rate)	kg/s	0.1001	0.2002	0.2002	0.2155
$\dot{Q}_U$ (Utilized heat rate for desalination)	kW	242.5	429	502.2	540.5
$T_{waste\ out,Eva}$(Waste water evaporator outlet temperature)	˚C	82	82	82	82
$T_{waste\ out,Gen}$(Waste water generator outlet temperature)	˚C	82	75	73	72
Weak solution concentration		0.5926	0.5926	0.5926	0.5926
Strong solution concentration		0.6565	0.6243	0.6243	0.6243
$m_{distilled\ water}$(Distilled water produced)	kg/s	0.09281	0.1642	0.1922	0.2069

It can be seen in Fig.4.4 that as the absorber temperature increases, the COPs of all single stage AHT configurations having the condenser temperatures above 30˚C will

decrease sharply for the T_{abs} values above 120˚C. Among different configurations when the gross temperature lift ($\Delta T_G = T_{abs} - T_{eva}$) is not beyond 45˚C the COP is basically unchanged for configurations 3 and 4. However, it decreases very rapidly for configuration 2, compared to a moderate drop for configuration 1. Configuration 4 achieves the highest COP while configuration 2 delivers the lowest. The maximum COP of configuration 4 is 12-13% higher than that of accomplished by configuration 2. For T_{con}=25 ˚C, T_{eva}=80 ˚C and T_{abs}=130 ˚C, the COPs for configurations 1 to 4 are evaluated to be 0.4876, 0.4584, 0.4976 and 0.516, respectively, as seen in Fig. 4.4.

It is also observed that the lower the condenser temperature is, the higher the COP and thus the available temperature lift will be. This observation was also made by other researchers, who studied configuration 1[6, 23, 32] .Out of all configurations, configuration 4 stands out as the best performer in a colder weather.

Fig. 4.5 shows the variation of COP with the absorption temperature under different generation or evaporation temperature conditions. As it can be seen, any increase in the absorber temperature above T_{abs}=122˚C will cause a steeper drop in the COP and the absorber heat capacity (as discussed later in Figure 4.8). This is due to the fact that as T_{abs} increases, the concentration of the weak solution and consequently the flow ratio (f) increase, resulting in a decrease in the absorber heat capacity. This result is in agreement with that reported in the literature [23, 32, 33].

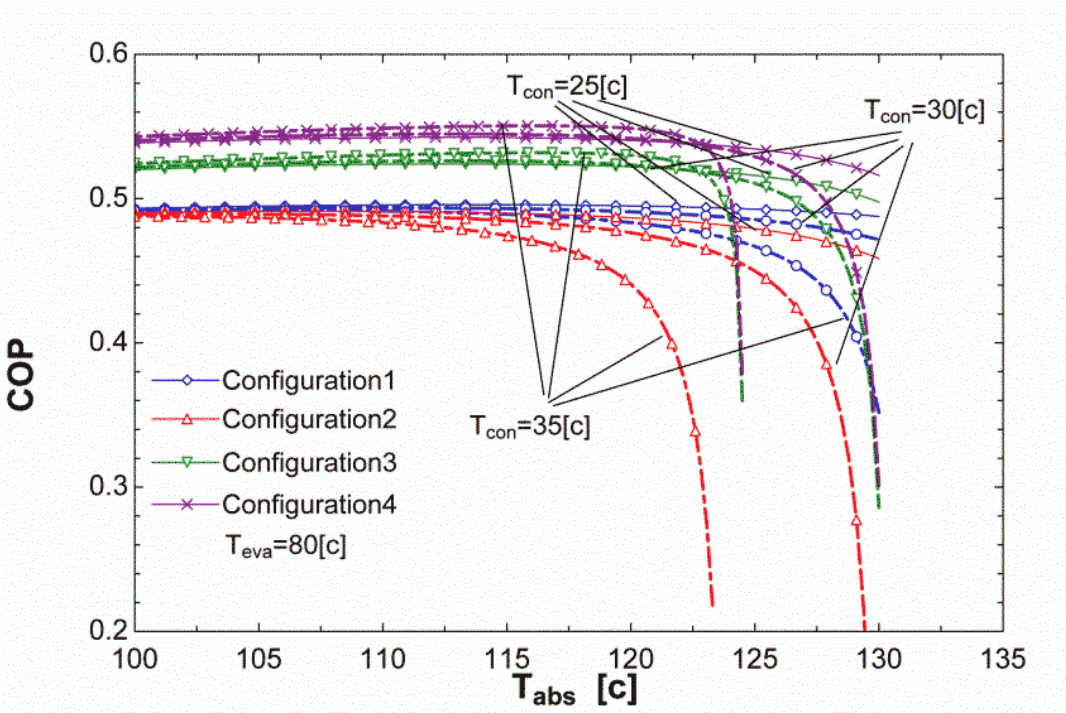

Figure 4. 4. Effects of T_{abs} on COP for different configurations at different condenser temperatures

As shown in Fig. 4.5 the higher the generation or evaporation temperature is, the higher the absorption and corresponding gross temperatures. It is still consistent here that the COP follows the order of configuration 4, 3, 1 and 2 under different generation or evaporation temperature conditions.

The variations in the concentrations of strong and weak solutions are plotted against T_{abs} in Fig. 4.6. The absorber will absorb more refrigerant vapor with higher concentrations of LiBr solutions leaving the generator. The strong solution is denoted with x_s. When generating and condensing temperatures are kept unchanged, the x_s does not vary with the T_{abs} , but the weak solution increases with the $T_{abs.}$ The higher the absorbing temperature or GTL, ΔT is, the denser the weak solution is. As shown in Fig. 4.6, x_s in configuration 1 is more than that of other configurations while weal solution in all the configurations is the same. The higher x_s results in the higher flow

ratio and can also cause crystallization problem of LiBr [1]. So, it can be concluded that the possibility of crystallization within configuration 1 is higher than those of other three configurations [34].

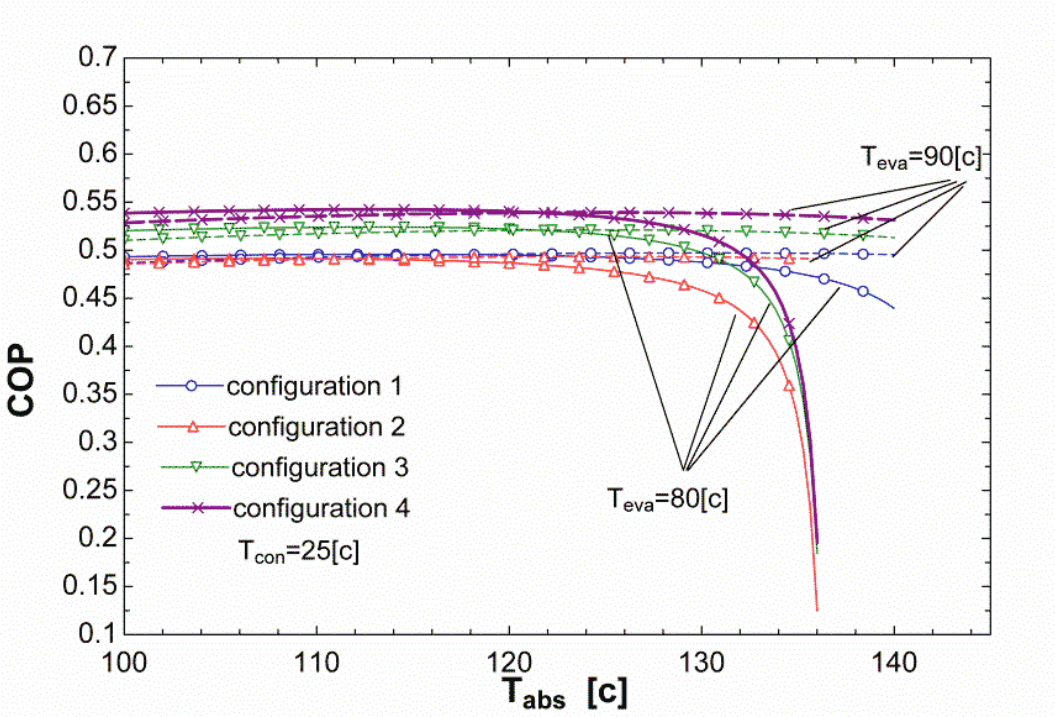

Figure 4. 5. Effects of Tabs on COP for different configurations at different evaporation temperatures

As the concentration of the weak solution increases with T_{abs}, the concentration, the concentration difference (ΔX) will decrease linearly and the flow ratio, f will exhibit a parabolic increase as shown in Fig.4.7. As mentioned earlier, when the generation, evaporation and condensing temperatures are constant, the ΔX and T_{abs} will only vary with f, which is an important and easily controllable operation parameter. Larger f also results in higher T_{abs} and more mechanical power losses. Under the same operation conditions, the f is in the order of configuration 1 > configurations 2, 3 and 4. According to the results reported in the literature, the larger the

concentration difference is, the larger the driving force for the mass transfer in the generator or absorber [6].

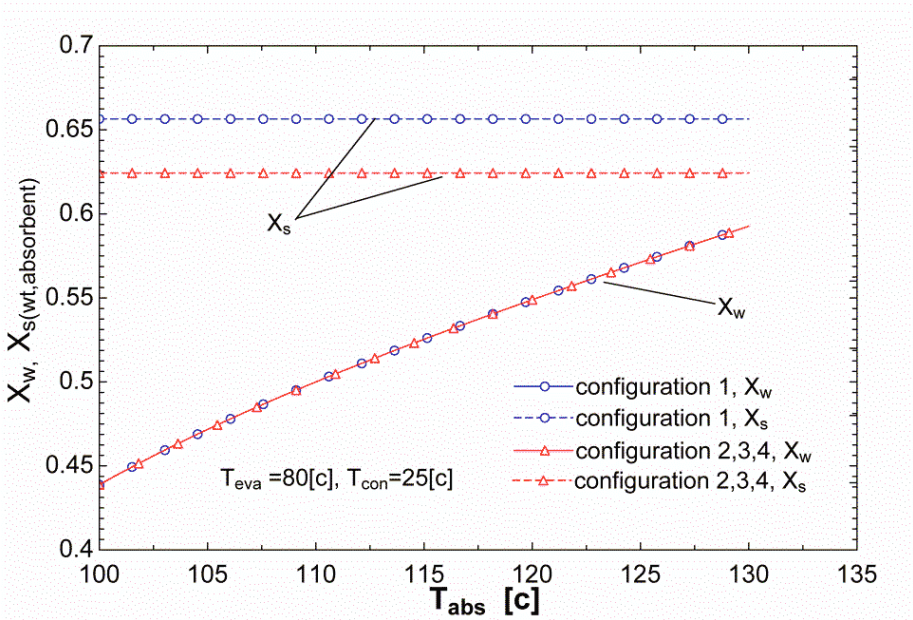

Figure 4. 6. Effects of Tabs on Xs and Xw for four different configurations

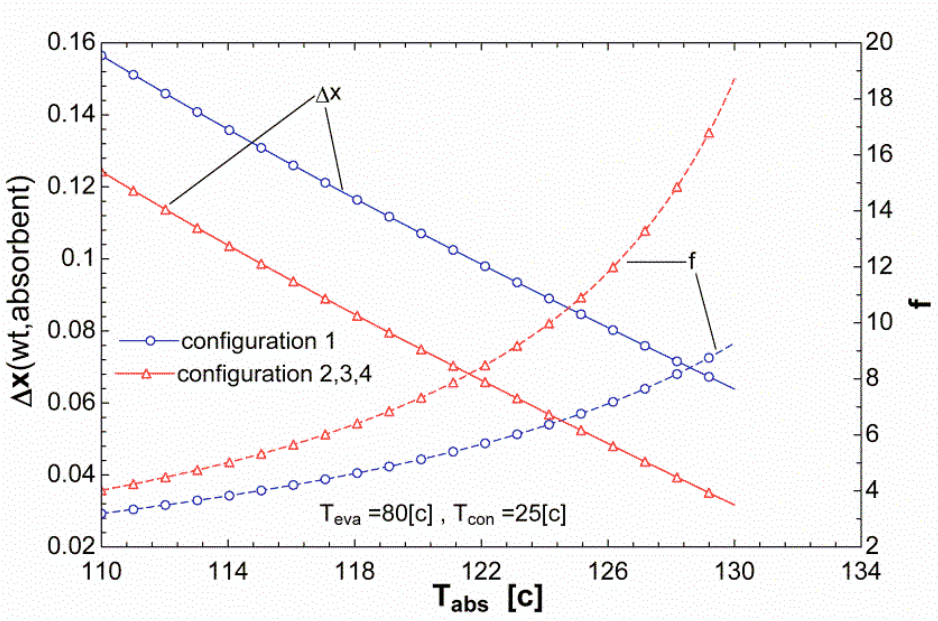

Figure 4. 7. Effects of Tabs on ΔX and f for four configurations

Fig.4.8 shows the variation of utilized heat output delivered to the desalination system by AHT cycle at absorbing temperature T_{abs}. It is clear that as T_{abs} increases, the absorber heat capacity and totally $\dot{Q}_u$ decrease. This is due to the fact that as T_{abs} increases, X_w and consequently flow ratio (f) increases, resulting in a decrease in the absorber heat capacity. This result is in agreement with that reported in the literature [23, 32]. It should be noted that for T_{eva}=80˚C and T_{con}=25˚C configuration 4 provides the maximum $\dot{Q}_u$ for desalination purpose. The other configurations follow in the order of 3,2 and 1. The increment of $\dot{Q}_u$ for the second configuration is due to the fact that when the evaporator temperature is higher than the generator temperature, the absorber heat capacity increases [1, 33]. In configuration 3, in addition to the waste hot water system of configuration 2, an absorber heat exchanger is included instead of solution heat exchanger, which boosts the quantity of the utilized heat for desalination. Finally, as mentioned earlier, configuration 4 is based on configuration 3, which additionally incorporates a heat exchanger before the evaporator that recovers the waste heat from the condenser, would have the maximum heat output for desalination.

The effect of the AHT heat source temperature on the AHT performance and pure water production rate are shown in Figs. 4.9 and 4.10. Figs indicate that as heat source temperature inrcreases, the absorber heat capacity, the COP of the AHT and the pure water production rate increases. This is due to the fact that, increasing waste heat or heat source temperature results in the increased AHT evaporator temperature (and pressure) leading to a lower weak solution concentration and flow ratio (f). The lower flow ratio results in a higher absorption heat capacity and a higher COP [1].

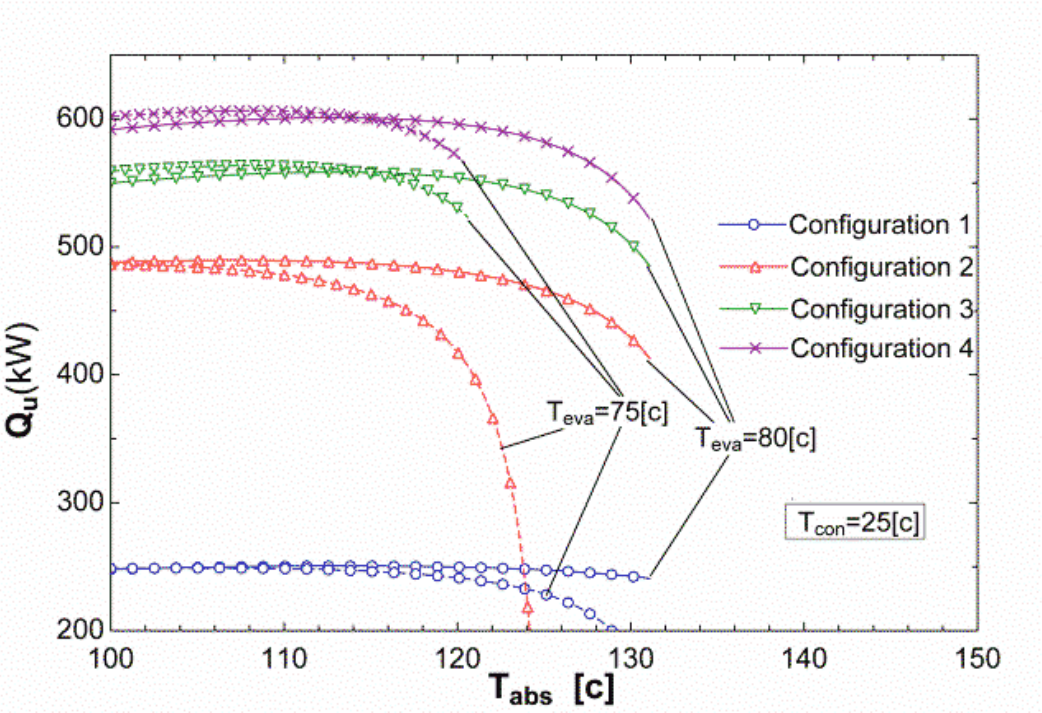

Figure 4. 8. Effect of Tabs on Utilized heat for the aim of desalination

Therefore the energy input to the desalination system increases causing a higher pure water production rate, as shown in Fig. 4.10. Figs. 4.10 and 4.11 also indicate the improvement of the proposed latter configurations of AHT systems (2-4) to the basic AHT configuration (1) for the aim of desalination. In configurations 3 and 4 an absorber heat exchanger and a refrigerant heat exchanger have been added, which decreases the absorption heat capacity, but increases the total utilized heat for the desalination purpose. Therefore the pure water production in configurations 3 and 4 are higher than the other two configurations.

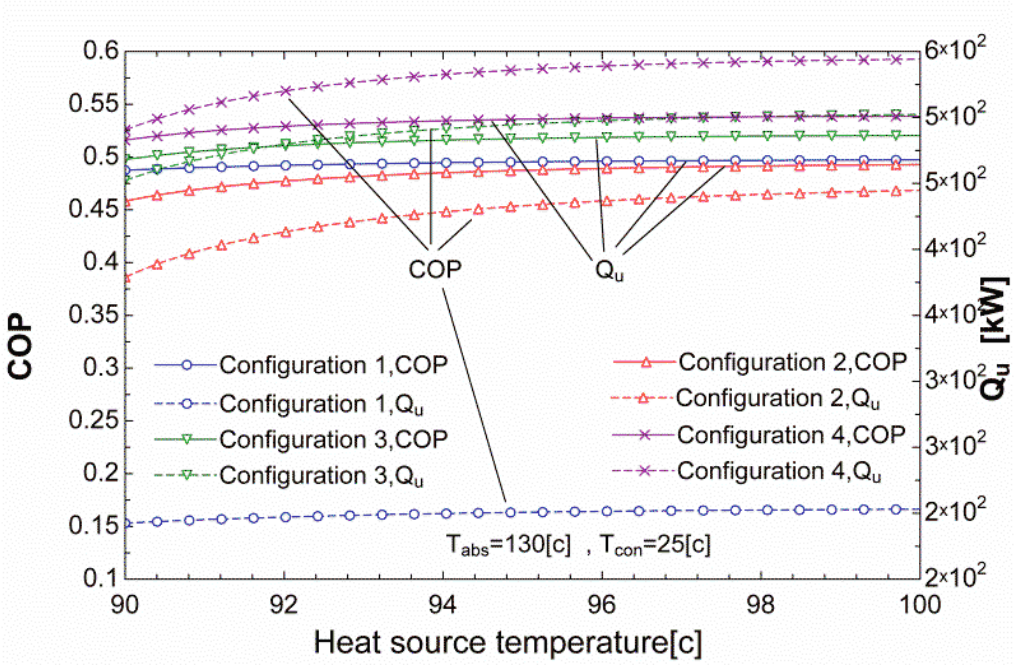

Figure 4. 9. Effect of heat source temperature on COP and utilized heat water for desalination

The pure water production rates were investigated for T_{con}=25˚C, T_{eva}=75 and 80˚C with respect to T_{abs} as shown in Fig. 4.11. The curves indicate similarity to Fig. 4.8 where the quantity of utilized heat for desalination purpose decreases with increasing $T_{abs.}$ The trends observed in these curves have been also reported by Yari et al [25, 33]. The figure also reveals that a higher pure water production rate is achieved when configuration 4 is utilized, which is in coherence with the results indicated in Fig. 4.5. The distilled mass flow rates in all configurations demonstrate a rapid decline when T_{eva} decreases from 80˚C to 75˚C.

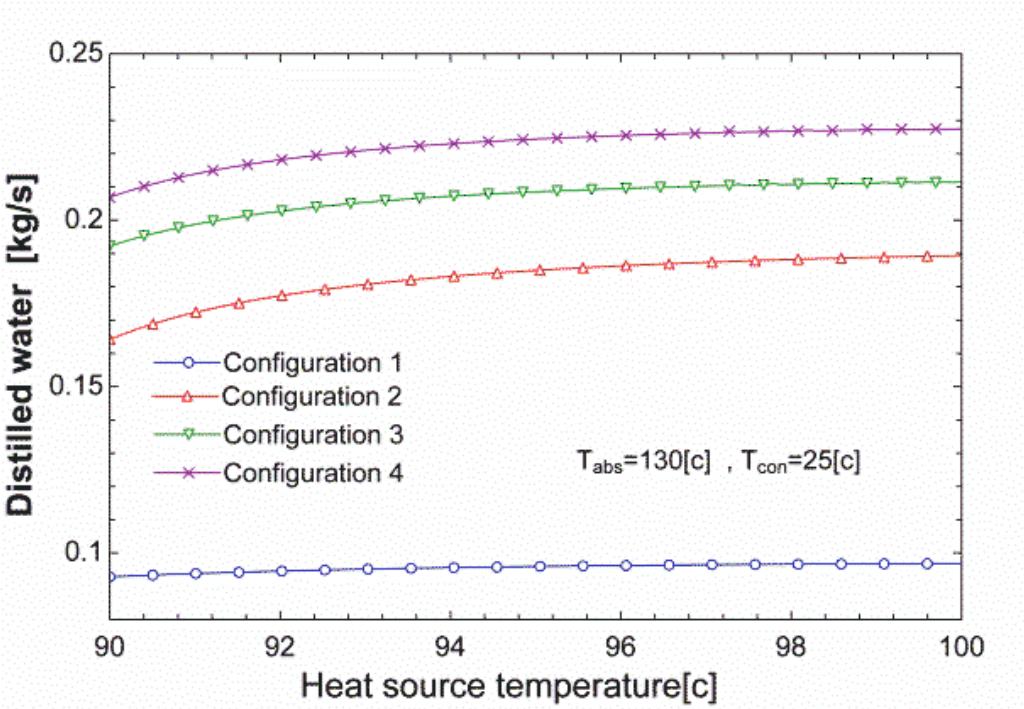

Figure 4. 10. Effect of heat source temperature on the magnitude of distilled water

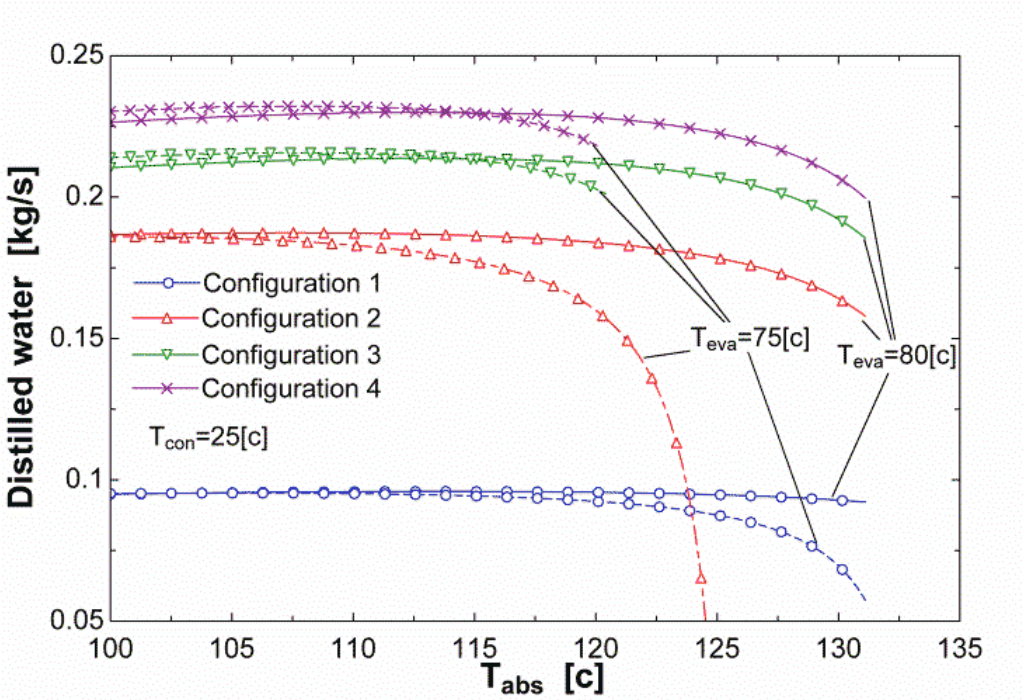

Figure 4. 11. Effects of absorber temperature on the magnitude of distilled water

The effect of the GTL on the COPs of different configurations were investigated as ΔT increased from 20 °C to 50 °C for T_{con}=25 ˚C and T_{eva}=80 ˚C (Fig. 4.12). It can be seen that the COP remains almost constant till the ΔT magnitudes of (38-40) °C and then decreases rapidly at ΔT higher than 40 °C. From equation ($\Delta T_G=T_{abs}- T_{eva}$) and considering that T_{eva}=80 °C, the absorber temperature varies in this plot from 100-130 °C which are the highest system temperatures, furthermore, from the first law of thermodynamics it is clear that the system has to reduce its efficiency as the absorber increases its temperature which is in agreement with the results available in the literature [26, 35].

The maximum COP levels are achieved with configuration 4 for T_{con}=25˚C and T_{eva}= 80˚C. The other configurations follow in the order of 3, 1 and 2.

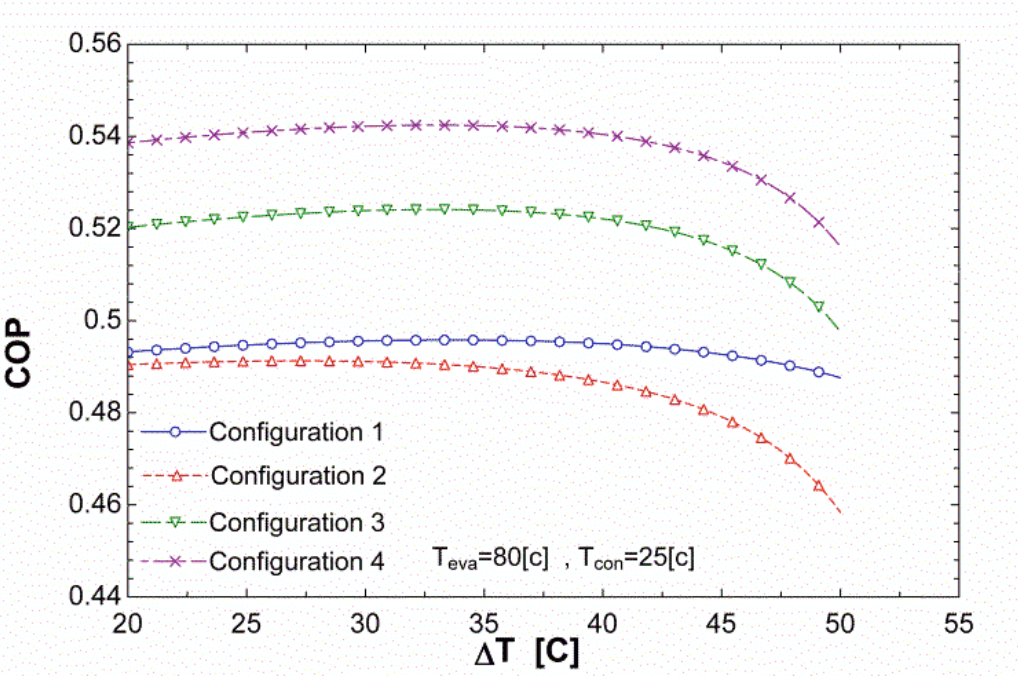

Figure 4. 12. Effect of Gross temperatures lift on COP for different configurations

Fig. 4.13 examines the COP trends against the recirculation flow ratio for different configurations and for the equal absorber and condenser temperatures of 130 ˚C and 25 ˚C. As it is seen, the COP decreases in all configurations as the recirculation flow ratio increases [36]. This is because when the evaporator temperature increases, the maximum system pressure will increase and the weak solution concentration will decrease by decreasing the flow ratio. The lower flow ratio results in a higher absorption heat capacity and a higher COP [1, 33]. Again the order of the COPs is similar to figure 4.9.

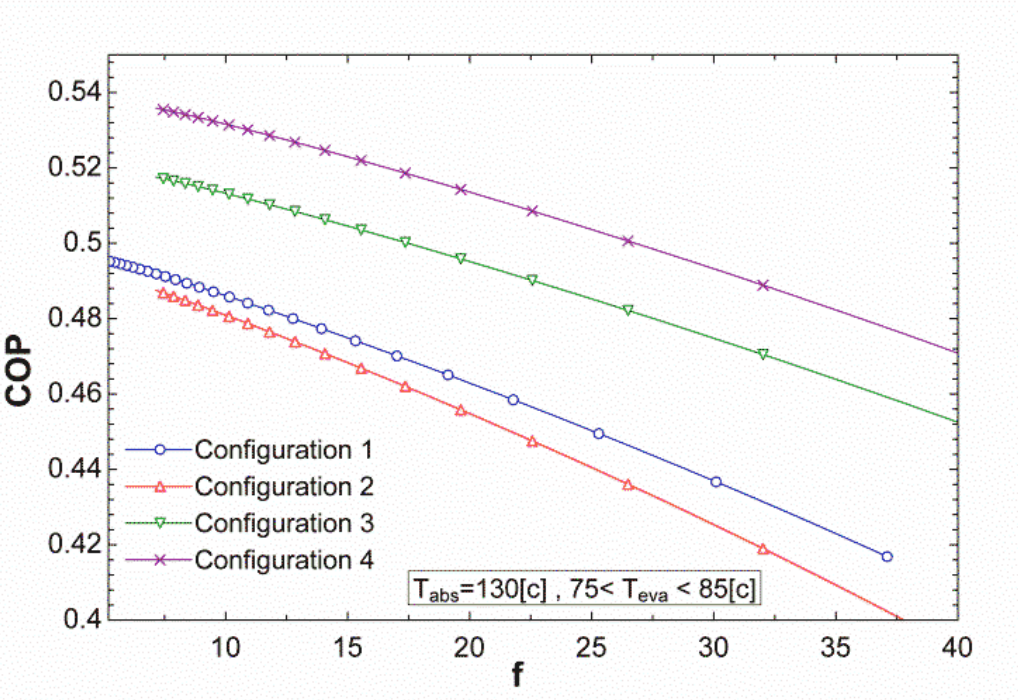

Figure 4. 13. Effect of flow ratio on COP for different configurations

4.3 Optimization

Using direct search method in the EES software, the amount of the distilled water produced by each configuration has been optimized with respect to the temperatures of the evaporator, absorber, condenser and generator. It was discovered that, the

optimized temperatures for the condenser and generator are unchanged for each case. The results are outlined in Tables 4.2-4.5. For all configurations the optimization was performed for five different values of T_{eva}, as mentioned above.

Table 4. 2. The results of optimization for maximum amount of distilled water in Configuration 1

T_eva(˚C)	COP	f	$\dot{m}_w$(kg/s)	T_abs(˚C)	T_con(˚C)	T_gen(˚C)	$\dot{Q}_u$(kW)	X_s	X_w
80	0.5024	3.475	0.09921	123.8	20	90	259.2	0.7289	0.566
82	0.5016	3.416	0.09882	125.6	20	90	258.2	0.7289	0.5639
84	0.5009	3.365	0.09844	127.5	20	90	257.2	0.7289	0.5619
86	0.5001	3.313	0.09806	129.3	20	90	256.2	0.7289	0.5599
88	0.4993	3.138	0.09768	130	20	90	255.2	0.7289	0.5528
90	0.4984	2.909	0.09728	130	20	90	254.2	0.7289	0.5425

Table 4. 3. The results of optimization for maximum amount of distilled water in Configuration 2

T_eva(˚C)	COP	f	$\dot{m}_w$(kg/s)	T_abs(˚C)	T_con(˚C)	T_gen(˚C)	$\dot{Q}_u$(kW)	X_s	X_w
80	0.4977	3.629	0.1933	117.3	20	80	505	0.6845	0.5366
82	0.4969	3.556	0.1925	119.1	20	80	503	0.6845	0.5342
84	0.4961	3.485	0.1917	120.9	20	80	501	0.6845	0.5319
86	0.4953	3.416	0.191	122.7	20	80	499	0.6845	0.5295
88	0.4944	3.35	0.1902	124.4	20	80	497	0.6845	0.5271
90	0.4936	3.285	0.1895	126.2	20	80	495.1	0.6845	0.5247

Table 4. 4 The results of optimization for maximum amount of distilled water in Configuration 3

T_eva(˚C)	COP	f	$\dot{m}_w$(kg/s)	T_abs(˚C)	T_con(˚C)	T_gen(˚C)	$\dot{Q}_u$(kW)	X_s	X_w
80	0.5364	12.44	0.226	122	35	80	589.6	0.6028	0.5579
82	0.5321	8.52	0.2218	120.2	35	80	579.1	0.6028	0.5395
84	0.5287	6.861	0.2188	119.7	35	80	570.8	0.6028	0.5261
86	0.5258	5.899	0.2161	119.8	35	80	563.7	0.6028	0.5154
88	0.5232	5.056	0.2137	119.7	34.94	80	557.4	0.6031	0.5035
90	0.5207	4.764	0.2115	121.1	34.76	80	551.6	0.6041	0.4993

Table 4. 5.The results of optimization for maximum amount of distilled water in Configuration 4

T_eva(˚C)	COP	f	$\dot{m}_w$(kg/s)	T_abs(˚C)	T_con(˚C)	T_gen(˚C)	$\dot{Q}_u$(kW)	X_s	X_w
80	0.5549	12.48	0.2435	122	35	80	635.4	0.6028	0.5581
82	0.5506	8.525	0.2391	120.2	35	80	624	0.6028	0.5395
84	0.5472	6.804	0.2356	119.6	34.98	80	614.9	0.6029	0.5256
86	0.5444	5.823	0.2327	119.6	35	80	607.3	0.6028	0.5144
88	0.5417	5.047	0.2302	119.7	34.91	80	600.4	0.6033	0.5035
90	0.5394	4.696	0.2279	120.7	35	80	594.4	0.6028	0.497

In all cases the highest COP and the maximum production of pure water are obtained at T_{eva}=80˚c. Configuration 4 displays the best performance, then configuration 3, 1 and 2 follow in descending order. The optimized COP of configuration 4 is 0.5549, allowing a production rate of 0.2435 kg/s, which is almost 2.5 times better than that of configuration 1. As T_{eva} increases, this ratio decreases. It is noticed that as T_{eva} increases all the other quantities (except T_{con}, T_{gen} and $X_{s,}$ which tends to stay

unchanged) are decreased and T_{abs} increased. As the evaporator temperature increases, so does the maximum pressure of the system, which causes a decrease in the weak solution concentration. The weaker solution concentration results in the lower flow ratio [1]. Since generator temperature is constant in optimal conditions and strong solution concentration is a function of T_{gen} therefore, the strong solution concentration will remain fixed under the optimization conditions.

Jradi et al. [28] indicated that 10 L of fresh water per day is adequate for a typical residential use. Therefore, assuming that configuration 4 operates non-stop, it will be able to produce enough water for 2100 residential units.

4.4 Final Remarks

An analysis and optimization of four different configurations integrated in to desalination system were presented in this study. A thermodynamic model was developed by applying the energy analyses for each system components. Furthermore, an optimization was performed using the EES software regarding the quantity of distilled water rate. The model was verified through comparison between results obtained from current model and those available in the literature for similar operating conditions. Based on the analysis and optimization results, following conclusions are drawn:

- Configuration 4 has the maximum COP value which is 13-14 % more than the COP of configuration 2 which has the lowest value amongst the four configurations.
- The lower the condensing temperature is, the higher the COP or available temperatures lift will be.

- The higher the generation or evaporation temperature is, the higher the absorption temperature and corresponding gross temperature achieved.
- Crystallization possibility within configuration 1 is higher than other configurations.
- Configuration 1 has the highest flow rate ratio among all the configurations.
- As heat source temperature is raised, the utilized heat for desalination purpose, the COP of the AHT and the pure water production rate are decreased.
- The order of utilized heat capacity and hence the pure water production rate's order for different configurations are: configuration 4 > configuration 3 > configuration 2 > configuration 1.
- Distilled mass flow rate increases with the increase in the COP.
- The maximum pure water rate of 0.2435 kg/s was obtained in the last configuration.

Chapter 5

ABSORPTION HEAT TRANSFORMER CONFIGURATIONS INTEGRATED WITH A NOVEL COGENERATION CYCLE USING SUPERCRITICAL CARBON DIOXIDE AS WORKING FLUID

The supercritical carbon dioxide (S-CO_2) power cycle has emerged as a promising alternative for producing higher efficiency due to its simplicity, compactness, sustainability, enriched safety and superior economy. The S-CO_2 cycle has also various advantages over helium and water based power cycles. With growing interest in renewable energy sources, cycles with high efficiency are critical for achieving cost-parity with non-renewable sources. Recently S-CO_2 cycles are not only integrated with solar-thermal technologies [37], but also they are combined with nuclear [25, 38] and geothermal application [39]. The turbo-machinery used in the S-CO_2 cycle is more compact than that of conventional cycles due to the higher density of CO2. Over the past decade, there has been a significant amount of researches conducted on S-CO_2 power cycles and the heat transfer associated with its components [40-45]. In the recompression S-CO_2 cycle, circulating CO_2, which has to be compressed in two successive stages, cools the reactor core. For thermodynamic reasons, these compression stages require pre-cooling of the CO2 to about 32^{O}C through using a pre- cooler. Approximately 50% of the input energy is inevitably rejected through pre-cooler exchangers into the heat sink [38, 46-48]. The temperature of the working fluid entering the pre-cooler is typically in the range of 130-190^{O}C [38, 46, 48] which makes it an usable energy source in transcritical CO2 cycles [49-52].

Recently, Yari et.al made some efforts [53-55] to recover this thermal energy in S-CO2 and He-Brayton cycles. In Ref. [53] they utilized this waste heat energy to produce power through the transcritical CO2 power cycle to enhance the performance of the cycle. In that work, the recompression S-CO2 cycle was designed without using inter-cooling and reheating sections and the waste heat generated from the pre-cooler was utilized in a transcritical CO2 power cycle.

It was shown that both the first and second law efficiencies of the proposed S-CO2 cycle were 5.5 to 26 % higher than that of the simple S-CO2 cycle. On the other hand exergy destruction for the proposed S-CO2 cycle was also about 6.7-28.8% lower than that of the simple S-CO2 cycle. The study also showed that no more than half of the lost thermal energy in the bottoming cycle is recoverable. This thermal energy is rejected to the environment in the pre-cooler 2. The inlet temperature of the CO2 in the pre-cooler 2, depending on the design and operating conditions, could vary between 75 and 80^{O}C. This temperature range could be desirable for a LiBr/H2O absorption heat transformer (AHT) in the desalination applications [10, 22, 23, 29, 35, 56, 57].

In the subsequent work they utilized this available heat in AHT where a desalination system was coupled to it [25]. They found that not only the energy and exergy efficiencies of the new S-CO2 cycle were higher than that of the simple S-CO2 cycle, but also a maximum pure water flow production of 3.317 kg/s was obtained under the analyzed conditions for the new S-CO2 cycle. Recently Horuz and Kurt [1] introduced four different configurations of AHTs and showed that their performances can be modified. The objective of the present chapter is to examine in detail the

performance of alternative AHT configurations introduced by Horuz [1], coupled with cogeneration cycle investigated by Yari [25].

A thorough and comprehensive thermodynamics analysis and efficiency assessment of the proposed configurations are performed. In order to identify the effects of some parameters such as; main compressor inlet temperature, compressor pressure ratio, heat source temperature of AHT and flow ratio, concentration of weak and strong solutions on the cogeneration cycle performance and the quantity of distilled water, a parametric study is carried out and validated with the experimental data available in the literature. Furthermore the whole cycle is optimized thermodynamically using the EES software [58].

5.1 Alternative Configurations Of AHTs Integrated To The Cogeneration Cycle

Figs. 5.1 (a-d) displays four different configurations of a combined heat and power cycle that incorporates a S-CO2 Brayton Cycle, a transcritical CO2 Cycle and an absorption heat transformer which is integrated to a single-effect evaporation desalination system. A high temperature reactor is used as a thermal reservoir to supply the heat input into the combined cycle.

As can be seen from the figures, starting with the Brayton cycle, in the main compressor (process 1-2) a fraction of the fluid flow (CO2) is compressed to high pressure. In the low temperature recuperator (LTR) fluid is pre-heated to the recompressing compressor outlet temperature (process 2-3). Then, the fluid flow is merged with the rest of the fluid flow from the recompressing compressor (point 3). The entire fluid flow is further heated in the high temperature recuperator (HTR) up

to the reactor core inlet temperature (process 3-4). The fluid leaves the reactor core at the highest cycle temperature (T_{max}). At this temperature, it enters turbine-1, where fluid expansion (process 5-6) generates rotational energy, which is converted into electricity in the generator. After leaving the turbine, the high temperature fluid is cooled in the high and low temperature recuperators (processes 6-7 and 7-8, respectively), where the available heat is transferred to the cooler high pressure side fluid flow. The fluid flow is split before entering the pre-cooler (point 8) in which one part is recompressed to high pressure (process 8-3) and the other cooled in the pre-cooler 1 to the temperature of T_{13} (process 8-13). Subsequently, the fluid flow is further cooled in the AHT and pre-cooler 2 to the main compressor inlet temperature i.e., T_1 (process 13-1).

The processes of the transcritical CO2 which takes place in the Rankine cycle are as follows: a constant-pressure heat absorption in the pre-cooler 1 (process 10-11), a non-isentropic expansion process in turbine 2 (process 11-12) leading to electricity production, a constant-pressure heat rejection process in the condenser (process 12-9), and a non-isentropic compression process in the pump (process 9-10).

The AHT system mainly consists of a generator, an absorber, a condenser, an evaporator; two pumps, an expansion valve and a heat exchanger. In this system heat is transferred to the working fluid ($LiBr/H_2O$) in the evaporator and the generator from the output flow of pre-cooler 1. The system rejects heat from the absorber and condenser. The rejected heat in the absorber is utilized to provide the required energy in the desalination system. The sequence of processes in the $LiBr/H_2O$ absorption heat transformer (AHT) is as follows: the weak $LiBr/H_2O$ solution (with lower concentration of LiBr) from the absorber goes to the generator via the solution heat

exchanger and the expansion valve respectively. Superheated water vapor comes out of the generator and then enters the condenser where it is condensed to the saturated liquid. Water pressure is then raised to that of the evaporator by the pump. In the evaporator, the water is heated by the waste heat until it becomes saturated vapor. This vapor is then absorbed in the absorber by the strong $LiBr/H_2O$ solution, which comes from the generator (state 23).

The heat of absorption released in the absorber is in the temperature range of 100–130 °C. This upgraded energy now can be used in the water purification systems as Fig. 5.1 (a) suggests. The water purification system receives its required thermal energy from the absorber of the AHT system. The impure water is heated in the absorber where it is partially evaporated. The two phase flow enters the separator vessel where it is separated into liquid and vapor. The liquid water mixes with the entering impure water before returning to the suction pump.

As can be seen from Fig. 5.1 (a), when a basic AHT is used, output flow from the pre-cooler 1 is supplied both to the generator and the evaporator. The system shown in Fig. 5.1 (b) has such a configuration that the hot flow from pre-cooler 1 is initially directed to the evaporator and then to the generator. In the third system (see Fig. 5.1 c), an absorber heat exchanger is included instead of the solution heat exchanger, which was used in configuration 2. Finally, the last system incorporates the second and the third system with the addition of a refrigerant heat exchanger at the evaporator inlet as can be seen in Fig. 5.1 (d).

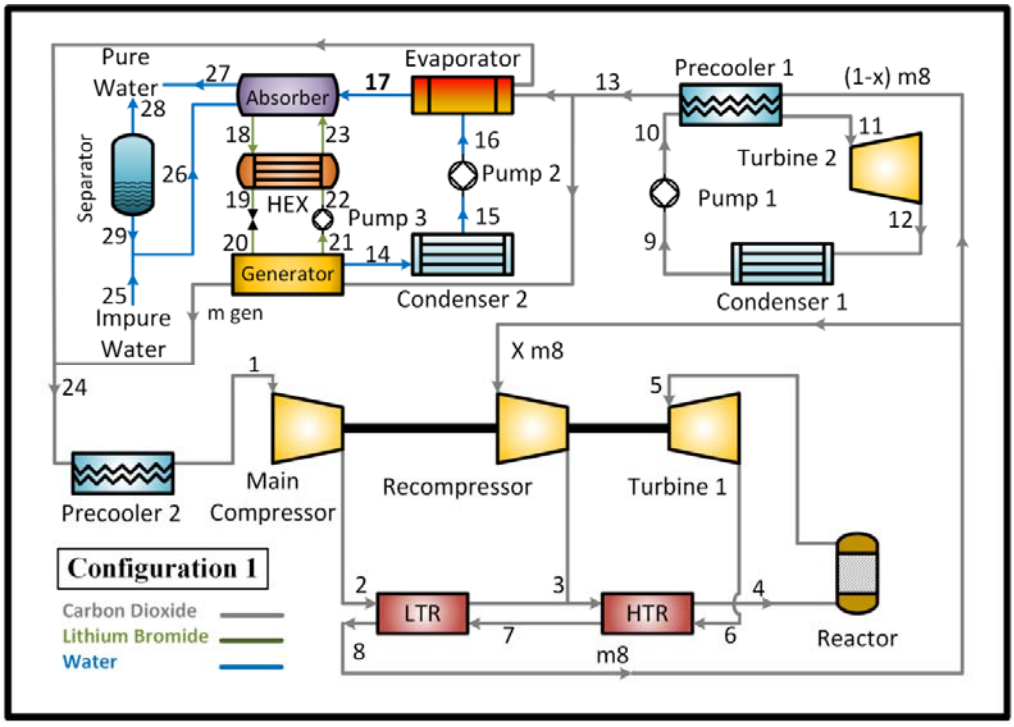

Figure 5.1 1.Schematic diagram of the cogeneration cycles coupled to AHT and desalination system (Configuration 1)

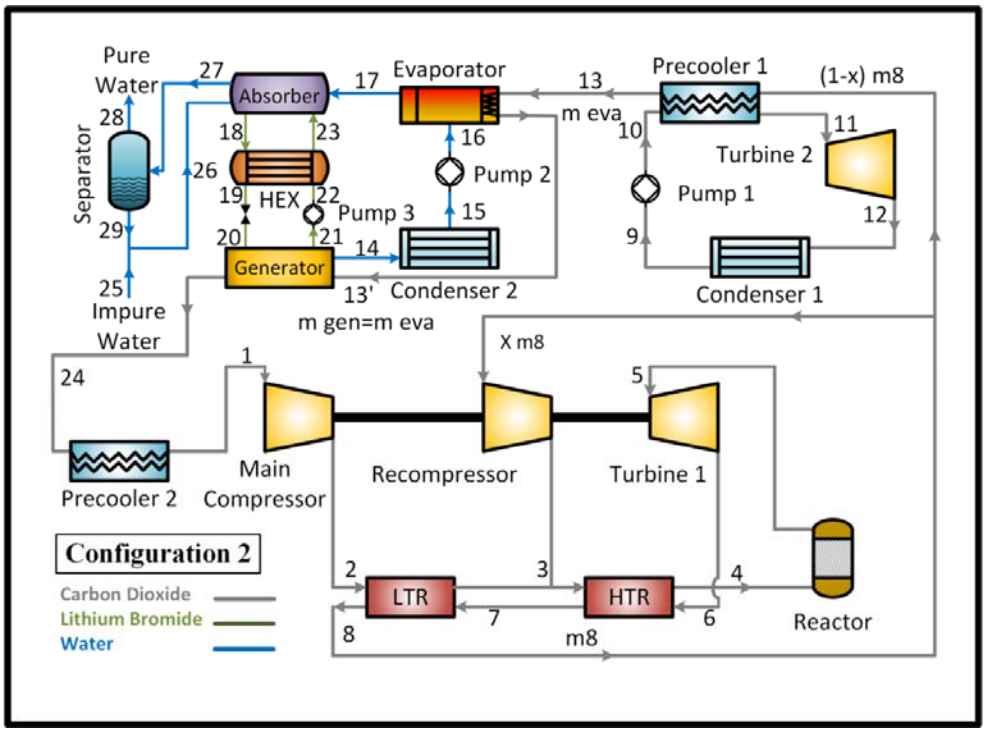

Figure 5.1 2.Schematic diagram of the cogeneration cycles coupled to AHT and desalination system (Configuration 2)

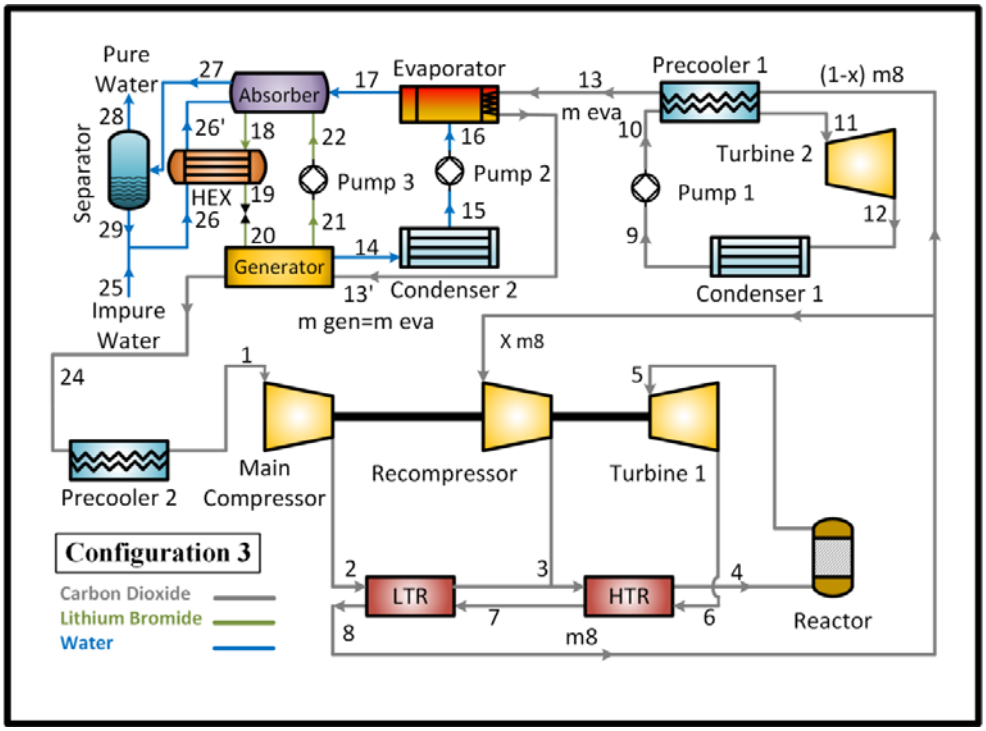

Figure 5.1 3. Schematic diagram of the cogeneration cycles coupled to AHT and desalination system (Configuration 3)

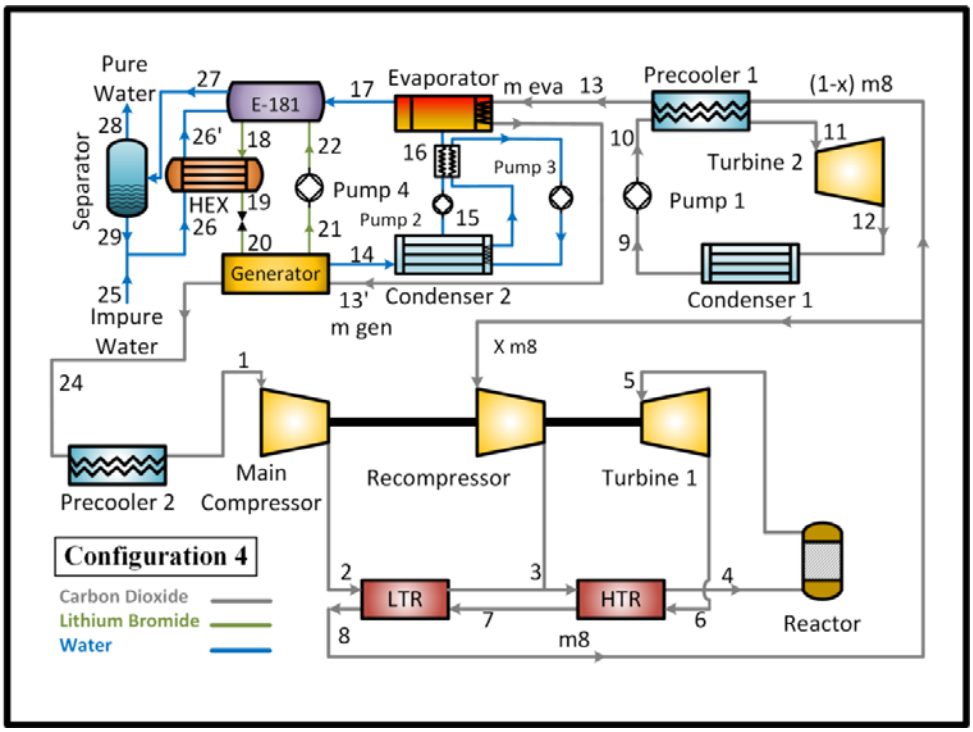

Figure 5.1 4. Schematic diagram of the cogeneration cycles coupled to AHT and desalination system (Configuration 4)

5.2 Thermodynamic Analysis

This section describes the thermodynamic model used for the simulation of the four different configurations of the cogeneration cycle. Each component of the considered system has been treated as a control volume and the principles of mass, energy and exergy balances are applied to them. EES software is used for solving the equations. The equations outlined in table. 5.1 are for the first configuration [23, 25, 52, 53].

In configurations of 2, 3 and 4 added elements have been considered in the calculations.

Table 5. 1. Energy and exergy relations for the studied cogeneration cycles

Subsystems	Energy relations	Exergy relations
Main compressor	$\eta_c = \frac{h_{2s}-h_1}{h_2-h_1}$, $w_{mc} = m_1(h_2 - h_1)$ $m_1 = (1-x)m_8$	$E_{D,mc} = m_1 T_o(S_2 - S_1)$
Pre-cooler 2	$Q_{pc2} = m_1(h_8 - h_1)$	$E_{D,pc2} = m_1 T_o(h_8 - h_1 - T_o(S_8 - S_1))$
Recompression compressor	$\eta_c = (h_{3s} - h_8)/(h_3 - h_8)$ $W_{rc} = m_3(h_3 - h_8)$ $m_3 = xm_8$	$E_{D,rc} = m_3 T_o(S_3 - S_8)$
LTR	$m_2(h_3 - h_2) = m_7(h_7 - h_8)$ $\varepsilon_{LTR} = (T_7 - T_8)/(T_7 - T_2)$	$E_{D,LTR} = m_7 T_o(S_8 - S_7 - (1-x)(S_3 - S_2))$
HTR	$m_4(h_4 - h_3) = m_6(h_6 - h_7)$ $\varepsilon_{HTR} = (T_6 - T_7)/(T_6 - T_3)$	$E_{D,HTR} = m_4 T_o(S_7 + S_4 - S_3 - S_6)$
Turbine 1	$\eta_c = (h_5 - h_6)/(h_5 - h_{6s})$ $W_{T1} = m_5(h_5 - h_6)$	$E_{D,T1} = m_5 T_o(S_3 - S_5)$

Reactor core	$Q_{core} = m_4(h_5 - h_4)$	$Q_{core}\left(1 - \frac{T_o}{T_r}\right) + E_4 = E_5 + E_{D,core}$
Pump 1	$\eta_p = V_9(P_{10} - P_9)/(h_{10} - h_9)$ $W_p = V_9(h_{10} - h_9)$	$E_{D,p1} = m_9 T_o(S_{10} - S_9)$
Pre-cooler 1	$m_9(h_{11} - h_{10}) = m_1(h_8 - h_{13})$	$E_{D,pc1} = T_o(m_8(S_{13} - S_8) + m_{10}(S_{11} - S_{10})$
Turbine 2	$\eta_{T2} = (h_{11} - P_{12})/(h_{11} - h_{12s})$ $W_{T,2} = m_{10}(h_{11} - h_{12})$	$E_{D,T2} = m_{10} T_o(S_{12} - S_{11})$
Condenser 1	$Q_{cond} = m_9(h_{12} - h_9)$	$E_{D,cond} = m_9(h_{12} - h_9 - T_o(S_{12} - S_9)$
Absorber	$m_{26}(h_{27} - h_{26}) = m_{18}h_{18} - m_{17}h_{17}$ $- m_{23}h_{23}$	$E_{D,a} = T_o(m_{18}S_{18} + m_{27}S_{27} - m_{17}S_{17}$ $- m_{23}S_{23} - m_{26}S_{26})$
Condenser 2	$Q_{cond,2} = m_{14}(h_{14} - h_{15})$	$E_{D,cond,2} = m_{14}(h_{14} - h_{15} - T_o(S_{14} - S_{15}))$
Evaporator	$m_{eva}(h_{13} - h_{24}) = m_{16}(h_{17} - h_{16})$	$E_{D,eva} = T_o(m_{17}S_{17} + m_{eva}S_{24} - m_{16}S_{16}$ $- m_{eva}S_{13})$
Expansion valve	$h_{19} = h_{20}$	$E_{D,ExV} = T_o m_{19}(S_{20} - S_{19})$
Geneartor	$m_{gen}(h_{13} - h_{24}) = m_{14}h_{14} + m_{21}h_{21}$ $- m_{20}h_{20}$	$E_{D,gen} = T_o(m_{14}S_{14} + m_{21}S_{21} + m_{gen}S_{24}$ $- m_{20}S_{20} - m_{gen}S_{13})$
HeX	$m_{22}(h_{23} - h_{22}) = m_{18}(h_{18} - h_{19})$ $\varepsilon_{HeX} = (T_{23} - T_{22})/(T_{18} - T_{22})$	$E_{D,HeX} = T_o(m_{19}S_{19} + m_{23}S_{23} - m_{18}S_{18}$ $- m_{22})$
Pump 2	$\eta_p = V_{15}(P_{16} - P_{15})/(h_{16} - h_{15})$ $W_{p,2} = V_{15}(h_{16} - h_{15})$	$E_{D,p2} = m_{15} T_o(S_{16} - S_{15})$
Pump 3	$\eta_p = V_{21}(P_{22} - P_{21})/(h_{22} - h_{21})$ $W_{p,3} = V_{21}(h_{22} - h_{21})$	$E_{D,p3} = m_{21} T_o(S_{22} - S_{21})$

5.3 Assumptions

The following assumptions are made in this study:

I. All the processes are assumed to be steady flow processes.

II. Changes in kinetic and potential energies are neglected.

III. The pressure losses due to the frictional effects in the connecting pipes are neglected.

IV. The turbines and the pumps have constant isentropic efficiencies [25, 53].

V. Some proper values of effectiveness are considered for the heat exchangers [25, 53, 59].

VI. The condenser outlet state is saturated liquid and its temperature is assumed to be higher than the environment temperature [25, 59].

VII. In the AHT, the solution at the generator and the absorber outlets, as well as the refrigerant at the condenser and the evaporator outlets are all at saturated states [1, 59].

VIII. The evaporator and the generator of the AHT work at the same temperature for configuration 1, since heat is supplied to them from the same source. This assumption is made by other researchers previously [1, 21-23, 27, 59]. Meanwhile in configurations 2, 3 and 4 temperature of the generator is less than that of the evaporator ($T_{gen} = T_{eva} - 7$ °C) [1, 59].

IX. Absorber heat is transferred to impure water as latent and sensible heat [33, 59].

X. The distilled water is salt free [33, 59].

Table 5.2 summarizes the basic assumptions and presents the input parameters used in the simulation according to the streams numbers shown in Figs 4.1(a-d).

Table 5. 2. The input data in the simulation

Parameters	value	Ref
P_o[kPa]	100	-
P_1 [kPa]	7400	[46]
PR[-]	1.5 – 5	[38]
T_o [^oC]	15	-
T_{11} [^oC]	T_8-10	[51]
T_{13} [^oC]	75 – 80	[35] and [60]
T_9 [^oC]= T_{15} [^oC]	T_o+5	[49], [51] and [52]
T_a [^oC]	105 – 120	[29, 56, 57] and [10]
T_g=T_{ev} [^oC] ; (Configuration 1)	T_{24}-3	[22] and [23]
T_g [^oC] ; (Configurations 2,3 and 4)	T_{ev}-7	[59] and [1]
T_{24} [^oC]	T_{13}-5	[22] and [23]
T_{max} [^oC]	550 – 750	[38], [47] and [48]
T_1 [^oC]	35 – 50	[38], [47] and [48]
T_r [^oC]	800	[38], [47] and [48]
η_c[%]	85	[47] and [48]
η_p[%]	80	[49] and [52]
η_{T1}[%]	90	[49] and [52]
η_{T2}[%]	80	[49] and [52]
ε_{LTR}=ε_{HTR} [%]	86	[47] and [48]
ε_{HEX} [%]	70	[22] and [23]
Q_{core} [MW]	600	-

5.3 Performance Evaluation

The first-law efficiencies of the cogeneration cycles may be expressed as: [53, 61, 62]

$$\eta_I = \frac{W_{net}+m_{13}(h_{13}-h_{24})}{Q_{core}} = \frac{W_{net}+m_{13}(h_{13}-h_{24})}{m_4(h_5-h_4)} \quad \textbf{(5.1)}$$

where,

$$W_{net} = W_{net,1} + W_{net,2} - (W_{p2} + W_{p3}) = (W_{T1} - W_{mc} - W_{rc}) + (W_{T2} - W_{p1}) - (W_{p2} + W_{p3}) \quad \textbf{(5.2)}$$

Using the exergy released in the reactor core as the input to the plant, the second-law efficiency of the recompression S-CO2 cogeneration cycle can be defined as: [51, 53, 61]

$$\eta_{II} = \frac{W_{net}+E_T}{E_{in}} = \frac{W_{net}+m_{13}((h_{13}-h_{24})-T_o(S_{13}-S_{24})}{m_4(h_5-h_4)} \quad \textbf{(5.3)}$$

The total exergy destruction in the basic cogeneration cycle is as follows:

$$E_D = E_{D,mc} + E_{D,rc} + E_{D,pc2} + E_{D,HTR} + E_{D,LTR} + E_{D,T1} + E_{D,core} + E_{D,p1} + E_{D,pc1} + E_{D,T2} + E_{D,cond1} + E_{D,a} + E_{D,cond2} + E_{D,ev} + E_{D,exv} + E_{D,gen} + E_{D,HEX} + E_{D,p2} + E_{D,pc3} \quad \textbf{(5.4)}$$

It should be noted that in the cases of 2, 3 and 4 the exergy destruction rate of the added elements have been considered.

For an AHT system the coefficient of performance (COP) is a measure of the cycle's ability to upgrade the thermal energy given to the generator and the evaporator of the system. It is defined as follows: [1]

$$COP_{AHT} = \frac{Q_{abs}}{Q_{gen}+Q_{eva}} \quad \text{(Configuration 1 and 2)} \tag{5.5}$$

$$COP_{AHT} = \frac{Q_{abs}+Q_{abs-ex}}{Q_{gen}+Q_{eva}} \quad \text{(Configuration 3 and 4)} \tag{5.6}$$

The flow ratio (f) is an important design and optimization parameter in the AHT system. It is defined as the ratio of the strong solution mass flow rate; $\dot{m}_s$ to the refrigerant mass flow rate; $\dot{m}_r$:

$$f = \frac{m_s}{m_r} = \frac{m_{21}}{m_{14}} = \frac{x_{20}}{x_{21}-x_{20}} \tag{5.7}$$

where, x is the LiBr concentration in the solution. The heat capacities of the absorber and the generator as a function of flow ratio can be calculated by using the following equations [1]:

$$q_{abs} = \frac{Q_{abs}}{m_{17}} = (f+1)h_{18} - fh_{23} - h_{17} \tag{5.8}$$

$$q_{gen} = \frac{Q_{gen}}{m_{14}} = h_{14} + fh_{21} - (f+1)h_{20} \tag{5.9}$$

5.4 Optimization Method

The results obtained from the mathematical model reveal that the optimum performance of the cogeneration cycle depends on the following design/operating parameters:

I. Pressure ratio (PR)
II. Main compressor inlet temperature (T_1)
III. Outlet temperature of the pre-cooler 1 (T_{13})
IV. AHT's absorber temperature (T_a)
V. Turbine inlet temperature (T_{max})

Therefore the optimum value of the first and second law efficiencies of the cogeneration cycle can be expressed as a function of five design/operating parameters as presented in the following equation:

$$\text{Maximize } \eta_I(PR, T_1, T_{13}, T_a, T_{\max}) \quad \textbf{(5.10)}$$

Subject to: **(5.11)**

$$1.5 \leq \text{PR } [-] \leq 5$$

$$32 \leq T_1(^{o}C) \leq 5$$

$$75 \leq T_{13}(^{o}C) \leq 80$$

$$105 \leq T_{abs}(^{o}C) \leq 120$$

$$550 \leq T_{max}(^{o}C) \leq 750$$

Using direct search method and applying the constraints on each variable by setting the bounds, the performance of the whole cycle is optimized by the EES software from the viewpoint of first and second law efficiencies. The direct search method is based on a successive search intended to find an extremum by directly comparing function values at a sequence of trial points without involving derivatives. This method is deemed suitable for problems involving simulation-based optimization or optimizing non-numerical functions, as well as, in practice, problems involving non-smooth or discontinuous functions [28].

5.5 Model Validation

In order to validate the simulation results, the available data in literature were used. For the case of the absorption heat transformer, the thermodynamic model was validated using the previously published data [22, 23, 29, 35, 57, 60]. In the cases of supercritical transcritical CO2 and recompression S-CO2 cycles, the models were validated using the previously published data from [49, 50, 52, 61, 62] and [46-48],

respectively. All the comparisons between the obtained results and data available in the literature have been previously studied by Yari [25] and acceptable agreement is witnessed.

5.6 Results and discussion

The energy, mass flow rate, flow ratio, the heat lost in pre-coolers 1 and 2 and concentration values for four different configurations are compared for the same absorber and condenser temperatures in Table 4.3. As the table indicates, in configuration 4, heat lost in pre-cooler 2 is 10.83 % less than that of configuration 1. Meanwhile there is a huge increase in the quantity of distilled water.

Table 5. 3.The Comparison of input and calculated properties of different AHT configurations

	Unit	**Configuration 1**	**Configuration 2**	**Configuration**	**Configuration 4**
Absorber temperature(T_{abs})	˚C	110	110	110	110
Condenser temperature(T_{con})	˚C	20	20	20	20
Generator temperature(T_{gen})	˚C	67	60	60	60
Evaporator temperature(T_{eva})	˚C	67	67	67	67
Solution heat exchanger outlet temperature (T_{23})	˚C	97.1	95	-	-
Absorber heat exchanger outlet temperature ($T_{26'}$)	˚C	-	-	101.4	101.6
Evaporator heat exchanger outlet temperature ($T_{16'}$)	˚C	-	-	-	63
f (flow ratio)		11.09	29.62	29.62	29.62
COP_{AHT}		0.4759	0.399	0.6458	0.6686
m_r(Refrigerant flow rate)	kg/s	3.08	5.888	5.888	6.337

Weak solution concentration		0.5769	0.5769	0.5769	0.5769
Strong Solution concentration		0.6289	0.5964	0.5964	0.5964
$m_{distilled\ water}$(Distilled water produced)	kg/s	2.721	3.782	7.645	8.229
$Q_{pre\text{-}cooler\ 1}$	MW	190.036	190.036	190.036	190.036
$Q_{pre\text{-}cooler\ 2}$	MW	158.899	149.068	142.904	141.686
Q_{core}	MW	600	600	600	600
T_o=15 ^{0}C, T_{max}=550 ^{0}C,T_1=35 ^{0}C, PR=3.435,T_{13}=75 ^{0}C					

Fig.5.2 demonstrates the effects of main compressor and the turbine inlet temperatures on the first law efficiency of the proposed configurations. It is evident that as the main compressor inlet temperature increases, the thermal energy efficiency for all the configurations stays almost constant. This is due to the fact that as the main compressor inlet temperature of the S-CO2 cycle increases, the main compressor work increases due to increase in the inlet temperature and flow rate. On the other hand, turbine power generation decreases which leads to decrease in the cycle net power generation. Thus, a gain in cycle efficiency can be achieved by simply lowering the main compressor inlet temperature [46-48]. But in the case of the proposed configurations; the main compressor work increase is compensated by the increase of power generation in the second turbine.

As a result, any increase in the main compressor inlet temperature causes the energy efficiency to be constant. In fact, a smaller pre-cooler having a lower cost is required. Figure 5.2 also shows that the maximum energy efficiency for configuration 4 is 5.56-6.2% higher than that of configurations 1 and follows the order of configurations 4, 3, 2 and 1 under different turbine inlet and main compressor temperatures.

It should be also noted that the thermal efficiency of the proposed configurations will decreases by 8.3-9.5 % if the temperature of the turbine inlet decreases from 650°C to 550°C.

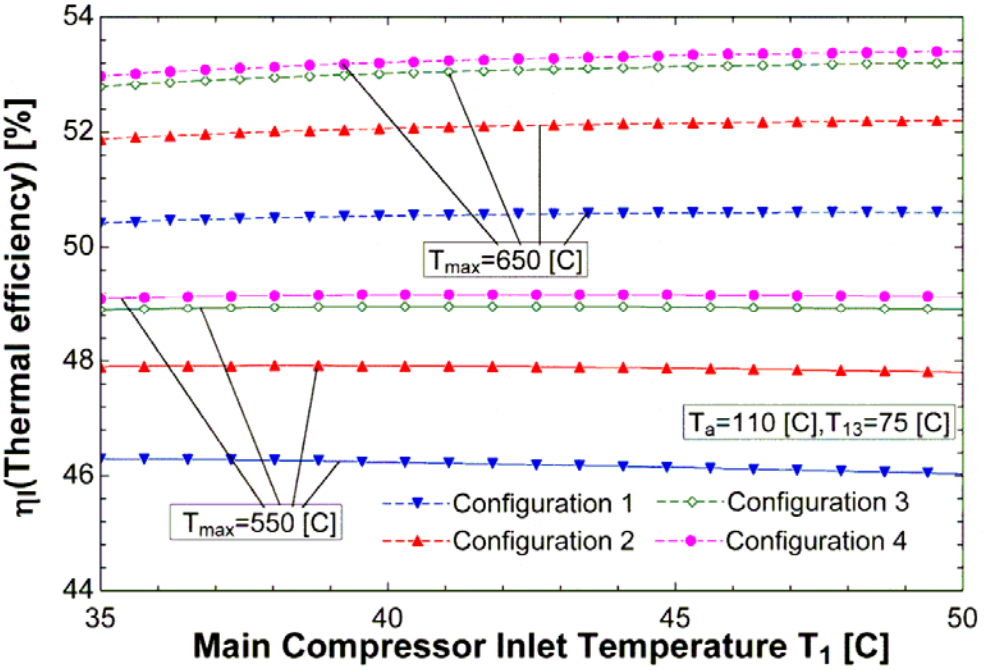

Figure 5. 1. Energy efficiency vs. main compressor inlet temperature under two different turbine inlet temperatures

The influence of the minimum cycle and turbine inlet temperatures on the exergy efficiencies is shown in Figure 5.3. The exergy efficiency for all the configurations is slightly increased as the minimum cycle temperature increases. It can be explained in the same manner as stated in Fig.5.2. Figure 5.3 exhibits that the configuration 1 has the highest exergy efficiency and configuration 2 possesses the lowest. This is completely in agreement with the results shown later in Fig.5.4. Another interesting point is that a decrease of 9.97-10.2% between the highest and lowest maximum exergy efficiency will occur if the AHT configurations are changed.

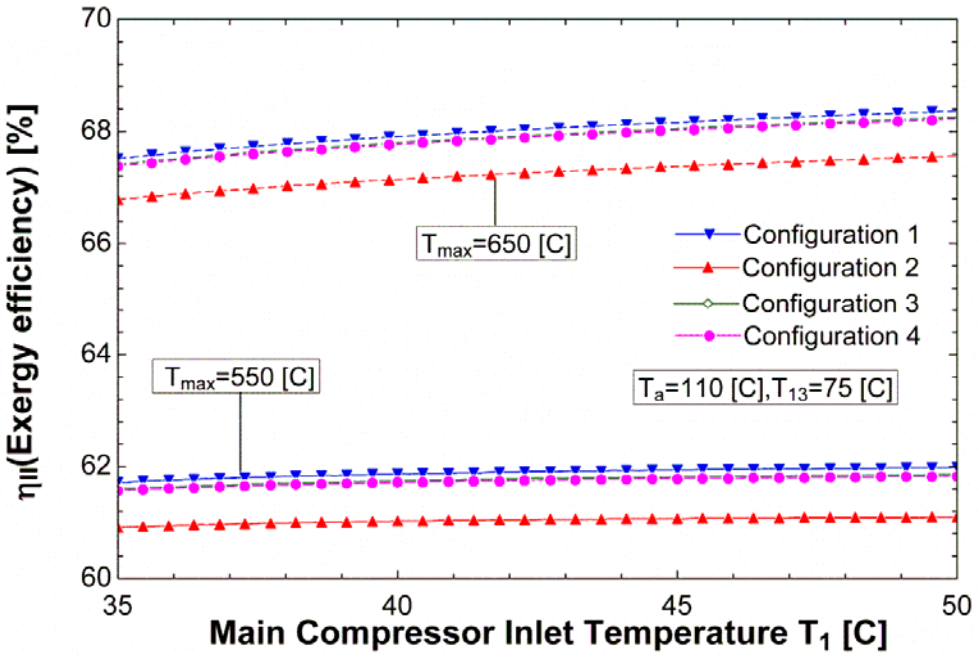

Figure 5. 2. Exergy efficiency vs. main compressor inlet temperature under two different turbine inlet temperatures

Fig. 5.4 depicts the variation of the exergy destruction of the proposed cycles vs. the main compressor inlet temperature under two different turbine inlet temperatures. As shown in Figure 5.4, the exergy destruction of the systems decrease by increasing the turbine inlet temperature as well as by decreasing the main compressor inlet temperature. This is because of decrease in the difference between the minimum and maximum temperatures. Configuration 2 possesses the highest exergy destruction which is the main reason for having the lowest exergy efficiency shown in Fig.5.3. Other configurations approximately have similar exergy destructions.

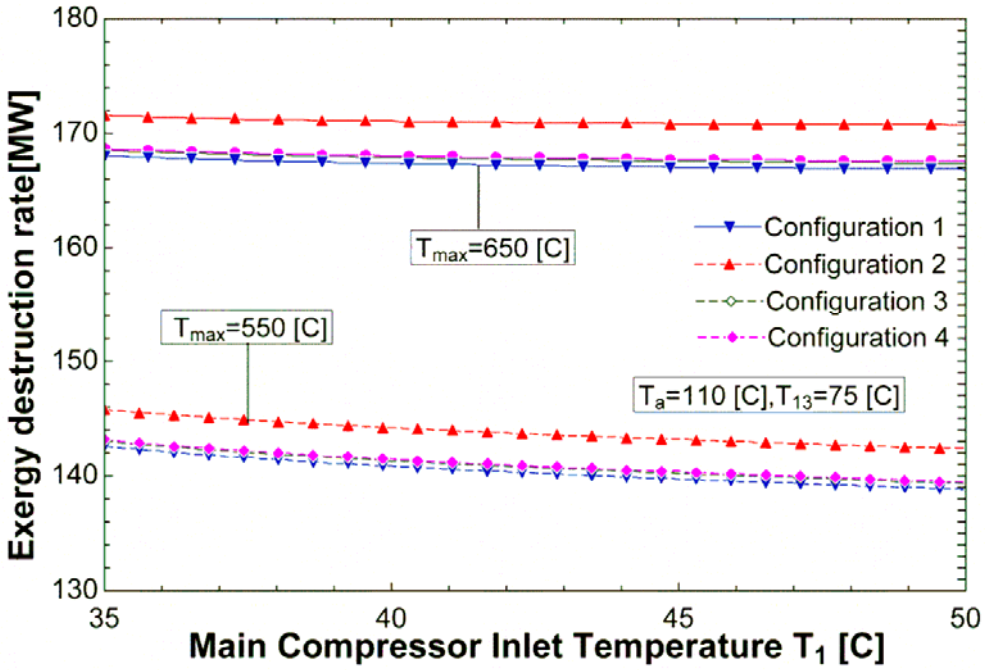

Figure 5. 3. Exergy destruction vs. main compressor inlet temperature under two different turbine inlet temperatures

Fig.5.5 shows the effect of compressor pressure ratio on the first and second law efficiencies of different configurations of combined cogeneration cycle (CC). This figure indicates higher thermal efficiency values for configuration 4 which is very close to configuration 3, compared to that of other configurations. However, the amount of efficiency enhancement is more pronounced at lower pressure ratios being maximum 18.84 %.

In comparison to the first law efficiency, a negligible influence on the second law efficiency of the CC cycles is detected from the figure when the configurations of AHT system is changed which is in agreement with the results from Fig.5.2. Fig. 5.5 also indicates that there are optimum values of pressure ratio at which the efficiencies are maximized.

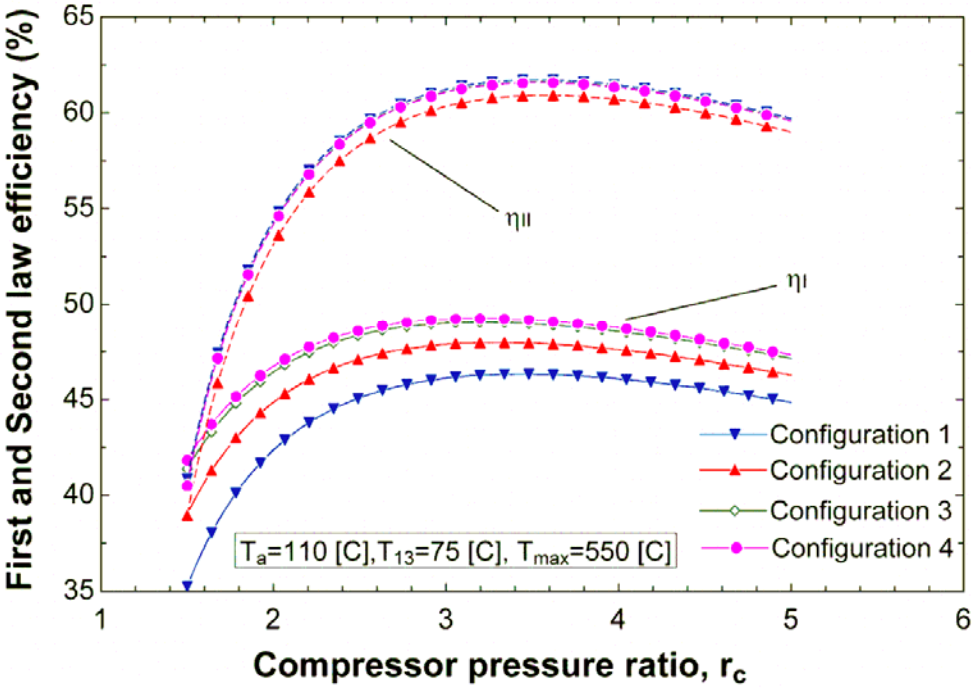

Figure 5. 4. Effect of compressor pressure ratio on the first and second law efficiencies of different configurations of CC cycle

The pure water production rates on behalf of four different configurations were investigated for T_{13}=75^{0}C, T_{max}=550, 650^{0}C and T_a=100-110^{0}C with respect to the main compressor inlet temperature as shown in Figs 5.5 (a-c). As seen, generally the pure water mass flow rate is increased either by increasing the main compressor inlet and absorber temperatures or by decreasing the turbine inlet temperature. The trends observed in these figues have been also reported in the literature [10, 23, 25]. The figures also reveal that a higher pure water production is achieved when the last configuration of AHT is utilized which is in coherence with the results reported in [59].

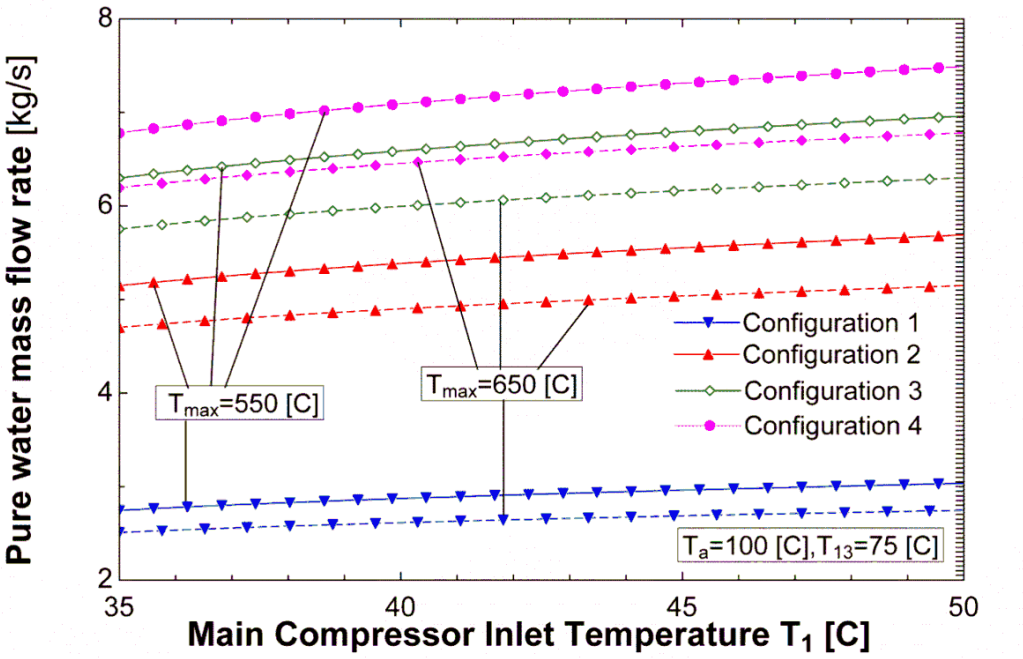

Figure 5. 5 a. T_a=100˚C

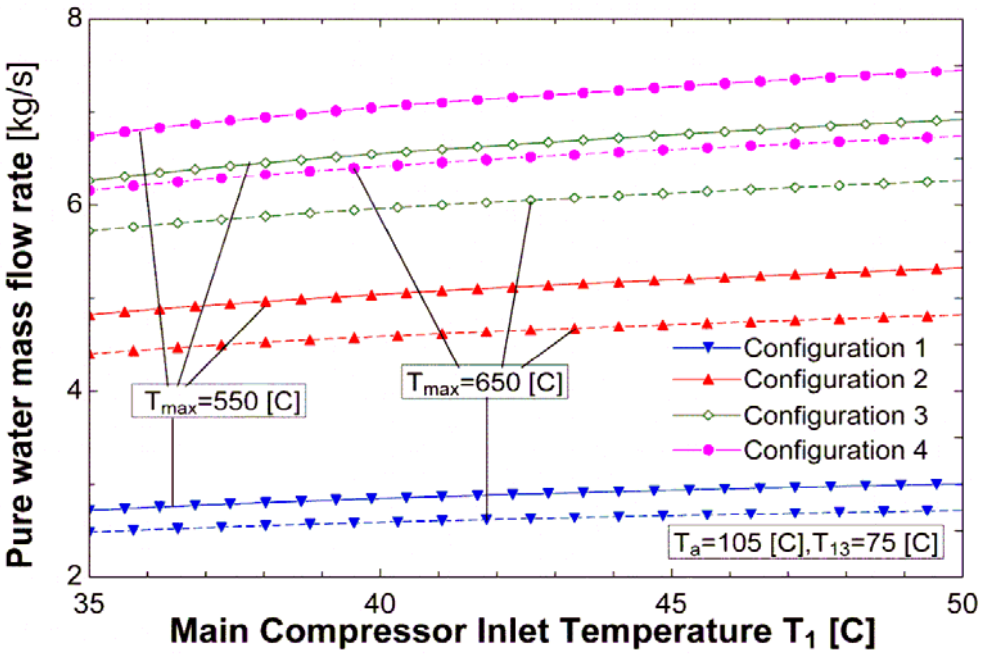

Figure 5. 5 b. Ta=105˚C

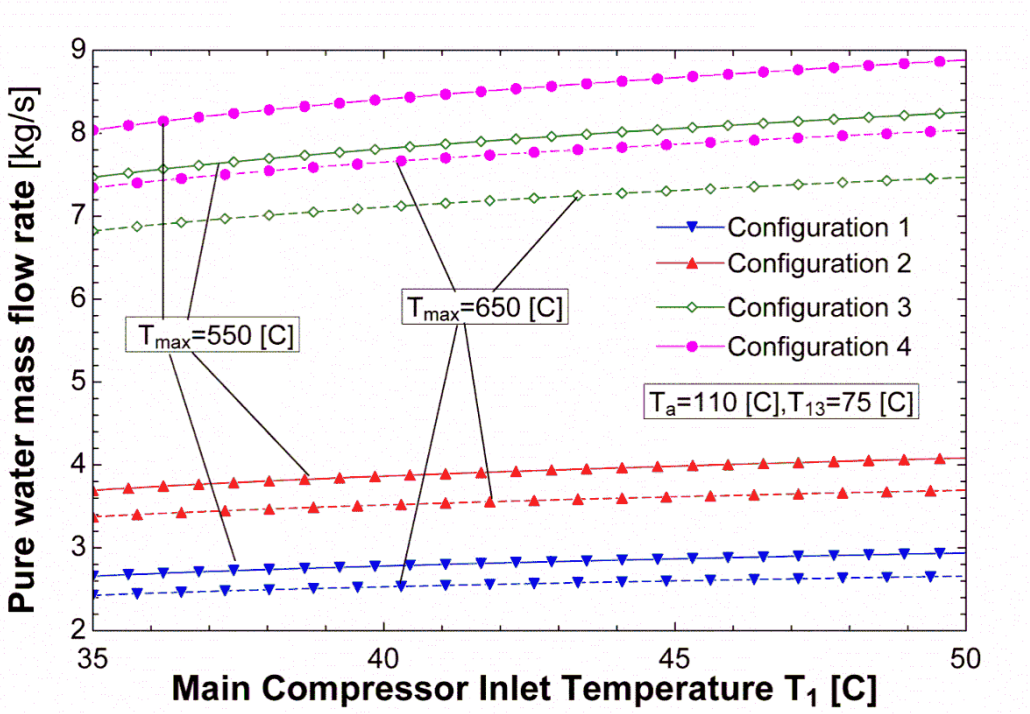

Figure 5. 5 c..Ta=110˚C

Figure 5. 5. Pure water production rate vs. main compressor inlet temperature under two different turbine inlet temperatures

The variation of the first and second law efficiencies of the CC cycle with the temperature of state point 13 which is essentially the heat source for the AHT is shown in Figs. 5.7 and 5.8. Fig.5.7 indicates that as T_{13} increases the efficiency decreases slightly. This is expected because, with increasing T_{13}, the temperature of S-CO_2 entering the main compressor, is increased.

The increase of the main compressor inlet temperature will result in higher power consumption and consequently a lower W_{net}. In addition, as the T_{13} increases, the heat recovery from recompression S-CO_2 cycle in the pre-cooler 1 of transcritical CO_2 cycle is decreased resulting in a lower power production in turbine 2. Therefore, according to the Eq. (1) the first law efficiency of the CC cycle decreases. Fig. 5.7 also reveals that as T_{max} is decreased by 100 °C, the CC cycle efficiency decreases by around 8-9%. The results obtained are in agreement with the results displayed in

Fig.5.2. The exergy efficiency has a similar behavior and it can be explained in the same manner as stated in Fig.5.7. From Fig.5.4 it is clear that the exergy destruction of configuration 2 is the highest and so it is reasonable to have the lowest exergy efficiency.

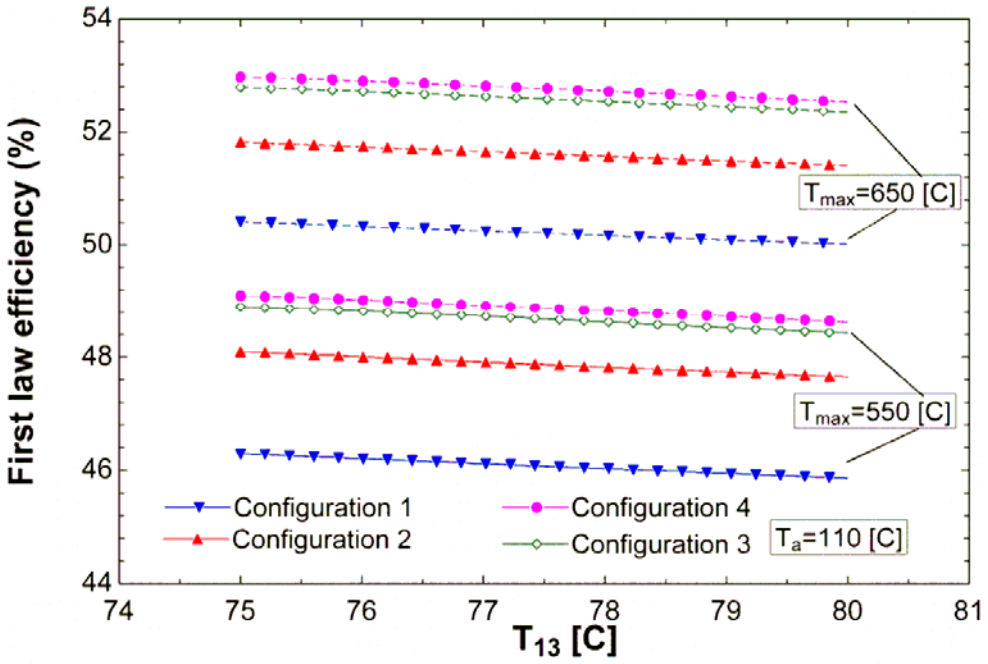

Figure 5. 6. Effect of T_{13} on the first law efficiency of the CC cycle

The effect T_{13} on the AHT performance and pure water production rate is shown in Fig. 5.5. It indicates that as T_{13} is raised, the COP of the AHT and the pure water production rate are increased. This is due to the fact that, increasing T_{13} results in an increase of the AHT evaporator temperature (and pressure) leading to a lower weak solution concentration and flow ratio. The lower flow ratio results in a higher absorption heat capacity and a higher COP [1, 33, 59]. Therefore the energy input to the desalination system increases causing a higher pure water production rate. Fig. 5.5 also indicate that the COP and pure water production follows the order of

configuration 4, 3, 1 and 2 which is in agreement with the results of Parham et.al [59].

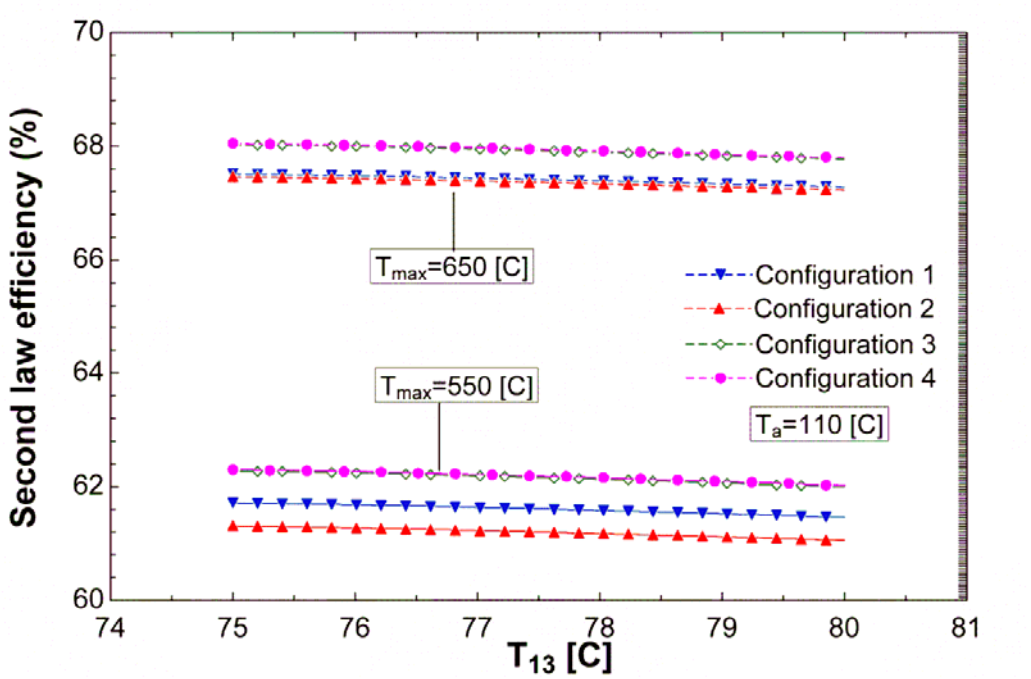

Figure 5. 7.. Effect of T13 on the second law efficiency of the CC cycle

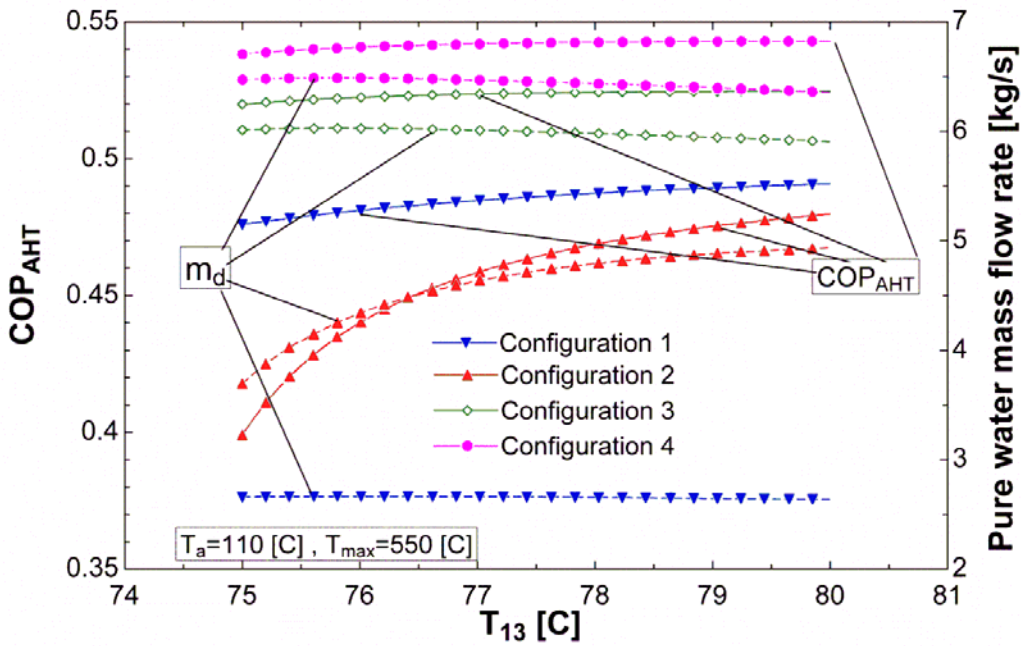

Figure 5. 8. Effect of T_{13} on COP and pure water production rate

The variations in the concentrations of strong and weak solutions are plotted against T_{13} in Fig. 5.10. The absorber will absorb more refrigerant vapor with higher concentrations of LiBr solutions leaving the generator. The strong and weak solutions are denoted by X_s and X_w respectively. When absorbing and condensing temperatures of the AHT are kept unchanged, the X_s increases with the T_{13}, but the weak solution does decrease with the T_{13}. The higher the heat source temperature is, the stronger the weak solution is. As shown in Fig. 5.9, X_s in configuration 1 is more than that of other configurations while X_w in all the configurations is the same. The higher X_s can cause crystallization problem of LiBr [1]. So it can be concluded that the possibility of crystallization within configuration 1 is higher than of other three configurations [59, 63].

As the concentration of the weak solution decreases with T_{13}, the concentration difference (ΔX) will increase linearly and the flow ratio (f) will exhibit a parabolic decrease as shown in Fig. 5.10. As mentioned earlier in [1, 59], when generation, evaporation, condensing and absorbing temperatures are constant, ΔX will only vary with f, which is an important and easily controllable operation parameter. Larger f also results in higher T_a and more mechanical power losses. Under the same operation conditions the f is in the order of configuration 1 < configurations 2, 3 and 4. According to the results reported in the literature, the larger the concentration difference is, the larger the driving force for mass transfer in the generator or the absorber [3, 64].

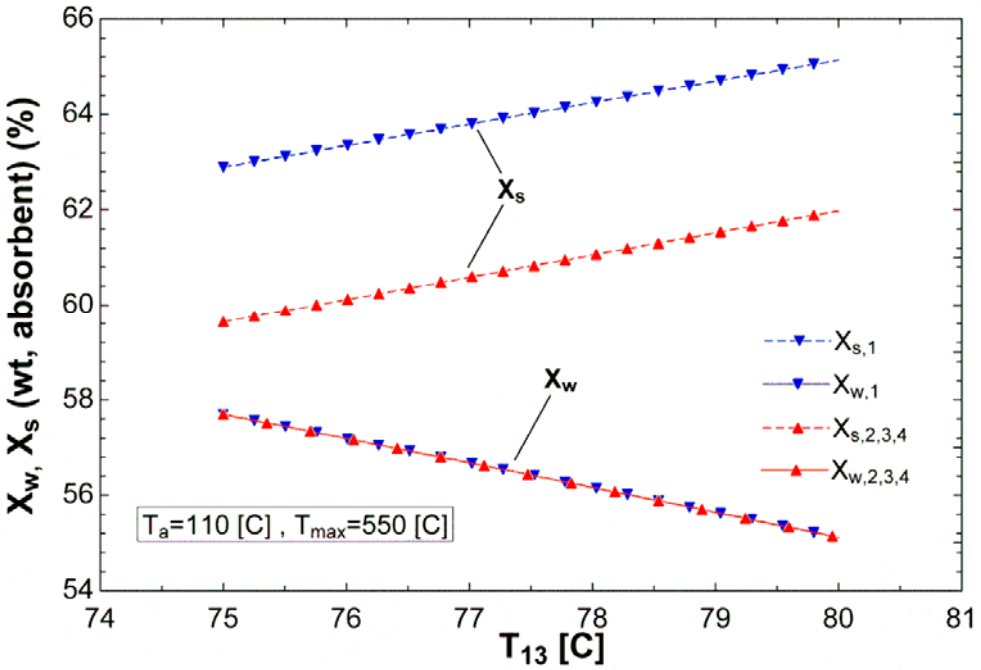

Figure 5. 9. Effect of T_{13} on Xs and Xw for different configurations

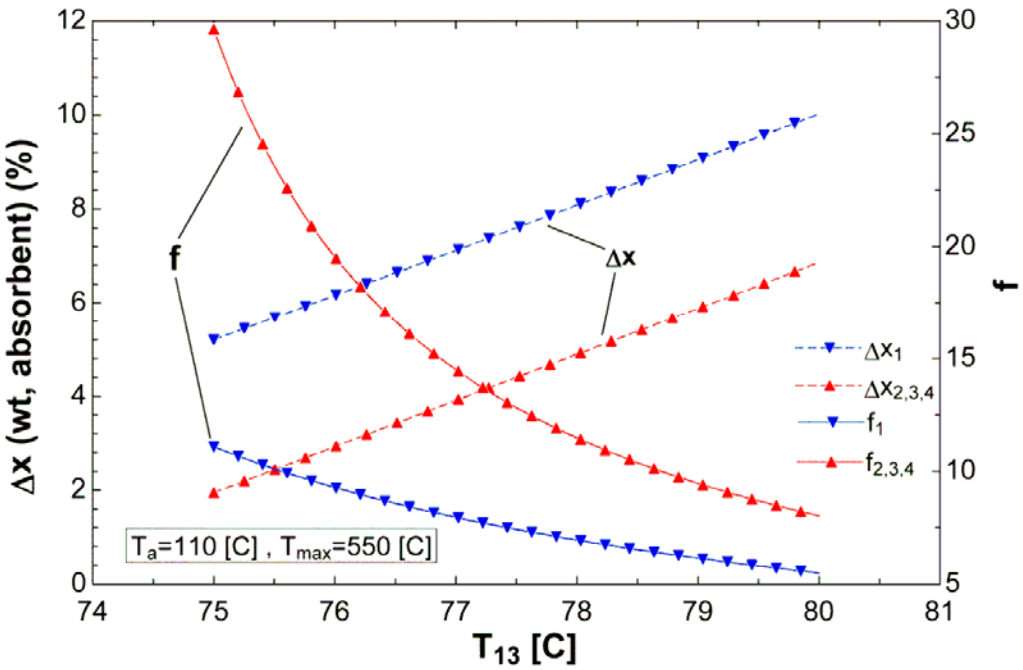

Figure 5. 10. Effect of T_{13} on ΔX and flow ratio for different configurations

Using direct search method in the EES software, both the first and second law efficiencies of the four configurations are optimized with respect to the main

compressor pressure ratio and inlet temperature, T_{13}, absorber temperature and turbine inlet temperature. The results are outlined in Tables 5.4–5.7. The optimization was performed for four main compressor inlet temperatures and five values of the maximum temperatures for any corresponding main compressor inlet temperature.

As the Tables indicate the optimum compressor pressure ratio for maximum first law efficiency is highest for the first configuration compared to that of others. Also, with increasing T_1, the first and second law efficiencies grow up as expected.

It should be noted that, as T_1 increases the enthalpy change of the S-CO_2 through the reactor core (Δh_{Core}) increases causing a decrease in the S-CO_2 mass flow rate across the reactor. Moreover, a decrease in the S-CO_2 mass flow rate will lead to a lower input energy to the AHT and desalination system. This lower input energy will in turn lead to a lower pure water production rate as Tables 5.4-5.7 indicate.

A comparison between Tables 5.4-5.7 reveals that when the configuration 4 is employed, the maximum first and second law efficiency and distilled water mass flow rate, are higher than that of other AHT configurations used and follows the order of configurations 4, 3, 2 and 1. On the other hand configuration 4 owns the lowest exergy destruction which is a chief advantage for it.

Table 5. 4.The results of optimization for maximum first law efficiency of the first configuration

T_1(°C)	T_{max}(°C)	T_{13}(°C)	T_a(°C)	Pr_{opt}	η_I(%)	η_{II}(%)	$\dot{m}_D$(kg/s)	E_D (kJ/kg)	COP_{AHT}
35	550	75.28	105.8	3.25	46.26	60.12	2.516	175	0.4809
	600	75.28	105.8	3.639	48.51	64.82	2.376	154.4	0.4809
	650	75.28	105.8	4.028	50.55	67.39	2.294	143.1	0.4809
	700	75.28	105.8	4.417	52.41	70.25	2.191	130.6	0.4809
	750	75.28	105.8	4.806	54.1	72.74	1.979	119.7	0.4809
40	550	75.28	105.8	3.25	46.31	60.64	2.624	172.7	0.4809
	600	75.28	105.8	3.639	48.55	65.03	2.563	153.5	0.4809
	650	75.28	105.8	4.028	50.58	67.98	2.503	140.5	0.4809
	700	75.28	105.8	4.417	52.43	70.4	2.13	129.9	0.4809
	750	75.28	105.8	4.417	54.13	72.79	2.187	119.4	0.4809
45	550	75.28	105.8	3.25	46.3	61.03	2.703	171	0.4809
	600	75.28	105.8	3.639	48.52	65.25	2.592	152.5	0.4809
	650	75.28	105.8	3.639	50.57	68	2.485	140.4	0.4809
	700	75.28	105.8	4.028	52.44	70.53	2.165	129.4	0.4809
	750	75.28	105.8	4.417	54.15	72.87	2.099	119.1	0.4809
50	550	75.28	105.8	3.25	46.27	61.36	2.662	169.6	0.4809
	600	75.28	105.8	3.25	48.53	64.2	2.638	157.1	0.4809
	650	75.28	105.8	3.639	50.58	68.31	2.546	139.1	0.4809
	700	75.28	105.8	4.028	52.44	70.68	2.406	128.7	0.4809
	750	75.28	105.8	4.417	54.14	73.06	2.139	118.2	0.4809

Table 5. 5. The results of optimization for maximum first law efficiency of the second configuration

T_1(°C)	T_{max}(°C)	T_{13}(°C)	T_a(°C)	Pr_{opt}	η_I(%)	η_{II}(%)	$\dot{m}_D$(kg/s)	E_D (kJ/kg)	COP_{AHT}
35	550	75	105	3.247	48.49	61.47	5.084	169.1	0.464
	600	75	105	3.584	50.52	64.74	4.604	154.8	0.464
	650	75	105	3.92	52.38	67.65	4.212	142	0.464
	700	75	105	4.264	54.09	70.27	3.881	130.5	0.464
	750	75	105	4.611	55.67	72.64	3.6	120.1	0.464
40	550	75.61	105	3.059	48.69	61.65	4.964	168.3	0.464
	600	75	105	3.385	50.69	64.94	4.509	153.9	0.464
	650	75	105	3.71	52.54	67.86	4.468	141.1	0.464
	700	75	105	4.041	54.24	70.49	4.132	129.5	0.464
	750	75	105	4.378	55.81	72.86	3.814	119.1	0.464
45	550	75	105	2.922	48.83	61.8	5.901	167.6	0.464
	600	75	105	3.241	50.81	65.1	5.265	153.2	0.464
	650	75	105	3.558	52.63	68.03	4.748	140.3	0.464
	700	75	105	3.88	54.32	70.65	4.332	128.8	0.464
	750	75	105	4.214	55.88	73.02	3.98	118.4	0.464
50	550	75	105	2.809	48.97	61.98	6.24	166.9	0.464
	600	75	105	3.117	50.91	65.27	5.527	152.4	0.464
	650	75	105	3.427	52.71	68.19	4.967	139.6	0.464
	700	75	105	3.745	54.39	54.39	4.511	128.2	0.464
	750	75	105	4.062	55.94	73.16	4.136	117.8	0.464

Table 5. 6.The results of optimization for maximum first law efficiency of the third configuration

T_1(°C)	T_{max}(°C)	T_{13}(°C)	T_a(°C)	Pr_{opt}	η_I(%)	η_{II}(%)	$\dot{m}_D$(kg/s)	E_D (kJ/kg)	COP_{AHT}
35	550	75	105	3.193	49.15	62.33	6.672	165.3	0.5295
	600	75	105	3.522	51.12	65.52	6.04	151.3	0.5295
	650	75	105	3.854	52.93	68.38	5.521	138.8	0.5295
	700	75	105	4.202	54.6	70.95	5.08	127.5	0.5295
	750	75	105	4.543	56.14	73.28	4.711	117.3	0.5295
40	550	75	105	2.996	49.41	62.56	7.289	164.3	0.5295
	600	75	105	3.312	51.34	65.77	6.538	150.2	0.5295
	650	75	105	3.641	53.13	68.64	5.924	137.6	0.5295
	700	75	105	3.97	54.78	71.21	5.422	126.4	0.5295
	750	75	105	4.305	56.31	73.53	5	116.2	0.5295
45	550	75	105	2.848	49.61	62.76	7.814	163.5	0.5295
	600	75	105	3.161	51.5	65.98	6.945	149.3	0.5295
	650	75	105	3.482	53.26	68.84	6.253	136.8	0.5295
	700	75	105	3.802	54.89	71.4	5.696	125.5	0.5295
	750	75	105	4.125	56.4	73.71	5.233	115.4	0.5295
50	550	75	105	2.722	49.79	62.96	8.316	162.6	0.5295
	600	75	105	3.033	51.64	66.18	7.325	148.4	0.5295
	650	75	105	3.346	53.37	69.03	6.559	135.9	0.5295
	700	75	105	3.664	54.98	71.58	5.942	124.7	0.5295
	750	75	105	3.986	56.48	73.88	5.435	114.6	0.5295

Table 5. 7.The results of optimization for maximum first law efficiency of the fourth configuration

T_1(°C)	T_{max}(°C)	T_{13}(°C)	T_a(°C)	Pr_{opt}	η_I(%)	η_{II}(%)	$\dot{m}_D$(kg/s)	E_D (kJ/kg)	COP_{AHT}
35	550	75	105	3.174	49.38	62.34	7.026	165.3	0.5478
	600	75	105	3.503	51.32	65.54	6.519	151.2	0.5478
	650	75	105	3.833	53.12	68.4	5.958	138.7	0.5478
	700	75	105	4.181	54.77	70.97	5.481	127.4	0.5478
	750	75	105	4.517	56.3	73.3	5.084	117.2	0.5478
40	550	75	105	2.971	49.66	62.57	7.89	164.3	0.5478
	600	75	105	3.288	51.56	65.79	7.067	150.2	0.5478
	650	75	105	3.617	53.32	68.66	6.399	137.6	0.5478
	700	75	105	3.946	54.96	71.23	5.854	126.3	0.5478
	750	75	105	4.277	56.47	73.55	5.399	116.1	0.5478
45	550	75	105	2.824	49.87	62.76	8.464	163.4	0.5478
	600	75	105	3.138	51.73	65.99	7.511	149.3	0.5478
	650	75	105	3.456	53.47	68.86	6.762	136.7	0.5478
	700	75	105	3.777	55.08	71.42	6.154	125.4	0.5478
	750	75	105	4.101	56.58	73.74	5.65	115.3	0.5478
50	550	75	105	2.69	50.07	62.94	9.034	162.6	0.5478
	600	75	105	3.004	51.88	66.19	7.939	148.4	0.5478
	650	75	105	3.314	53.58	69.04	7.103	135.9	0.5478
	700	75	105	3.639	55.18	71.6	6.422	124.6	0.5478
	750	75	105	3.958	56.66	73.91	5.873	114.5	0.5478

Based on the results indicated in Tables 5.4–5.7, it can be concluded that, the maximum first law efficiency, under optimized condition, for the fourth

configuration is around 6.5% higher than that of configuration 1 which owns the minimum first law efficiency. In the case of second law efficiency, a similar behavior is observed between configuration 4 and 2 which possess the maximum and minimum efficiencies. But the improvement of the second law efficiency is in the range of 2.6-3.7%. However, these enhancements are higher at higher pressure ratios. Under the optimum conditions for a minimum temperature of 50 °C in the main compressor inlet, the pure water flow rate of 9.034 kg/s is obtained at T_{max}=550 °C. Jradi et al.[28] indicated that 10 L of fresh water per day is adequate for a typical residential. Therefore, assuming that configuration 4 operates non-stop in the optimized situations, it will be able to produce enough water for 78'209 residential units that is 339.3 % higher than that of first (basic) configuration which is an impressing result. The value of minimum temperature has little effect on the optimization results as Tables 5.4-5.7 show. However, from these Tables it is found that increasing the minimum temperature will increase the first and second law efficiencies, compressor pressure ratio and decrease distilled mass flow rate as expected. It is noticed that T_a tends to stay unchanged in all the configurations and COP follows the order of configurations 4, 3, 1 and 2 which is completely in agreement with the results reported in the literature [1, 59].

5.7 Final Remarks

An analysis and optimization of a novel cogeneration cycle based on the recompression S-CO2 Brayton cycle for waste heat recovery through a transcritical CO_2 power cycle and pure water production by means of distillation process was presented in this study. Furthermore, performances of the four cycles were optimized for maximum first and second law efficiencies. The model was validated through

comparison between results obtained from current model and those available in the literature for similar operating conditions.

Based on the analysis and optimization results, following conclusions are drawn:

- ✓ When configuration 4 is employed, the first and second law efficiencies and distilled water mass flow rate, are higher than that of other configurations used and the efficiencies follow the descending order for configurations 4, 3, 2 and 1.
- ✓ Configuration 4 owns the lowest exergy destruction which is a major advantage for it.
- ✓ Crystallization possibility within configuration 1 is higher than the other configurations.
- ✓ As heat source temperature is raised, the utilized heat for desalination purpose, the COP of the AHT and the pure water production rate are decreased.
- ✓ The maximum pure water rate of 9.034 kg/s was obtained by configuration 4 under the analyzed conditions.

Chapter 6

ALTERNATIVE WORKING FLUIDS IN ABSORPTION CYCLES

The cycle performance of refrigeration cycles not only depends on their configuration, but also on the thermodynamic properties of working pairs regularly composed of refrigerant and absorbent. The commonly used working pairs in absorption cycles are aqueous solutions of either lithium bromide–water or ammonia–water. However, corrosion, crystallization, high working pressure and toxicity are their major disadvantages in industrial applications. Therefore, seeking more advantageous working pairs with good thermal stability, minimum corrosion and without crystallization has become the research focus in the past two decades. In this chapter, the objective is to review the novel working pairs of working fluids from the family of ionic liquid and utilizing one of them as a representative in an absorption chiller.

6.1 Ionic Liquids In Absorption Cycles

Ionic liquids (ILs) are room-temperature melting salts that can remain in the liquid state at near or below room temperature. ILs have attracted considerable attentions due to their unique properties, such as negligible vapor pressure, non-flammability, thermal stability, good solubility, low melting points and staying in the liquid state over a wide temperature range from room temperature to about 300°C.

The above-mentioned highly favorable properties of ILs motivated us for carrying out a review of the available ILS found in the literature as the working fluids of

absorption cycles. Absorption cycles contain absorption heat pumps, absorption chillers and absorption transformers.

The requirements of working fluids of absorption cycles are as follows [3]:

1. The difference in the boiling point between the pure refrigerant and the mixture at the same pressure should be as large as possible,
2. Refrigerant should have high heat of vaporization and high concentration within the absorbent in order to maintain low circulation rate between the generator and the absorber per unit of cooling capacity,
3. Transport properties that influence heat and mass transfer, e.g., viscosity, thermal conductivity, and diffusion coefficient should be favorable,
4. Both refrigerant and absorbent should be non-corrosive, environmental friendly, and low-cost.

Ionic liquids (IL) are a class of low-temperature molten salts, which are constituted by an organic cation and an inorganic anion. During recent years, ILs have been used as organic green solvent in catalysis, separation process, electrochemistry and many other industries for their unique physical and chemical properties, such as negligible vapor pressure [65], negligible flammability and thermal stability [66], low melting temperature and liquid state over a wide temperature range and good solubility[67]. In particular, the low volatility of the ILs enables easy separation of the volatile working fluid from the ILs by thermal stratification with the minimum harmful impacts on environment [68].ILs can be a substitute for some of the most used toxic working fluids (such as ammonia/water) in absorption cycles. Since many of the Ionic Liquids have melting points below the lowest solution temperature in the

absorption system (~300) [69]. They also wipe out the crystallization and metal-compatibility problems of water/LiBr system.

As illustrated in Table 6.1 a comparison was made among different Ionic liquids in order to choose suitable working pairs. Among the most of ionic liquids, water was chosen as refrigerant due to its superior properties as a heat transfer fluid; such as large latent heat of evaporation followed by extremely small flow ratio resulted in its high performance. Selecting working fluids for absorption cycles should be suitable for initial operating conditions and limitations, such as crystallization, corrosion problems, and environmental limits and also material requirement should be considered.

Table 6. 1. Characteristic comparison of different working fluids.

Working pair	References	Absorption cycle	Remarks
H_2O + [EMIM][DMP]	[64]	AC	COP lower than that of H_2O + LiBr by 7%, but still higher than 0.7
H_2O +[EMIM][BF4]	[70]	AHP	High COP due to: -Suitable compatibility of water with [EMIM][BF4] -Superior properties of water as a heat transfer fluid, such as large latent heat of evaporation -Extremely small refrigerant (water) flow rate
H_2O + [EMISE]	[71] and [72]	AHP	Colorless ionic liquid, EMISE is easy to absorb the water vapor in the air.

H_2O + [DMIM] DMP	[73]	AC	Less crystallization and corrosion risk thanH_2O+LiBr in air cooled absorption chiller
CO_2+ [BMPYRR][Tf2 N]	[74] and [75]	AHP	Non-toxicity, non-flammability and low cost, high circulation ratios in comparison with conventional absorption refrigerators, increases the energy necessities of heating and pumping processes
Methanol+[EMIM][DMP] Ethanol+[EMIM][DMP]	[76]	AHP	Strong absorbing ability for coolant
[MMIM][DMP] + water/ethanol/ methanol	[72]	AHP	Suitable vapor pressure, heat capacity, excess enthalpy, low viscosity
[MMIM][(CH 3) 2PO4]	[77]	AC	High COP, low flow ratio
[EMIM][(CH3) 2PO4]	[77]	AC	High COP, low flow ratio
CH3OH + [MMIM][DMP]	[3]	AHP	High COP, high refrigerant capacity, higher gas-emission scope and circulation ratio than NH_3+H_2O, fewer requirements of generating pressure and condensing pressure than conventional system.

6.2 Absorption Chiller Utilizing (Licl+H_2o) As The Working Pair

The investigated study case in this section is a single stage absorption chiller using (LiCl+H2O) as the working pair. Recently has been an unprecedented research interest in vapor absorption refrigeration and heat pumping in order to reduce CO2 emissions for a healthy environment and balanced ecology. To pursue the desire to reduce the greenhouse gas CO_2 to levels of 1990s, the United Nation Framework Convention on Climate is urging a phase out of CFC and HCFC fluids. This movement has encouraged research into environmental friendly refrigerants such as water and other binary solutions. These researches have led to the use of low grade energy systems like vapour-compression cycle systems for heating and cooling as compared to other heating and cooling systems. Aside from economic benefits, improving the efficiency of like vapour-compression cycle systems are effective means of curbing CO_2 emissions. The vapour-absorption cycle is considered to be the best in terms of energy performance today. In addition, it has the potential to be improved among the several heat-powered cycles [78]. In comparison with other vapour-compression cycle, the absorption cycle has a low efficiency reputation although this is a result of an unfair comparison between them, but the environmental concern calls for high efficiency, pollution-free refrigerators and heat pumps.

The essential condition in absorption chillers is the availability of an inexpensive or even free heat source such as waste (or rejected) heat. Several studies have been made using solar energy [79, 80]. Absorption cooling is based on the strong chemical affinity between two working fluids; the refrigerant and the absorbent, the former having a much lower vapour pressure than the latter. In a single-effect absorption chiller, at a lower pressure and temperature level, the refrigerant is evaporated using

the heat removed from the conditioned space and absorbed by the absorbent solution. At a higher pressure and temperature level, a heat source provides the energy needed to extract the absorbed refrigerant vapour from the solution, which is subsequently regenerated and ready for the next cycle. Water, as a refrigerant and lithium-bromide as an absorbent are one of the most used working fluid pairs in current absorption chillers [81].

One of the earliest dynamic simulations of absorption refrigeration systems has been performed by Jeong et al.[82] for a steam driven heat pump. The model assumes solution mass storage in the vessels, thermal capacity heat storage, and flow rates (vapour and solution) are calculated according to the pressure differences between vessels. Later, Fu et al. [83] developed a library of elemental dynamic models for absorption refrigeration systems (CHP applications), in which the components are described as lumped processes involving two-phase equilibriums. In a series of two papers, Kohlenbach and Ziegler [84] presented a simulation model and its experimental verification for a single-effect water/LiBr chiller. As a special feature, all of the thermal capacities have been divided into an external part (influenced by the temperature of the external heat carriers) and an internal part (influenced by the temperature of the refrigerant or the absorbent). Moreover, a transport delay time has been assumed in the solution cycle. Matsushima et al. [85] developed a program using object-oriented formulation and parallel processing to simulate the transient operation of a triple-effect absorption chiller.

A special algorithm based on the pressure difference and flow resistance between the generators and the absorber has been used to calculate the flow rate of solution. Wu et al. [86] experimentally studied the equilibrium pressure, equilibrium temperature

and gas composition of NH_3-H_2O-LiBr ternary mixture for its application in industrial absorption chillers and heat pumps. Me et al. [87] investigated the relationship of coefficient of performance (COP) of a lithium-bromide absorption chiller with solution concentration of LiBr/H2O. Papaefthimiou et al. [88] developed a mathematical model for analyzing the heat and mass transfer process of LiBr-H2O absorption on a horizontal tube, and a good agreement with the test data was obtained. Lucan et al. [89] added formats and lithium-nitrates in the lithium bromide solution and analyzed the effect of generation temperature, condensing temperature, and evaporation temperature on system performance. This action was found to increase the COP by 30% and the solution circulation rate to decrease by 12%.

In recent years, finding ways to improve absorption-system efficiency has been a great challenge for researchers [3, 59, 78] .Works have mainly focused on inventing new or hybrid cycles, finding new working fluids and improving the heat and mass transfers of the absorption refrigerator. The performance of absorption cycles are attributed to the thermodynamic properties of the working pairs which consist of the refrigerant and the absorbent. Most commonly used working pairs are ammonia + water solution (NH3+H2O) and aqueous solution of lithium bromide (H2O+LiBr). However, Zhang and Hu [90] have identified corrosion, crystallization and toxicity as inevitable weaknesses of these working pairs. The need for working pairs not susceptible to these weaknesses has become the focus of research. In this study, we have used LiCl+H2O as a working pair in the absorption cycle, for the aim of a comprehensive study and optimization. The studied working pairs have the advantages of availability and environmentally friendly and are suitable for moderate temperature applications [36]. LiCl/H2O is preferred over LiBr/H2O for the reason of cost and long-term stability while it is preferred over CaCl2/water for its better

hygrocopic properties leading to better cycle performance [91]. Furthermore the small chemical potential of LiCl relative to LiBr leads to a larger absorber area and shows a larger performance reduction than LiBr [92]. A detailed review of Thermodynamic properties of ($LiCl/H_2O$) can be seen in the work of Patek and Klomfar [93].

6.2.1 The Performance Simulation

Figure 6.1 presents the schematic of the single effect absorption refrigeration.

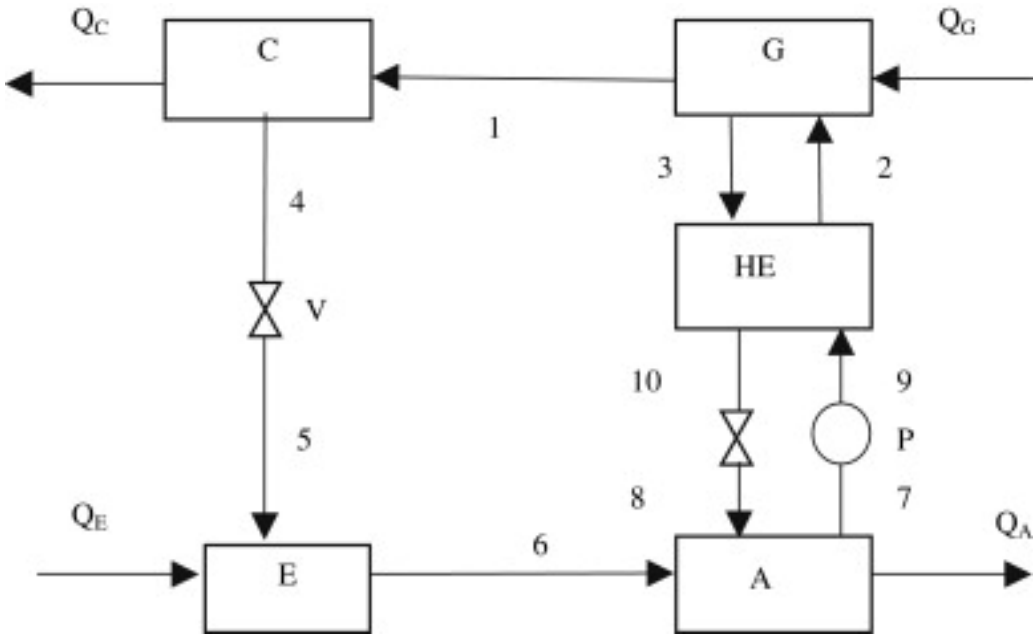

Figure 6. 1. Schematic diagram of absorption refrigeration. A – Absorber, C – Condenser, E – Evaporator, G – Generator, HX – Solution heat exchanger, P – Pump, v – Valve.

6.2.2 Assumptions

The following assumptions are made through simulating the thermodynamic performance of the absorption refrigeration cycle [90, 94]:

I. The entire system runs under steady state conditions

II. Solutions leaving the generator and the absorber are at a saturated liquid temperature

III. Refrigerant leaving the condenser is in a saturated liquid phase

IV. In the whole cycle, pressure losses are neglected

V. Throttling valves is an isenthalpic device

VI. (6)Temperature difference between the cold and hot streams at the cold end of solution heat exchange (HX) is 10 °C

VII. (7)The consumption of mechanical energy by the pump is negligible.

VIII. (8)The difference of the concentration between the strong and weak solutions is 5% (wt%, LiCl or LiBr).

6.2.3 Mass and Energy Balance Equations

Mass and energy balance equations for any component in the cycle for the aim of thermodynamic cycle performance simulation are given as follows:

Generator

$$m_2=m_1+m_3 \quad \textbf{(6.1)}$$

$$m_2x_2=m_3x_3 \quad \textbf{(6.2)}$$

$$Q_{gen}= m_3h_3+m_1h_1-m_2h_2 \quad \textbf{(6.3)}$$

$$P_3=P(T_3,x_3) \quad \textbf{(6.4)}$$

Condenser

$$m_1=m_4 \quad \textbf{(6.5)}$$

$$Q_{con} = m_1 h_1 - m_4 h_4 \quad \textbf{(6.6)}$$

$$P_4 = P_s(T_4) \quad \textbf{(6.7)}$$

Evaporator

$$m_5 = m_6 \quad \textbf{(6.8)}$$

$$Q_{gen} = m_6 h_6 - m_5 h_5 \quad \textbf{(6.9)}$$

$$P_6 = P_s(T_6) \quad \textbf{(6.10)}$$

Absorber

$$m_7 = m_6 + m_7 \quad \textbf{(6.11)}$$

$$m_8 x_8 = m_7 x_7 \quad \textbf{(6.12)}$$

$$Q_{abs=} m_6 h_6 + m_8 h_8 - m_7 h_7 \quad \textbf{(6.13)}$$

$$P_7 = P(T_7, x_7) \quad \textbf{(6.14)}$$

Solution Heat Exchanger

$$m_3 h_3 + m_9 h_9 = m_2 h_2 + m_{10} h_{10} \quad \textbf{(6.15)}$$

$$T_{10} = T_9 + 10 \quad \textbf{(6.16)}$$

$$m_1 = 1 \text{ kg/s} \quad \textbf{(6.17)}$$

The saturation pressure of water and working solutions (H2O + LiBr or H2O + LiCl) are shown respectively with $P_s(T)$ and $P(T,x)$.

A computer program has been developed using Engineering Equation Solver (EES) [95] to carry out the thermodynamic analysis of the absorption chiller cycle. For the previously mentioned properties, we have used the available date in the library of EES Software.

By applying the mass, energy and phase balance equations around any element in the cycle, and by utilizing the above stated assumptions, the heat load of the generator, absorber, evaporator and condenser, the concentration of strong and weak solution and flow rate ratio were obtained.

The coefficient of performance, COP, exergetic efficiency, ECOP, which is based on the second law of thermodynamics [96] and the flow rate ratio, F, are defined as follows:

$$\mathrm{COP} = \frac{\mathrm{Qe}}{\mathrm{Qg}} \quad \textbf{(6.18)}$$

$$\mathrm{ECOP} = \frac{\mathrm{Qe}(\frac{\mathrm{To}}{\mathrm{Te}}-1)}{\mathrm{Qh}(1-\frac{\mathrm{To}}{\mathrm{Th}})} = \mathrm{COP}\frac{(\frac{\mathrm{To}}{\mathrm{Te}}-1)}{(1-\frac{\mathrm{To}}{\mathrm{Th}})} \quad \textbf{(6.19)}$$

$$\mathrm{f} = \frac{\mathrm{m2}}{\mathrm{m1}} \quad \textbf{(6.20)}$$

T_0 = 298.15 K (Environmental Temperature) **(6.21)**

$T_h = T_G$ +10 K (Heat source temperature) **(6.22)**

6.2.4 Optimization Method

The results obtained from the mathematical model reveal that the optimum performance of the absorption chiller cycle depends on the following design/operating parameters:

• Condenser temperature

• Evaporator temperature

• Absorber temperature

•Generator temperature

Therefore, the optimum value of the coefficient of performance for the absorption chiller cycle can be expressed as a function of four design/operating parameters, as shown in the following equation:

Maximize COP(T_{con}, T_{eva}, T_{abs}, T_{gen}) **(6.23)**

Subject to: **(6.24)**

$30 < T_{con}(^0C) < 45$

$5 < T_{eva}(^0C) < 15$

$25 < T_{abs}(^0C) < 40$

$70 < T_{gen}(^0C) < 95$

Using direct search method and applying the constraints on each variable by setting the bounds, the performance of the whole cycle is optimized by the EES software from the viewpoint of quantity of produced distilled water. The direct search method is based on a successive search intended to find an extremum by directly comparing function values at a sequence of trial points without involving derivatives. This method is deemed suitable for problems involving simulation-based optimization or optimizing non-numerical functions, as well as, in practice, problems involving non-smooth or discontinuous functions [97].

6.2.5 Model Validation

For validating the models developed for the single-effect absorption refrigeration cycle the theoretical data given by Kaushik and Arora [98] and Yari et al.[94] are used.

The results of comparisons are shown in Table 6.2, which indicate that there is a good agreement between the present work and numerical data reported in the literature.

Table 6. 2. Comparison of results obtained in this work with numerical data given by Kaushikand Arora [98] and Yari et al.[94]for single-effect absorption refrigeration cycle using LiBr/H2O as working pair

Component	Kaushik and Arora [98]	Yari et al. [99]	Present work	Difference percentage (%) with data available in [98]	Difference percentage (%) with data available in [94]
	$\dot{Q}$(kW)	$\dot{Q}$(kW)	$\dot{Q}$(kW)	$\dot{Q}$(kW)	$\dot{Q}$(kW)
Generator	3095.7	3092	3087	-0.28	-0.16
ABS	2945.27	2943	2960	0.5	0.57
Evaporator	2355.45	2355	2349	-0.27	-0.25
Condenser	2505.91	2506	2476	-1.19	-1.19
HE	518.72	522.6	516	-0.52	-1.26
COP	0.7609 (-)	0.7615 (-)	0.7609 (-)	0	-0.07

Input parameter values: (T_{gen}= 87.8 ^{0}C, T_{evap}=7.2 ^{0}C, T_{abs}=T_{cond}=37.8 ^{0}C, ε_{HX}= 0.7, $\dot{m}_r$=1 kg/s)

6.2.6 Results And Discussion

Figs 6.2-6.9 demonstrate the results of absorption chiller using (H2O + LiBr) and (H2O + LiCl). Fig 6.2 shows coefficients of performance versus evaporator temperature for both working pairs. (H_2O + LiCl)'s performance is approximately

equal to (H_2O + LiBr). Moreover, for both pairs the coefficient of performance will increase with the increase of evaporation temperature.

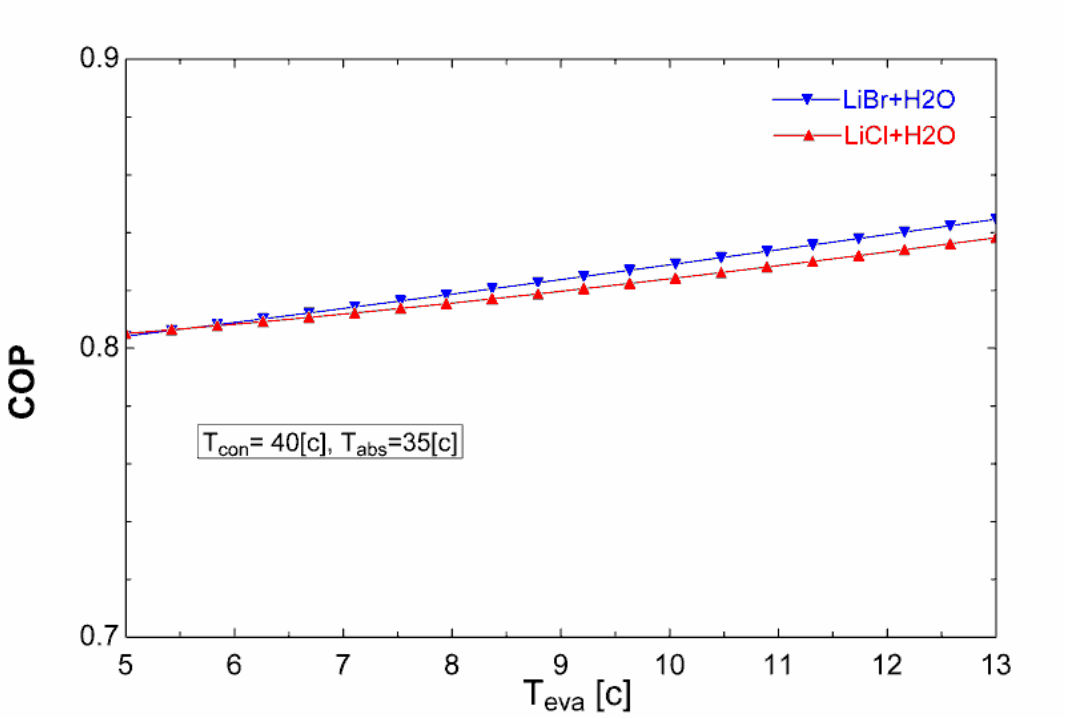

Figure 6. 2. Effect of Evaporator Temperature on COP

The variation of ECOP with the evaporation temperature for two working pairs is shown in figure 6.3. The evaporation temperature's effect on COP and ECOP are completely different from each other which are very interesting and are in agreement with the results available in literature [79, 96]. The COP will increase with the increase of T_{eva} while ECOP will decrease with the increase of T_{eva}. The reason for the difference between COP and ECOP is that the former only takes account of the quantity of the heat, but the latter not only takes account of the heat but also of quality of the heat. In other words, the cooling load of Q_{eva} and the temperature level of T_{eva} are all important for the refrigeration process, namely, the lower the T_{eva}, the higher quality of cooling load Q_{eva} is. This was why the ECOP will decrease with the increase of T_{eva}. It was also discovered that the ECOP for working pair H_2O + LiCl is

slightly higher than that for $H_2O + LiBr$ (5-6%). This is an advantage for ($H_2O + LiCl$).

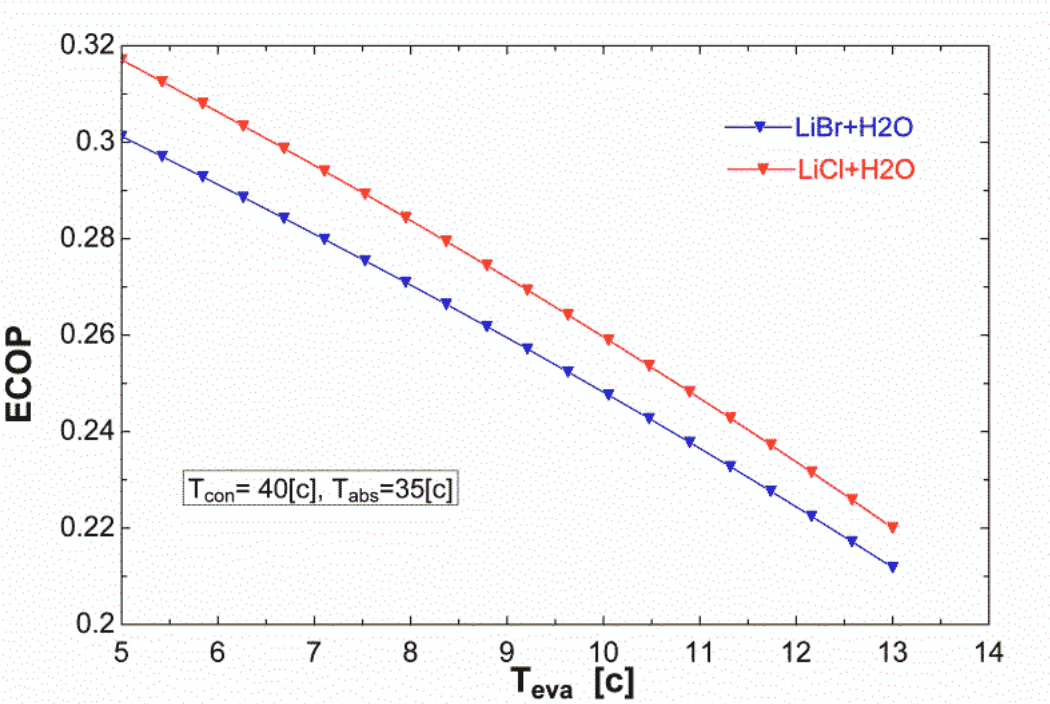

Figure 6. 3. Effect of Evaporator Temperature on ECOP

Figure 6.4 demonstrates that the generation temperature for ($H_2O + LiCl$) is lower than that for ($H_2O + LiBr$), which designates that absorption chiller using ($H_2O + LiCl$)as working fluid can be driven by lower temperature level waste heat under the same operating conditions. Moreover, the generation temperature will decrease with the increase of the evaporation temperature.

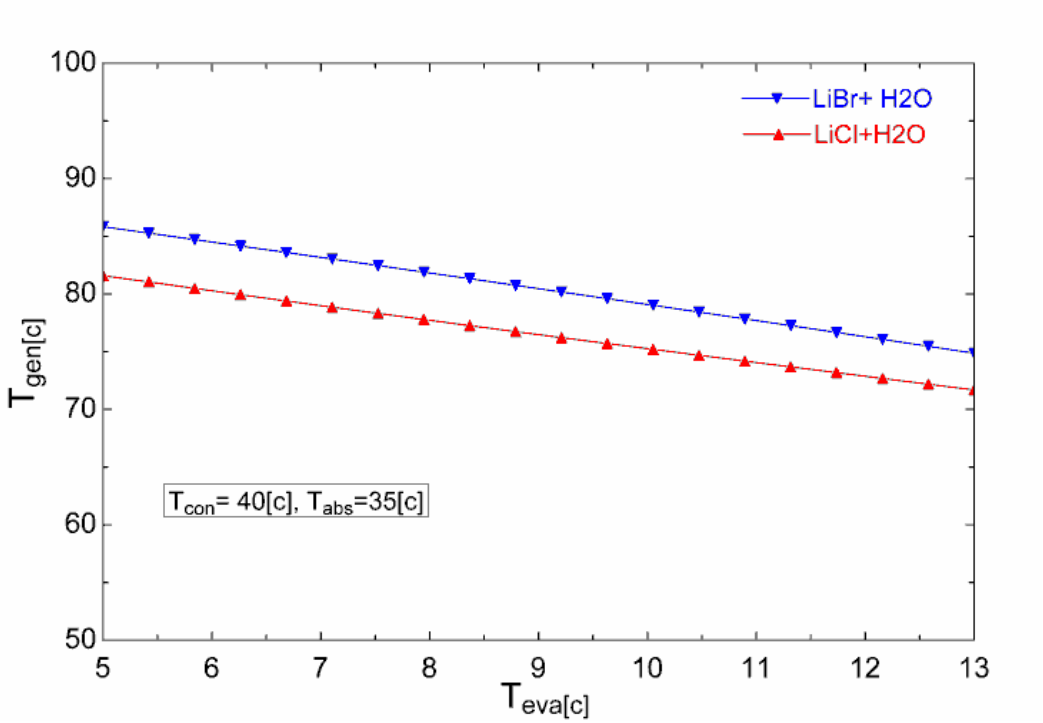

Figure 6. 4. Effect of Evaporator Temperature on Generator Temperature

According to Figures 6.5 and 6.6, the concentration of strong solution and flow rate ratio, f, for (H_2O + LiBr), are both higher than those for (H_2O + LiCl), and they both decreased with the increase of the evaporation temperature. It is obvious that having smaller flow ratio for a working pair is a major advantage from the view point of performance and lesser amount of mechanical power losses [3, 59, 70].

Fig.6.7 shows the flow ratio variation with respect to the generator outlet temperature. The generator outlet temperature rises with the increment of flow ratio due to a decrease in the mass fraction of the weak solution. Equation (5.9) can be rewritten to yield Equation (6.25) [70].

$$Q_{gen}/m_r = f\,(h_3 - h_2) - h_3 + h_1 \qquad \textbf{(6.25a)}$$

$$Q_{gen}/m_r = h_3\,(f - 1) + h_1 - fh_2 \qquad \textbf{(6.25b)}$$

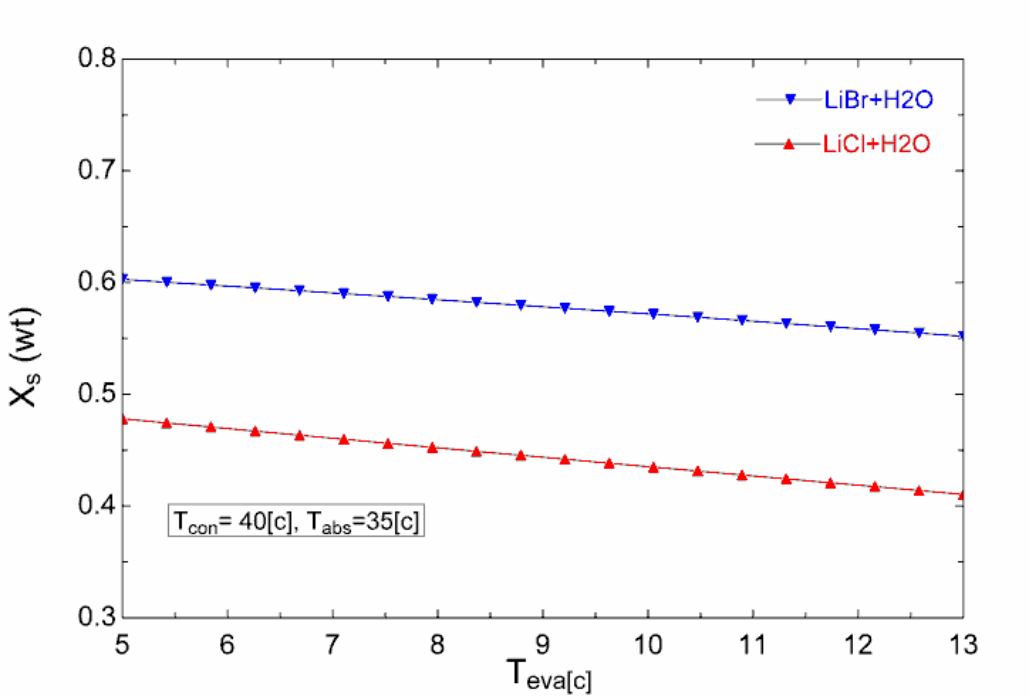

Figure 6. 5. Effect of Evaporator Temperature on concentration of strong solution

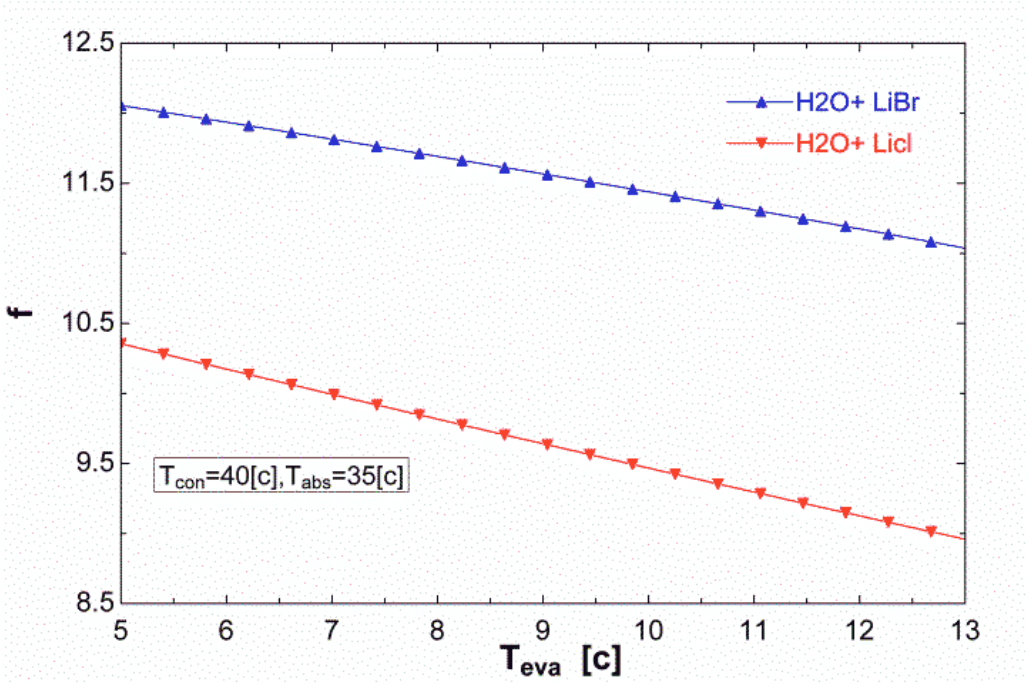

Figure 6. 6. Effect of Evaporator Temperature on Flow rate Ratio

Equation (6.25a) shows that a smaller flow ratio results in less heat input to the generator for the same amount of cooling at the evaporator, which would increase COP [70] (Far ahead shown in fig f-COP).

These results are in agreement with that shown figs 6.4 and 6.6.

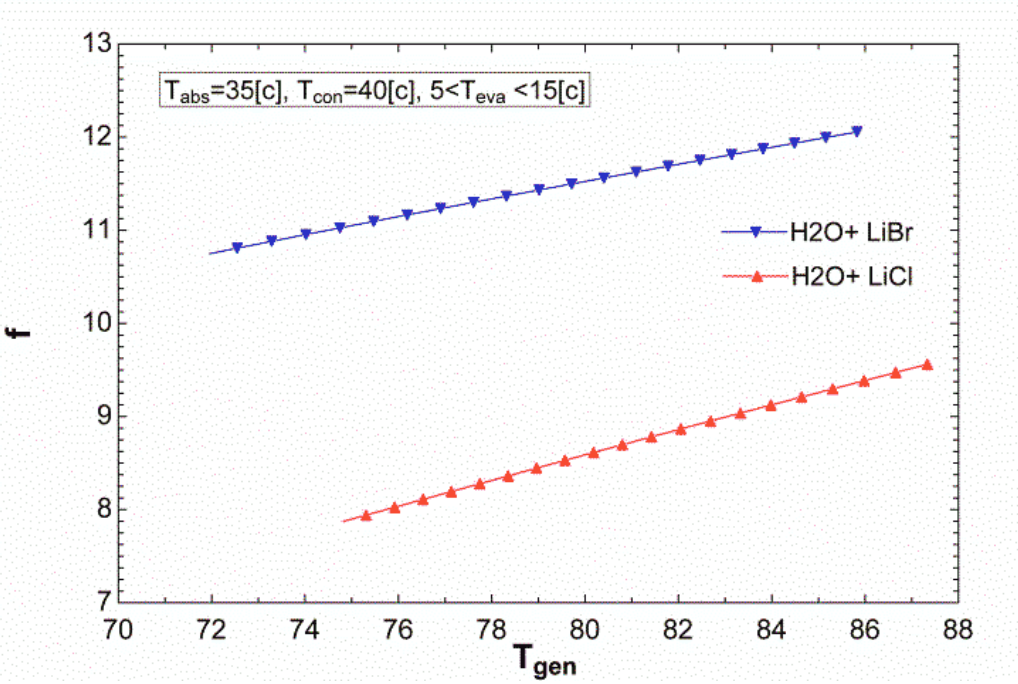

Figure 6. 7.Flow ratios of the absorption system with respect to the generator outlet temperature using (H2O + LiBr) and (H2O + LiCl)

Fig 6.8 examines the COP trends against the recirculation flow ratio for different condenser and evaporator temperatures and for equal evaporator temperature ranges of 5-15°C. As is seen, the COP decreases in all cases as the recirculation flow ratio increases. This is because when the evaporator temperature increases, the minimum system pressure will increase and the strong solution concentration will decrease by decreasing the flow ratio. (According to fig 5.5) The lower flow ratio results in a higher absorption heat capacity and a higher COP.

Coefficients of performance for both working pairs are approximately equal to each other while (H_2O+LiCl) owns less magnitude of flow ratio.

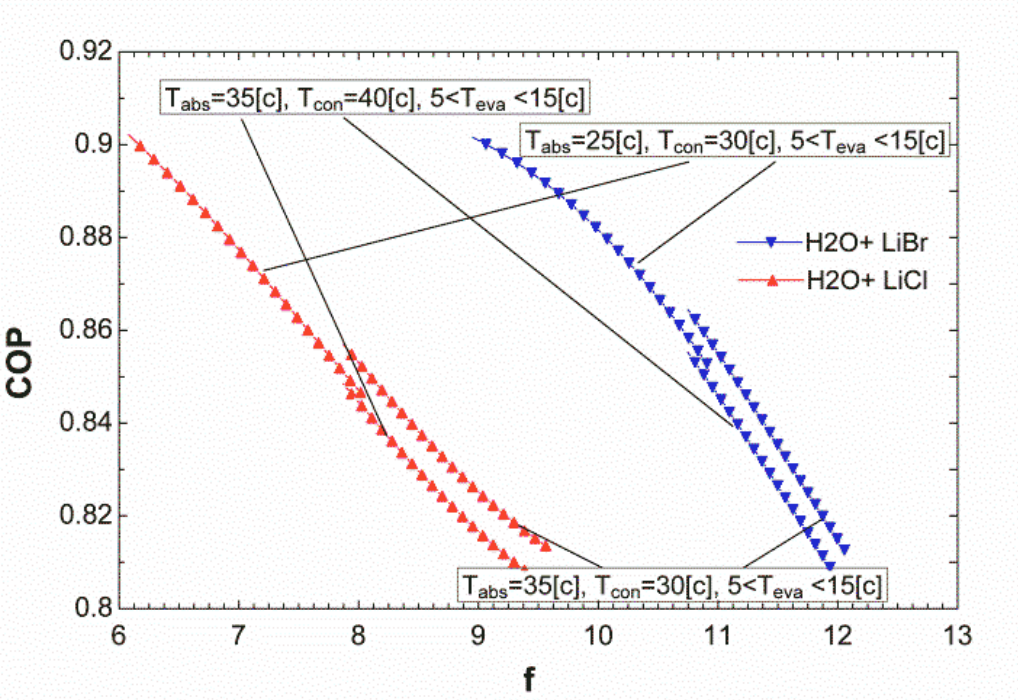

Figure 6. 8. Effect of flow ratio on COP for different conditions

It can be seen in Fig 5.8 that as the absorber temperature is increased, the COPs of both pairs decrease and flow ratio increase very rapidly. A similar behavior is observed as condenser temperature is decreased.

Fig 6.9 shows the variation of COP with the generator temperature under different condenser temperature and equal evaporator temperature ranges of (5-15)°C conditions. The COP of the system decreases as T_{con} increases for both working pairs. Increasing the generator temperature T_{gen} tends to decrease the COP at constant condenser temperature. At the same working conditions, COP of the system utilizing H2O+LiBr is (0.6-0.8%) more than that of H2O+LiCl. But on the other hand the desirable generator temperature for the H2O+LiCl is (2-2.5)˚C less than that

of H2O+LiBr. Our results for H2O+LiBr are in agreement with those reported in the literature[100].

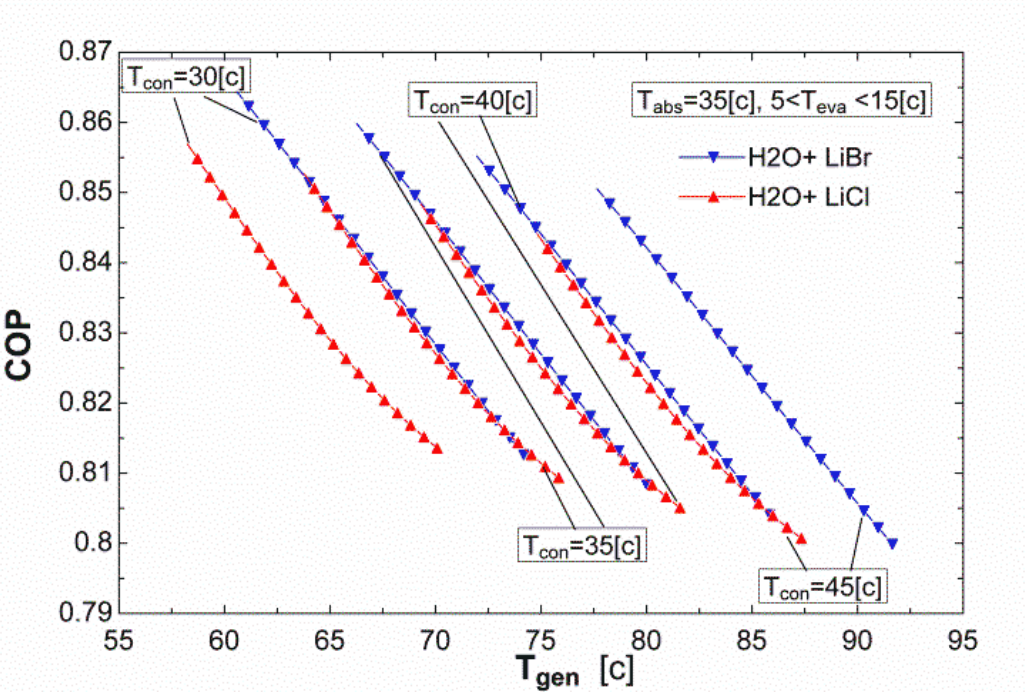

Figure 6. 9. Relationship between COP and generator temperature under different condenser temperature and equal evaporator temperature

6.2.7 Optimization

Using the direct search function in the EES software, the coefficient of performance of the absorption chiller cycle is optimized with respect to the condenser, evaporator, absorber and generator temperatures for the two cases using (LiBr+H2O) and (LiCl+H2O) working pairs. The results are outlined in Tables 6.3 and 6.4.

Table 6. 3. The results of optimization for maximum coefficient of performance of the absorption chiller cycle using (LiBr-H2O)

T_{abs}(c)	T_{con}(c)	T_{eva}(c)	T_{gen}(c)	f	COP	ECOP
25	30	15	46.24	8.952	0.9016	0.3299
30	30	15	53.78	9.996	0.8848	0.2668
35	30	15	60.57	10.75	0.8645	0.2263
40	30	15	66.78	11.36	0.8436	0.1979

Table 6. 4.The results of optimization for maximum coefficient of performance of the absorption chiller cycle using (LiCl-H2O)

T_{abs}(c)	T_{con}(c)	T_{eva}(c)	T_{gen}(c)	f	COP	ECOP
25	30	15	46.26	6.08	0.9015	0.3299
3 0	30	15	52.61	7.059	0.8788	0.2723
35	30	15	58.25	7.873	0.8569	0.2347
40	30	15	63.49	8.627	0.8376	0.2078

As the Tables indicate the optimum mass flow ratio for maximum coefficient of performance is higher for the case of (LiBr+H2O) compared to that for the (LiCl+H2O). Also, with increasing T_{abs}, the coefficient of performance and exergetic efficiency decreases as expected. A comparison between Table 6.3 and Table 6.4 reveals that when the (LiCl+H2O) is employed as a working fluid, the maximum coefficient of performance is slightly less than (1.5-2%) that when (LiBr+H2O) is used. However, regarding the smaller crystallization risk, the former maybe preferred in spite of the difference in the performance criterion.

6.3 Conclusion

In the first section of this chapter, a number of researches about working fluids of absorption cycles, which contain absorption heat pumps, absorption chillers, and absorption heat transformers including ionic liquids, were reviewed. Using ionic liquids as the working fluids of absorption cycles can lead us to benefit from factors

such as less crystallization, less corrosion, low toxicity, and non-flammability in comparison with conventional working fluids.

In the case of absorption chiller using (H_2O+LiCl) the major conclusions drawn from the simulation are as follows:

1. Under the same condensation and absorption temperatures, the generation temperature of refrigeration cycle for H_2O + LiCl was somewhat lower than that for H_2O + LiBr, so it was possible that the absorption chiller was driven by lower temperature level waste heat by means of adopting H_2O + LiCl as a working fluid.

2. At the same condensing and absorbing temperature, the simulating results indicated that the temperature was lower than that for H_2O + LiBr.

3. The exergetic efficiency ECOP for H_2O + LiCl was somewhat higher than for H_2O + LiBr and they will all decrease with the evaporation temperature T_{eva}.

4. The concentration of strong solution and flow rate ratio, f, for (H_2O + LiBr), are both higher than those for (H2O + LiCl), and they both decreased with the increase of evaporation temperature.

5. The results show that the coefficient of performance of the absorption chiller, using (H_2O + LiBr) at the optimum conditions is around 1.5-2% higher than that of (H_2O + LiCl).

6. As the absorber temperature is increased, the COPs of both pairs decrease and flow ratio increase very rapidly. A similar behavior is observed as condenser temperature is decreased.

7. At the same working conditions, COP of the system utilizing H2O+LiBr is (0.6-0.8%) more than that of H2O+LiCl. But on the other hand the desirable generator temperature for the H2O+LiCl is (2-2.5)˚C less than that of H2O+LiBr.

Chapter 7

CONCLUSION

The present work investigated the role of different cyclic configurations of AHTs on the COP of the cycles, gross temperature lift, flow fraction (of the refrigerant and absorbent) and the amount of distilled water for combined systems of AHT-desalination and AHT-cogeneration-desalination. Furthermore, the effect of alternative working pairs on the performance of absorption cycles was also examined. A thermodynamic model was developed, in which, energy balance was established for each component of the mentioned systems.

Based on the analysis and the optimization of results, following major conclusions are drawn:

- Configuration 4, in which all the other configurations have been put together, has the maximum COP value and configuration 2, wherein the feed heat is directed firstly to the evaporator and then generator has the lowest COP value amongst the four configurations.
- The lower the condensing temperature is, the higher the COP or available temperatures lift will be.
- The higher the generation or evaporation temperature is, the higher the absorption temperature and corresponding gross temperature achieved.
- Crystallization possibility within the basic configuration is higher than other configurations.

- Configuration 1 has the highest flow rate ratio among all the configurations.
- As heat source temperature is raised, the utilized heat for desalination purpose, the COP of the AHT and the pure water production rate are decreased.
- The order of the utilized heat capacity and hence the pure water production rate's order for different configurations are as follows: configuration 4 > configuration 3 > configuration 2 > configuration 1.
- Distilled water mass flow rate increases with the increase in COP.
- Configuration 4 owns the lowest exergy destruction which is a major advantage for it.

And finally it was shown that $LiCl+H_2O$ can be an acceptable working pair in absorption cycles.

REFERENCES

1. Horuz, I. and B. Kurt, Absorption heat transformers and an industrial application. Renewable Energy, 2010. 35(10): p. 2175-2181.

2. Kurem, E. and I. Horuz, A comparison between ammonia-water and water-lithium bromide solutions in absorption heat transformers. International Communications in Heat and Mass Transfer, 2001. 28(3): p. 427-438.

3. Khamooshi, M., K. Parham, and U. Atikol, Overview of ionic liquids used as working fluids in absorption cycles. Advances in Mechanical Engineering, 2013. 2013.

4. Ma, X., et al., Application of absorption heat transformer to recover waste heat from a synthetic rubber plant. Applied Thermal Engineering, 2003. 23(7): p. 797-806.

5. Sotelo, S.S. and R.J. Romero. Improvement of recovery energy in the absorption heat transformer process using water - Carrol™ for steam generation. 2009. Rome.

6. Zhang, X.D. and D.P. Hu, Performance analysis of the single-stage absorption heat transformer using a new working pair composed of ionic liquid and water. Applied Thermal Engineering, 2012. 37: p. 129-135.

7. Zebbar, D., et al., Thermodynamic optimization of an absorption heat transformer. International Journal of Refrigeration, 2012. 35(5): p. 1393-1401.

8. Rivera, W., et al., Theoretical and experimental comparison of the performance of a single-stage heat transformer operating with water/lithium bromide and water/Carrol ™. International Journal of Energy Research, 2002. 26(8): p. 747-762.

9. Rivera, W. and J. Cerezo, Experimental study of the use of additives in the performance of a single-stage heat transformer operating with water-lithium bromide. International Journal of Energy Research, 2005. 29(2): p. 121-130.

10. Rivera, W., et al., Exergy analysis of an experimental single-stage heat transformer operating with single water/lithium bromide and using additives (1-octanol and 2-ethyl-1-hexanol). Applied Thermal Engineering, 2011. 31(16): p. 3526-3532.

11. Shi, L., et al., Study on a new ejection-absorption heat transformer. Applied Energy, 2001. 68(2): p. 161-171.

12. Sozen, A. and H.S. Yucesu, Performance improvement of absorption heat transformer. Renewable Energy, 2007. 32(2): p. 267-284.

13. Sözen, A., Effect of irreversibilities on performance of an absorption heat transformer used to increase solar pond's temperature. Renewable Energy, 2004. 29(4): p. 501-515.

14. Shi, L., et al., Study on a new ejection-absorption heat transformer. Applied Energy, 2001. 68(2): p. 161-171.

15. Guo, P.J., J. Sui, and H.G. Jin, Off-design performance of a vertical LiBr/H 2O absorption heat transformer. Kung Cheng Je Wu Li Hsueh Pao/Journal of Engineering Thermophysics, 2012. 33(6): p. 907-912.

16. Olarte-Cortés, J., J. Torres-Merino, and J. Siqueiros, Experimental study of a graphite disks absorber couple to a heat transformer. Experimental Thermal and Fluid Science, 2013. 46: p. 29-36.

17. Kotenko, O., H. Moser, and R. Rieberer, Thermodynamic simulation of alternative absorption heat pumping processes using natural working fluids. International Journal of Refrigeration, 2012. 35(3): p. 594-604.

18. Niang, M., T. Cachot, and P.L. Goff, Evaluation of the performance of an absorption-demixtion heat pump for upgrading thermal waste heat. Applied Thermal Engineering, 1998. 18(12): p. 1277-1294.

19. Alonso, D., T. Cachot, and J.M. Hornut, Experimental study of an innovative absorption heat transformer using partially miscible working mixtures. International Journal of Thermal Sciences, 2003. 42(6): p. 631-638.

20. Rivera, W., et al., Theoretical and experimental comparison of the performance of a single-stage heat transformer operating with water/lithium bromide and water/Carrol (TM). International Journal of Energy Research, 2002. 26(8): p. 747-762.

21. Siqueiros, J. and R.J. Romero, Increase of COP for heat transformer in water purification systems. Part I – Increasing heat source temperature. Applied Thermal Engineering, 2007. 27(5–6): p. 1043-1053.

22. Gomri, R., Energy and exergy analyses of seawater desalination system integrated in a solar heat transformer. Desalination, 2009. 249(1): p. 188-196.

23. Gomri, R., Thermal seawater desalination: Possibilities of using single effect and double effect absorption heat transformer systems. Desalination, 2010. 253(1–3): p. 112-118.

24. Şencan, A., et al., Different methods for modeling absorption heat transformer powered by solar pond. Energy Conversion and Management, 2007. 48(3): p. 724-735.

25. Yari, M., A novel cogeneration cycle based on a recompression supercritical carbon dioxide cycle for waste heat recovery in nuclear power plants. International Journal of Exergy, 2012. 10(3): p. 346-364.

26. Rivera, W., J. Cerezo, and H. Martínez, Energy and exergy analysis of an experimental single-stage heat transformer operating with the water/lithium

bromide mixture. International Journal of Energy Research, 2010. 34(13): p. 1121-1131.

27. Romero, R.J., J. Siqueiros, and A. Huicochea, Increase of COP for heat transformer in water purification systems. Part II – Without increasing heat source temperature. Applied Thermal Engineering, 2007. 27(5–6): p. 1054-1061.

28. Jradi, M., N. Ghaddar, and K. Ghali, Experimental and theoretical study of an integrated thermoelectric–photovoltaic system for air dehumidification and fresh water production. International Journal of Energy Research, 2012. 36(9): p. 963-974.

29. Rivera, W., et al., Single stage and double absorption heat transformers used to recover energy in a distillation column of butane and pentane. International Journal of Energy Research, 2003. 27(14): p. 1279-1292.

30. Khalil, E.E., Potable water technology development in Egypt. Desalination, 2001. 136(1-3): p. 57-62.

31. Garcia-Rodriguez, L. and C. Gomez-Camacho, Preliminary design and cost analysis of a solar distillation system. Desalination, 1999. 126(1-3): p. 109-114.

32. Romero, R.J. and A. Rodriguez-Martinez, Optimal water purification using low grade waste heat In an absorption heat transformer. Desalination, 2008. 220(1-3): p. 506-513.

33. Zare, V., M. Yari, and S.M.S. Mahmoudi, Proposal and analysis of a new combined cogeneration system based on the GT-MHR cycle. Desalination, 2012. 286: p. 417-428.

34. Farshi, L.G., S.M.S. Mahmoudi, and M.A. Rosen, Analysis of crystallization risk in double effect absorption refrigeration systems. Applied Thermal Engineering, 2011. 31(10): p. 1712-1717.

35. Sekar, S. and R. Saravanan, Exergetic performance of eco friendly absorption heat transformer for seawater desalination. International Journal of Exergy, 2011. 8(1): p. 51-67.

36. Reyes, R.M.B., V.M.A. Gomez, and A. Garcia-Gutierrez, Performance modelling of single and double absorption heat transformers. Current Applied Physics, 2010. 10: p. S244-S248.

37. Iverson, B.D., et al., Supercritical CO2 Brayton cycles for solar-thermal energy. Applied Energy, 2013. 111: p. 957-970.

38. Dostal, V., P. Hejzlar, and M.J. Driscoll, The supercritical carbon dioxide power cycle: Comparison to other advanced power cycles. Nuclear Technology, 2006. 154(3): p. 283-301.

39. Chen, H., D.Y. Goswami, and E.K. Stefanakos, A review of thermodynamic cycles and working fluids for the conversion of low-grade heat. Renewable and Sustainable Energy Reviews, 2010. 14(9): p. 3059-3067.

40. Ishizuka, T., et al., Thermal-hydraulic characteristics of a printed circuit heat exchanger in a supercritical CO2 loop Bull Res Lab Nucl. Reactor, 2006. 30: p. 109-116.

41. Floyd, J., et al., A numerical investigation of the sCO2 recompression cycle off-design behaviour, coupled to a sodium cooled fast reactor, for seasonal variation in the heat sink temperature. Nuclear Engineering and Design, 2013. 260: p. 78-92.

42. Jeong, W.S. and Y.H. Jeong, Performance of supercritical Brayton cycle using CO2-based binary mixture at varying critical points for SFR applications. Nuclear Engineering and Design, 2013. 262: p. 12-20.

43. Singh, R., M.P. Kearney, and C. Manzie, Extremum-seeking control of a supercritical carbon-dioxide closed Brayton cycle in a direct-heated solar thermal power plant. Energy, 2013. 60: p. 380-387.

44. Turchi, C.S., Z. Ma, and J. Dyreby. Supercritical carbon dioxide power cycle configurations for use in concentrating solar power systems. 2012.

45. Wells, T., et al. Waste heat energy supercritical carbon dioxide recovery cycle analysis and design. 2012.

46. Moisseytsev, A. and J.J. Sienicki, Investigation of alternative layouts for the supercritical carbon dioxide Brayton cycle for a sodium-cooled fast reactor. Nuclear Engineering and Design, 2009. 239(7): p. 1362-1371.

47. Sarkar, J., Second law analysis of supercritical CO2 recompression Brayton cycle. Energy, 2009. 34(9): p. 1172-1178.

48. Sarkar, J. and S. Bhattacharyya, Optimization of recompression S-CO2 power cycle with reheating. Energy Conversion and Management, 2009. 50(8): p. 1939-1945.

49. Cayer, E., et al., Analysis of a carbon dioxide transcritical power cycle using a low temperature source. Applied Energy, 2009. 86(7-8): p. 1055-1063.

50. Angelino, G. and C.M. Invernizzi, Carbon dioxide power cycles using liquid natural gas as heat sink. Applied Thermal Engineering, 2009. 29(14-15): p. 2935-2941.

51. Wang, J., et al., Parametric optimization design for supercritical CO2 power cycle using genetic algorithm and artificial neural network. Applied Energy, 2010. 87(4): p. 1317-1324.

52. Cayer, E., N. Galanis, and H. Nesreddine, Parametric study and optimization of a transcritical power cycle using a low temperature source. Applied Energy, 2010. 87(4): p. 1349-1357.

53. Yari, M. and M. Sirousazar, A novel recompression S-CO2 Brayton cycle with pre-cooler exergy utilization. Proceedings of the Institution of Mechanical Engineers, Part A: Journal of Power and Energy, 2010. 224(7): p. 931-946.

54. Yari, M. and S.M.S. Mahmoudi, Utilization of waste heat from GT-MHR for power generation in organic Rankine cycles. Applied Thermal Engineering, 2010. 30(4): p. 366-375.

55. Yari, M. and S.M.S. Mahmoudi, A thermodynamic study of waste heat recovery from GT-MHR using organic Rankine cycles. Heat and Mass Transfer/Waerme- und Stoffuebertragung, 2011. 47(2): p. 181-196.

56. Rivera, W., et al., Exergy analysis of a heat transformer for water purification increasing heat source temperature. Applied Thermal Engineering, 2010. 30(14-15): p. 2088-2095.

57. Rivera, W., et al., Exergy analysis of an experimental heat transformer for water purification. Energy, 2011. 36(1): p. 320-327.

58. S.A. Klein and F. Alvarado, Engineering Equation Solver (EES), F Chart Software. 2010.

59. Parham, K., M. Yari, and U. Atikol, Alternative absorption heat transformer configurations integrated with water desalination system. Desalination, 2013. 328(0): p. 74-82.

60. Sekar, S. and R. Saravanan, Experimental studies on absorption heat transformer coupled distillation system. Desalination, 2011. 274(1-3): p. 292-301.

61. Wang, Y. and N. Lior, Proposal and analysis of a high-efficiency combined desalination and refrigeration system based on the LiBr-H2O absorption cycle - Part 2: Thermal performance analysis and discussions. Energy Conversion and Management, 2011. 52(1): p. 228-235.

62. Wang, Y. and N. Lior, Proposal and analysis of a high-efficiency combined desalination and refrigeration system based on the LiBr-H2O absorption cycle-Part 1: System configuration and mathematical model. Energy Conversion and Management, 2011. 52(1): p. 220-227.

63. Garousi Farshi, L., S.M. Seyed Mahmoudi, and M.A. Rosen, Analysis of crystallization risk in double effect absorption refrigeration systems. Applied Thermal Engineering, 2011. 31(10): p. 1712-1717.

64. Zhang, X. and D. Hu, Performance analysis of the single-stage absorption heat transformer using a new working pair composed of ionic liquid and water. Applied Thermal Engineering, 2012. 37: p. 129-135.

65. Sun, J., L. Fu, and S. Zhang, A review of working fluids of absorption cycles. Renewable and Sustainable Energy Reviews, 2012. 16(4): p. 1899-1906.

66. Rogers, R.D. and K.R. Seddon, Ionic Liquids - Solvents of the Future? Science, 2003. 302(5646): p. 792-793.

67. Seddon, K.R., Ionic liquids: a taste of the future. Nat Mater, 2003. 2(6): p. 363-365.

68. Kim, S., et al., Absorption heat pump/refrigeration system utilizing ionic liquid and hydrofluorocarbon refrigerants. Journal of Electronic Packaging, Transactions of the ASME, 2012. 134(3).

69. Marsh, K.N., J.A. Boxall, and R. Lichtenthaler, Room temperature ionic liquids and their mixtures - A review. Fluid Phase Equilibria, 2004. 219(1): p. 93-98.

70. Kim, Y.J., et al., Thermodynamic analysis of an absorption refrigeration system with ionic-liquid/refrigerant mixture as a working fluid. Energy, 2012. 44(1): p. 1005-1016.

71. He, Z., et al., Thermodynamic properties of new heat pump working pairs: 1,3-Dimethylimidazolium dimethylphosphate and water, ethanol and methanol. Fluid Phase Equilibria, 2010. 298(1): p. 83-91.

72. Zuo, G., et al., Thermodynamic properties of a new working pair: 1-Ethyl-3-methylimidazolium ethylsulfate and water. Chemical Engineering Journal, 2010. 156(3): p. 613-617.

73. Dong, L., et al., Performance prediction of absorption refrigeration cycle based on the measurements of vapor pressure and heat capacity of H2O+[DMIM]DMP system. Applied Energy, 2012. 98: p. 326-332.

74. Kaynakli, O. and R. Yamankaradeniz, Thermodynamic analysis of absorption refrigeration system based on entropy generation. Current Science, 2007. 92(4): p. 472-479.

75. Martín, A. and M.D. Bermejo, Thermodynamic analysis of absorption refrigeration cycles using ionic liquid + supercritical CO2 pairs. Journal of Supercritical Fluids, 2010. 55(2): p. 852-859.

76. Ren, J., Z. Zhao, and X. Zhang, Vapor pressures, excess enthalpies, and specific heat capacities of the binary working pairs containing the ionic liquid 1-ethyl-3-methylimidazolium dimethylphosphate. Journal of Chemical Thermodynamics, 2011. 43(4): p. 576-583.

77. Yokozeki, A. and M.B. Shiflett, Ammonia solubilities in room-temperature ionic liquids. Industrial and Engineering Chemistry Research, 2007. 46(5): p. 1605-1610.

78. Wu, S.Y. and I.W. Eames, Innovations in vapour-absorption cycles. Applied Energy, 2000. 66(3): p. 251-266.

79. Li, C.S., et al., Design and model of absorption heat transformer. Huaxue Gongcheng/Chemical Engineering (China), 2001. 29(5): p. 48.

80. Hui, L., et al., Evaluation of a seasonal storage system of solar energy for house heating using different absorption couples. Energy Conversion and Management, 2011. 52(6): p. 2427-2436.

81. Zinet, M., R. Rulliere, and P. Haberschill, A numerical model for the dynamic simulation of a recirculation single-effect absorption chiller. Energy Conversion and Management, 2012. 62: p. 51-63.

82. Jeong, S., B.H. Kang, and S.W. Karng, Dynamic simulation of an absorption heat pump for recovering low grade waste heat. Applied Thermal Engineering, 1998. 18(1-2): p. 1-12.

83. Fu, D.G., G. Poncia, and Z. Lu, Implementation of an object-oriented dynamic modeling library for absorption refrigeration systems. Applied Thermal Engineering, 2006. 26(2-3): p. 217-225.

84. Kohlenbach, P. and F. Ziegler, A dynamic simulation model for transient absorption chiller performance. Part I: The model. International Journal of Refrigeration-Revue Internationale Du Froid, 2008. 31(2): p. 217-225.

85. Matsushima, H., et al., Dynamic simulation program with object-oriented formulation for absorption chillers (modelling, verification, and application to triple-effect absorption chiller). International Journal of Refrigeration-Revue Internationale Du Froid, 2010. 33(2): p. 259-268.

86. Wu, Y.Y., Y. Chen, and T.H. Wu, Experimental researches on characteristics of vapor-liquid equilibrium of NH3-H2O-LiBr system. International Journal of Refrigeration-Revue Internationale Du Froid, 2006. 29(2): p. 328-335.

87. Me, G.Z., et al., Absorber performance of a water/lithium-bromide absorption chiller. Applied Thermal Engineering, 2008. 28(13): p. 1557-1562.

88. Papaefthimiou, V.D., D.C. Karampinos, and E.D. Rogdakis, A detailed analysis of water-vapour absorption in LiBr-H2O solution on a cooled horizontal tube. Applied Thermal Engineering, 2006. 26(17-18): p. 2095-2102.

89. De Lucas, A., M. Donate, and J.F. Rodriguez, Absorption of water vapor into new working fluids for absorption refrigeration systems. Industrial & Engineering Chemistry Research, 2007. 46(1): p. 345-350.

90. Zhang, X.D. and D.P. Hu, Performance simulation of the absorption chiller using water and ionic liquid 1-ethyl-3-methylimidazolium dimethylphosphate as the working pair. Applied Thermal Engineering, 2011. 31(16): p. 3316-3321.

91. Gommed, K., G. Grossman, and F. Ziegler, Experimental investigation of a LiCl-water open absorption system for cooling and dehumidification. Journal of Solar Energy Engineering-Transactions of the Asme, 2004. 126(2): p. 710-715.

92. Kim, K.J., T.A. Ameel, and B.D. Wood, Performance evaluations of LiCl and LiBr for absorber design applications in the open-cycle absorption refrigeration system. Journal of Solar Energy Engineering-Transactions of the Asme, 1997. 119(2): p. 165-173.

93. Patek, J. and J. Klomfar, Thermodynamic properties of the LiCl-H2O system at vapor-liquid equilibrium from 273 K to 400 K. International Journal of Refrigeration-Revue Internationale Du Froid, 2008. 31(2): p. 287-303.

94. Yari, M., V. Zare, and S.M.S. Mahmoudi, Parametric study and optimization of an ejector-expansion TRCC cycle integrated with a water purification system. Proceedings of the Institution of Mechanical Engineers, Part A: Journal of Power and Energy, 2013. 227(3): p. 383-398.

95. S.A.Klein., F.Alvarda., and Alvarda., Engineering Equation Solver (EES), F-Chart Software, WI. 2010.

96. Chen, W., et al., Thermodynamic performances of mmim DMP/Methanol absorption refrigeration. Journal of Thermal Science, 2012. 21(6): p. 557-563.

97. Hvattum, L.M. and F. Glover, Finding local optima of high-dimensional functions using direct search methods. European Journal of Operational Research, 2009. 195(1): p. 31-45.

98. Kaushik, S.C. and A. Arora, Energy and exergy analysis of single effect and series flow double effect water-lithium bromide absorption refrigeration systems. International Journal of Refrigeration-Revue Internationale Du Froid, 2009. 32(6): p. 1247-1258.

99. Yari, M., A.S. Mehr, and S.M.S. Mahmoudi, Simulation study of the combination of absorption refrigeration and ejector-expansion systems. Renewable Energy, 2013. 60(0): p. 370-381.

100. Iyoki, S. and T. Uemura, PERFORMANCE-CHARACTERISTICS OF THE WATER LITHIUM BROMIDE ZINC-CHLORIDE CALCIUM BROMIDE ABSORPTION REFRIGERATING MACHINE, ABSORPTION HEAT-PUMP AND ABSORPTION HEAT TRANSFORMER. International Journal of Refrigeration-Revue Internationale Du Froid, 1990. 13(3): p. 191-196.